UNIVERSITY OF CALIFORNIA, SAN DIEGO

The upper limb of the North Atlantic overturning circulation: investigation of the subtropical-subpolar gyre exchange and Subpolar Mode Water

A dissertation submitted in partial satisfaction of the

requirements for the degree Doctor of Philosophy

in

Oceanography

by

Elena Brambilla

Committee in charge:

Lynne D. Talley, Chair
Arthur J. Miller
Peter P. Niiler
Paul E. Robbins
Sutanu Sarkar

2006

The dissertation of Elena Brambilla is approved, and it is acceptable in quality and form for publication on microfilm:

Chair

University of California, San Diego

2006

To those who, regardless geographical distances and annoying time differences,

always managed to be incredibly close to me.

TABLE OF CONTENTS

Signature Page iii

Dedication iv

Table of Contents v

List of Figures vii

List of Tables viii

Acknowledgments ix

Vita, Publications, and Fields of Study xi

Abstract xiii

1 Introduction 1

References 5

2 Surface drifter exchange between the North Atlantic subtropical and subpolar gyres 6
2.1 Conspectus 6
2.2 Introduction 7
2.3 Data and methods 11
2.3.1 Observed drifter tracks 11
2.3.2 Mean velocity at 15-m 14
2.3.3 Ekman velocity 14
2.3.4 Synthetic drifters 16
2.4 Cross gyre exchange observed by surface drifters 20
2.5 Causes for a low intergyre exchange experienced by drifters 32
2.5.1 Sampling issues 32
2.5.2 Ekman velocity bias and effects of eddies 41
2.6 Summary and conclusion 47
2.A Appendix: Lagrangian time scale 49

References 51

3 Subpolar Mode Water in the northeastern Atlantic. Part I: properties and circulation 55
3.1 Conspectus 55
3.2 Introduction 56
3.3 Data and methods 61
3.3.1 SPMW definition 62

3.3.2 Computation of the winter mixed layer 64
3.3.3 Absolute Streamfunctions 67
3.4 Northeastern Atlantic mixed layer 71
3.5 SPMW distribution 74
3.5.1 SPMW properties 74
3.5.2 SPMW on isopycnal surfaces 76
3.5.3 Seasonal variation of SPMW location 83
3.6 Circulation in the eastern subpolar gyre 84
3.6.1 Surface circulation 86
3.6.2 Streamfunctions on isopycnal surfaces 92
3.7 Summary and conclusions 97
3.A Appendix: Objective mapping 99
3.B Appendix: Mean velocity field from float measurements 102

References 104

4 Subpolar Mode Water in the northeastern Atlantic. Part II: origin and transformation 107
4.1 Conspectus 107
4.2 Introduction 108
4.3 Data and methods 112
4.3.1 Data 112
4.3.2 Computation of the water mass transformation and formation 113
4.4 Surface water mass transformation 118
4.4.1 Annual mean transformation rates 119
4.4.2 Regional distribution of the transformation rates 121
4.4.3 Temporal variability 128
4.5 SPMW formation/obduction 130
4.5.1 Annual mean formation/obduction rates 130
4.5.2 Regional distribution of the formation/obduction estimates 132
4.6 Geostrophic transport 139
4.7 Summary and conclusions 142

References 146

LIST OF FIGURES

Figure 2.1: Drifter density (buoy-days) in 0.5°squares. 12
Figure 2.2: Mean velocity field based on drifter data on a 1°×1° grid. 21
Figure 2.3: Trajectories of drifters deployed south of 45°N from 1990 to 2002. 27
Figure 2.4: A) Surface drifter trajectories passing through the Gulf Stream-box (brown). B) Initial location of surface drifter trajectories passing through the Iceland Basin. 28
Figure 2.5: Advection of synthetic drifters through the observed total mean velocity field 31
Figure 2.6: Probability density function of the surface temperature from drifter data 37
Figure 2.7: 600-day combined trajectories (section 2.5.1b). 40
Figure 2.8: Mean Ekman velocity field in 1°×1° calculated from wind data. 42
Figure 2.9: Advection of synthetic drifters through the observed mean velocity field. 44
Figure 2.10:Synthetic drifters advected through the mean velocity field with random turbulence added to it. 46

Figure 3.1: Study area 65
Figure 3.2: Depth of the winter mixed layer (m) 72
Figure 3.3: Properties at the PV minimum 77
Figure 3.4: Properties at $27.3\sigma_\theta$ 80
Figure 3.5: Properties at $27.4\sigma_\theta$. 81
Figure 3.6: Properties at $27.5\sigma_\theta$. 82
Figure 3.7: Monthly distribution of the hydrographic data 84
Figure 3.8: Seasonal potential vorticity values ($10^{-13} cm^{-1} s^{-1}$) 85
Figure 3.9: Absolute surface streamfunction (cm) 90
Figure 3.10:Joint probability density function (pdf) 91
Figure 3.11:Absolute isopycnal streamfunction 95

Figure 4.1: Annual mean transformation function $\overline{F(\sigma_\theta)}$ (Sv) 120
Figure 4.2: Regional distribution of the annual mean transformation function $\overline{F_{i,j}(\sigma_\theta)}$ (Sv) 124
Figure 4.3: Annual mean buoyancy flux ($kg\ m^{-1} s^{-3}$) 126
Figure 4.4: Regional distribution for the annual mean transformation function $\overline{F_{i,j}(\sigma_\theta)}$ (Sv) and SPMW 127
Figure 4.5: Time series of the transformation function (Sv) 129
Figure 4.6: Annual mean formation function $\overline{M(\sigma_\theta)}$ (Sv) 132
Figure 4.7: Annual mean formation/obduction rates (m/year) $\overline{S_{i,j}}$ . . 136
Figure 4.8: Annual mean formation/obduction rates (m/year) 138
Figure 4.9: Geostrophic transport (Sv) 140

LIST OF TABLES

Table 2.1: Speeds of the strongest currents in the North Atlantic. . . 23
Table 2.2: Summary of the actual drifters and all the synthetic drifter runs. 33

Table 3.1: Mean properties 83

ACKNOWLEDGMENTS

I am very grateful for the guidance provided by my advisor Lynne Talley. Lynne supported me with great enthusiasm since my first year of research, giving me the opportunity to study the ocean using data in my office, as well as discovering it "at sea" during several cruises. I thank Lynne for her infinite patience, suggestions, discussions, corrections, and explanations that allowed me to finish this dissertation.

I thank Peter Niiler, also member of my doctoral committee, for providing the surface drifter data, and for the help he gave me to better interpret the drifter results. Peter has always been very supportive of my Lagrangian studies and allowed me to attend to the LAPCOD meeting in Lerici (Italy), 2005.

Paul Robbins has been fundamental for the development of the last chapter of my thesis. Paul inspired my work suggesting very thoughtful readings and he has been very generous in offering his help to understand more deeply the results. I also thank the other members of my doctoral committee, Art Miller, Sutanu Sarkar, for contributing their time and providing useful comments.

I acknowledge the professors at Scripps who contributed to my education and among them, in particular, Sarah Gille, in the office of whom I ended up many times with numerous questions on data analysis.

The students at Scripps have been fun companions in my Ph.D. adventure, and among the many I am really grateful to Yueng Lenn for her fantastic cheerful attitude. Without my first year classmates, Genevieve Boisvert, Jessica

Kleiss, Liz Douglass, Sarah Zedler, Shane Elipot, the work load of the first year classes and the departmental exam would have been unbearable. I'm particular indebted to my officemate Shane Elipot, who has always been ready to spend time in scientific discussion or "philosophical" thoughts about life.

My research has been financially supported by the National Science Foundation-Ocean Science Division through grants part of the World Ocean Circulation Experiment (WOCE) and CLIVAR CLIMODE Experiment. I also received support for the Scripps Institution of Oceanography graduate department.

Chapter 2, in full, is a reprint of the material as it appears in:
Brambilla, E., L. D. Talley (2006), Surface drifter exchange between the North Atlantic subtropical and subpolar gyres, J. Geophys. Res., 111, C07026, doi:10.1029/2005JC003146. The dissertation author was the primary investigator and author of this paper.

VITA

2000	Laurea in Physics Universita' Statale di Milano (Italy)
2001–2006	Graduate Student Researcher Scripps Institution of Oceanography, University of California, San Diego
2006	Ph.D., Physical Oceanography Scripps Institution of Oceanography, University of California, San Diego.

PUBLICATIONS

Brambilla, E. L. D. Talley (2006): Surface drifter exchange between the North Atlantic subtropical and subpolar gyres. *J. Geophys. Res.*, 111, C07026, doi:10.1029/2005JC003146

Brambilla, E., and L. D. Talley, North Atlantic Subpolar Mode Water. Part I: properties and circulation in the eastern subpolar gyre, manuscript in preparation.

Brambilla, E., and L. D. Talley, North Atlantic Subpolar Mode Water. Part II: origin and transformation, manuscript in preparation.

Onken, R., and E. Brambilla (2003): Double diffusion in the Mediterranean Sea: Observation and parameterization of salt fingers convection. *J. Geophys. Res.*, 108 (C9), 8124, doi:10.1029/2002JC001349

FIELDS OF STUDY

Studies in Physical Oceanography
Professors M. C. Hendershott, P. E. Robbins, and D. Roemmich

Studies in Applied Mathematics
Professors S. G. Llewellyn Smith, G. Ierley, and W. R. Young

Studies in Fluid Mechanics
Professor C. Winant

Studies in Geophysical Fluid Dynamics
Professors P. Cessi and R. L. Salmon

Studies in Linear and Non-Linear Waves
Professors M. C. Hendershott, R. T. Guza, W. K. Melville

Studies in Data Analysis
Professors R. Pinkel, S. T. Gille, and D. L. Rudnick

Studies in Biological Oceanography
Professor P. J. S. Franks

Studies in Ocean Turbulence
Professor L. Armi

Studies in Atmospheric Dynamics
Professor R. C. J. Somerville

ABSTRACT OF THE DISSERTATION

The upper limb of the North Atlantic overturning circulation: investigation of the subtropical-subpolar gyre exchange and Subpolar Mode Water

by

Elena Brambilla

Doctor of Philosophy in Oceanography

University of California, San Diego, 2006

Professor Lynne D. Talley, Chair

Two aspects of the upper limb of the North Atlantic overturning circulation are studied: 1) surface drifter exchange between the subtropical and the subpolar gyres; and 2) characterization of the properties and formation of Subpolar Mode Waters (SPMW). With respect to the first, just one out of 273 drifters (drogued at 15 m) in the Gulf Stream region from 1990 to 2002, moved from subtropical to subpolar latitudes. Most of the drifters recirculated in the subtropical gyre without crossing the inter-gyre edge. This result was surprising because of the known transport of upper ocean water from the subtropical to the subpolar gyre. We suggest that undersampling and inadequate drifter life time lead to an underestimate the northward flow. Moreover, the Ekman flow and the eddy contribution affect the surface trajectories in opposite direction, nearly canceling each other.

The description of the properties of the SPMW and the analysis of its formation aim at better describing the warm and salty pathway that supplies water to the regions of dense water formation (Labrador and Nordic Seas). Lagrangian data (surface drifters and isopycnal floats) combined with historical hydrographic data show that each branch of the North Atlantic Current (NAC) in the eastern subpolar gyre is characterized by its own sequence of SPMW that increases in density following the downstream flow. Furthermore, since the branches of the NAC have a dominant northeastward direction, the newly observed distribution of SPMW, combined with the new streamfunctions calculated here, do not support the original hypothesis of McCartney and Talley (1982) of a smooth, cyclonic pathway for SPMW around the subpolar gyre. The transformation and the formation of SPMW are then investigated in terms of the diapycnal flux driven by buoyancy flux. We show that SPMW is transformed to increasingly dense SPMW along the major branches of the NAC. The continuous transformation of SPMW is not constant in density space, leading to "formation" (obduction) of SPMW. However, since the SPMWs are shown to be confined within the mixed layer, we interpret the SPMW formation as loss by entrainment to the dense overflows through Denmark Strait and Iceland-Scotland Ridge.

1

Introduction

The North Atlantic basin has long attracted the interest of oceanographers due to its important role in the activation and maintenance of the global thermohaline circulation (THC). Since the first physical oceanographical studies, the North Atlantic basin has been recognized to represent the junction between the deep and the upper flow of the THC (Stommel, 1955; Wüst, 1959). The formation of the dense water masses that constitute the deep southward flow of the THC takes place in various marginal seas of the North Atlantic: the Labrador Sea, the Nordic Seas, and possibly the Irminger Sea (Pickart et al., 2003). To balance the dense southward flow, warm and salty water flows in the upper layer of the North Atlantic (Gordon, 1986; Broecker, 1991; Schmitz and McCartney, 1993; Schmitz, 1995; Talley, 2003).

In this thesis, the focus is on the upper limb of the North Atlantic overturning circulation, studied from two different point of view: 1) the investigation of the surface drifter exchange between the subtropical and the

subpolar gyres; and 2) the characterization of the properties and the circulation of the Subpolar Mode Water (SPMW) in the northeastern Atlantic. These two studies represent, respectively, chapter 2 and chapters 3 and 4 of the dissertation.

The numerous Lagrangian data (surface drifters and subsurface floats) available in the North Atlantic can improve the accuracy of the circulation patterns of the flow compared with estimates from traditional hydrographic measurements. Therefore, it is useful to check if theses copious and relatively cheap (compared to ship time) Lagrangian data are adequate to investigate the upper flow of the thermohaline circulation. Moreover, recently, because of the possible connection between climate and the thermohaline circulation (THC), great attention has been given to the study of time variability of the THC. Thus, Lagrangian data, because of their increasingly long time coverage, could represent a useful tool to discuss this subject. However, it is necessary to first analyze their efficacy.

For these reasons, we initially concentrate on the efficiency of surface drifters in tracking the upper northward flow between the North Atlantic subtropical and subpolar gyre (chapter 2); secondly, we focus more in detail on the surface and subsurface flow of the subpolar gyre, in terms of both its path and the properties of its water masses (chapters 3 and 4).

In chapter 2, we conclude that the exclusive use of surface drifters is not adequate to track the northward flow between the subtropical and the subpolar gyre. We show that drifter lifetime and undersampling underestimate the northward flow. Moreover, Ekman flow and eddies affect the drifter trajectories in opposite manners that nearly cancel, therefore preventing the surface drifters

from flowing northward. However, these causes seem to explain, just partially, the difficulty that surface drifters have in tracking the northward flow. Thus, we propose that isopycnal Lagrangian measurements, for their capability in following obducting flow, might be more adequate.

In chapters 3 and 4, the study of the subpolar gyre flow is not limited to the identification and description of the surface and subsurface paths, but also includes description of the water masses in the eastern North Atlantic that characterize most of this upper circulation. McCartney and Talley (1982) propose that SPMWs constitute the upper flow of the North Atlantic thermohaline circulation; however they suggested that the main pathway is cyclonic in the subpolar gyre. Here, different from McCartney and Talley's (1982) hypothesis, taking advantage of the better spatial distribution of the hydrographic data and introducing Lagrangian data, we show that the main direction of the surface flow is northeastward, structured along two distinct branches of the North Atlantic Current (NAC). Hence, the SPMWs that constitute the upper flow of each NAC branch, move predominantly northeastward and, not cyclonically, in the subpolar gyre.

Chapter 4 further extends the investigation of SPMWs, focusing on their origin and formation. Estimates of the SPMW transformation rates are obtained using hydrographic and air-sea flux data with minor incorporation of Lagrangian data. We conclude that the diapycnal volume flux driven by the air-sea exchange is a dominant cause in the transformation of SPMWs. Due to air-sea exchange, SPMW progressively increases its density along the major branches of the North

Atlantic Current in the subpolar gyre. Moreover, the diapycnal volume flux is not constant in density space. Therefore it drives a continuous vertical exchange between the winter mixed layer and the ocean interior. Finally, we also observe that the isopycnal volume flux contribution to the SPMW throughput spans between 10% and 40% of the diapycnal component.

References

Broecker, W. S., 1991: The great ocean conveyor. *Oceanography*, **4**, 79–89.

Gordon, A. L., 1986: Interocean exchange of thermocline water. *J. Geophys. Res.*, **91**, 5037–5046.

McCartney, M. S., and Talley, L. D., 1982: The Subpolar Mode Water of the North Atlantic. *J. Phys. Oceanogr.*, **12**, 1169–1188.

Pickart, R., Straneo, F., and Moore, G. W. K., 2003: Is Labrador Sea Water formed in the Irminger Sea? *Deep-Sea Res. I*, **50**, 23–52.

Schmitz, W. J., 1995: On the interbasin-scale thermohaline circulation. *Rev. Geophys.*, **33**(2), 151–174.

Schmitz, W. J., and McCartney, M. S., 1993: On the North Atlantic circulation. *Rev. Geophys.*, **31**, 29–49.

Stommel, H., 1955: The anatomy of the Atlantic. *Scientific American*, **192**, 30–35.

Talley, L. D., 2003: Shallow, intermediate, and deep overturning components of the global heat budget. *J. Phys. Oceanogr.*, **33**, 530–559.

Wüst, G., 1959: New general study on oceanography. *Petermanns Geographisch Mitteilungen*, **103**, 276–277.

2

Surface drifter exchange between the North Atlantic subtropical and subpolar gyres

2.1 Conspectus

Surface drifters deployed in the subtropical and subpolar North Atlantic from 1990 to 2002 show almost no connection between the subtropical and subpolar gyres; only one drifter crosses the intergyre boundary even though other data types (e.g. dynamic topography and tracers) suggest a major connection. Two of several possible causes for the lack of intergyre connectivity in this two-dimensional data set are examined: (1) undersampling and short drifter lifetime leading to underestimation of the northward flow, and (2) the southward mean Ekman velocity. Advection of a large number of long-lived synthetic drifters through the

observed mean velocity results in a 5% increase in cross-gyre flux compared with that for synthetic drifters with realistic lifetimes. By further advecting synthetic drifters through the observed mean velocity field with and without the Ekman component, estimated from the wind field associated with the actual drifters, it is shown that removal of the Ekman component further increases the intergyre flux by up to 6%. With a turbulent component added to the mean velocity field to simulate the eddy field, there is a further increase in connection by 5%. Thus the Ekman and eddy contributions to the drifter trajectories nearly cancel each other. Consideration of three-dimensional processes (subduction and obduction) is reserved for complete modeling studies.

2.2 Introduction

Surface drifters have been extensively used to study the surface circulation in the North Atlantic (Fratantoni, 2001; Flatau et al., 2003; Reverdin et al., 2003; Niiler et al., 2003; McClean et al., 2002). Here, our attention moves beyond the description of Eulerian mean surface currents and we focus on the behavior of surface drifters at the subtropical/subpolar boundary in the North Atlantic, in a manner similar to Poulain et al.'s [1996] treatment of Lagrangian drifters in the Norwegian Sea.

We show that there is almost a complete separation between the North Atlantic drifters in the subtropical and subpolar gyres; only one crosses the intergyre boundary. Thus, almost none of the drifters deployed in the subtropical

gyre reach the Iceland Basin and the Norwegian Current. Similarly, drifters deployed in the subpolar gyre recirculate cyclonically in the gyre without leaving it.

This observation of so very few surface drifters entering the subpolar gyre contrasts with the known northward upper ocean flow based on surface dynamic topographies (Reid, 1994; Niiler et al., 2003) and transport analyses (Roemmich and Wunsch, 1985; Schmitz and McCartney, 1993; Macdonald, 1998; Koltermann et al., 1999; Ganachaud and Wunsch, 2003; Talley et al., 2003). The visual connectivity in the mean surface drifter velocity field from the Gulf Stream through the North Atlantic Current, shown below in section 3, also gives the impression of a northward surface flow from low to high latitudes.

This contrast between the surface drifter trajectories and known net flux based on hydrographic data sets is similar to the situation reported for subsurface floats exiting the Labrador Sea (Lavender et al., 2000). Although circulation analyses, mass transports and tracers indicate outflow into the Deep Western Boundary Current that heads southwest from Flemish Cap, the floats do not make the connection and instead move eastward, remaining in the subpolar gyre.

On the other hand, it is well-established that jets such as the Gulf Stream have little cross-frontal transport, based on numerous numerical and laboratory models (Liu and Yang, 1994; Yang, 1996; Pratt et al., 1995; Berloff et al., 2002). The front that drifters must cross to enter the subpolar gyre is the North Atlantic Current, as or after it turns eastward at the northwest corner (Rossby, 1996). Eddies in these strong currents are a primary mechanism for cross-

frontal transport through dispersion (Bower, 1991; Berloff et al., 2002; Ozgokmen et al., 2000; Dutkiewicz et al., 1993). Such an eddy component is of course part of the actual velocity field sampled by the surface drifters; the question is why it is not more effective in creating cross-frontal exchange. A partial answer is suggested by Owens (1984); Bower and Rossby (1989); Bower (1991); Lozier and Riser (1990), whose combined observational and modeling studies show that cross-frontal particle exchange is much more inhibited in the strongest frontal flows at the sea surface compared with weaker flows at depth.

Thus the observed dynamic topographies, transport and tracers indicate that there is more rather than less cross-frontal exchange whereas the observed surface drifters suggest that there is less rather than more. How can these two independent and apparently contradictory views of the same circulation be reconciled? We begin by assuming that there must be flow from the subtropical to the subpolar gyre, of up to 20 to 25% of the upper layer of the Gulf Stream, based on meridional transport calculations yielding a 15 to 20 Sv overturn in the northern North Atlantic (Hall and Bryden, 1982; Roemmich and Wunsch, 1985; Gordon, 1986; McCartney and Talley, 1982; Schmitz and McCartney, 1993; Richardson and Schmitz, 1993; Talley et al., 2003; Lumpkin and Speer, 2003; Ganachaud, 2003). This provides an upper limit to the intergyre exchange that we might expect.

We then use the surface drifter data observations to begin to evaluate possible mechanisms that could limit the intergyre flux. First, the limited drifter dataset and drifter lifetimes might bias the observations. Secondly, the net southward Ekman velocity beneath the westerly winds might counteract the

turbulent component of the flow that should cause dispersion of subtropical floats into the subpolar gyre as explored by Drijfhout et al. (2003); Tansley and Marshall (2001). Third, eddies could bias the drifter trajectories since drifters might be trapped in cyclonic eddies and avoid anticyclonic eddies (P. Niiler personal communication). Fourth, surface water subducts and obducts, particularly in the frontal zone related to the intergyre boundary Qiu and Huang (1995), but since drifters are constrained to remain at the surface, they cannot follow these three-dimensional pathways.

This paper is limited to investigation of the first two candidates: surface drifter sampling issues and the impact of the Ekman and turbulent components on the drifter trajectories. Analysis of the other possible causes is part of an ongoing study in cooperation with general circulation modelers, in which we are considering the three-dimensionality of the near-surface flow.

The paper is organized as follows: section 2 describes the data and methodology, in section 3 we show the basic drifter observations, focusing on the intergyre boundary, in section 4 the adequacy of the data set and the impact of the Ekman and turbulent components of the flow are analyzed, and section 5 is the summary and conclusions.

2.3 Data and methods

Surface drifters drogued at 15m are a large and readily accessible data set, which is expected to be continued indefinitely as part of the global ocean observing system. We examine the subtropical/subpolar northward flow as recorded by this dataset in the North Atlantic. As part of our exercise of understanding why the surface drifters do not show cross from the subtropical to the subpolar gyre, we construct a synthetic drifter data set using a simple model based on the surface flow from the actual drifters.

2.3.1 Observed drifter tracks

The Lagrangian surface drifters that are used in this study are part of a large set of drifters deployed in the North Atlantic from 1990 to 2002, under the aegis of the Surface Velocity Program (SVP) established during the WOCE and TOGA experiments, to have a long-term observing system of ocean currents (Sybrandy and Niiler, 1991).

All drifters used in the program were designed with a submerged cylindrical drogue centered at 15 m below the surface, to reduce the slippage due to the wind. The effects of the wind on the drifter trajectory have been estimated by Niiler (1995), who showed that the slippage due to the wind for drifters with the drogue attached is limited to 1 cm/s in 10 m/s at 10 m height. Pazan and Niiler (2001) compared the response to the wind of drogued and undrogued drifters. The

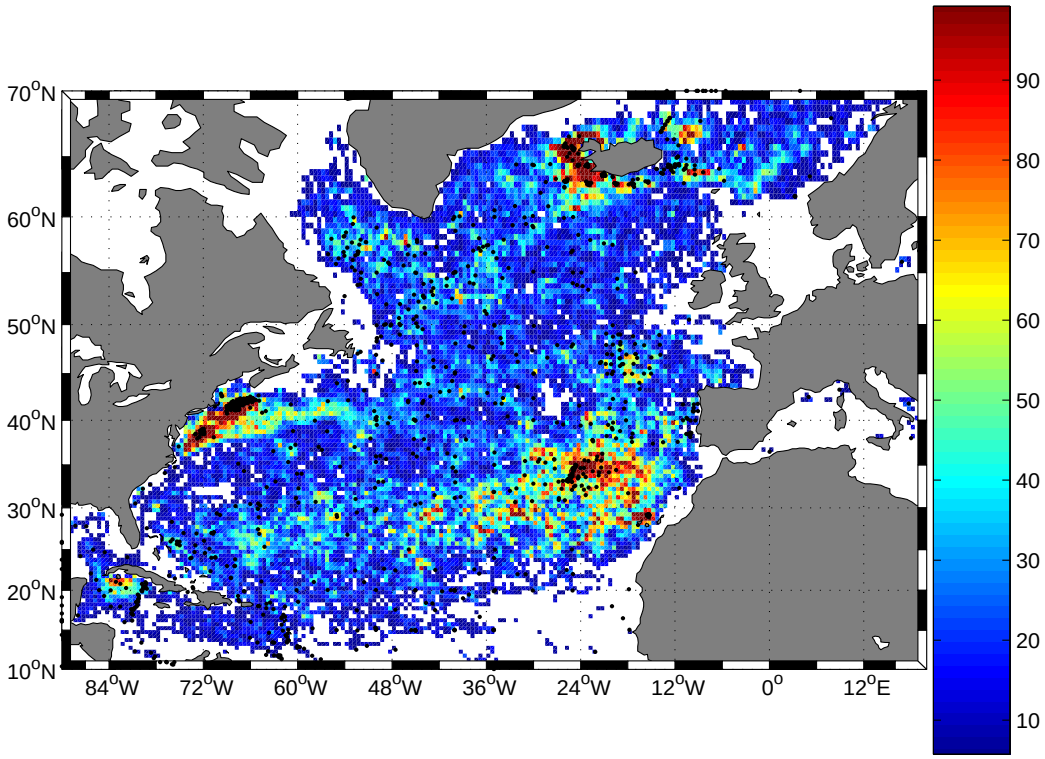

Figure 2.1: Drifter density (buoy-days) in 0.5°squares. The grid boxes with fewer than 5 buoy-days are not shown. Black dots are drifter deployment locations.

authors concluded that downwind slippage of an undrogued drifter relative to a drogued one is 8.8 cm/s per 10 m/s NCEP wind reanalysis at 10 m height. For a complete description of the SVP drifter refer to Pazan and Niiler (2001).

These studies led us to discard undrogued drifters from our data set. After this selection, 1108 drifters were left (98% of the total) to describe the surface circulation in the North Atlantic from 1990 to 2002. Each drifter continuously transmits position (longitude and latitude), temperature and time to the Argos satellite system. The data are processed at the Global Drifter Center at Atlantic Oceanographical and Metereological Laboratory (AOML) which provides them as a time series with a sampling interval of 6 hours. The time series includes: position (longitude and latitude), velocity (zonal and meridional), temperature, time and wind velocity (zonal and meridional). The wind velocity data are obtained by interpolation of the 10 m height NCEP wind reanalysis at 6-hourly intervals at the drifter locations. For a detailed explanation of the data processing see Reverdin et al. (2003).

The mean lifetime of the drogued surface drifters in this dataset is 271 days $\pm$ 260 days (the median is 182 days). The longest drifter has lifetime of 2024 days, the shortest 1 day.

2.3.2 Mean velocity at 15-m

The time series of velocity associated with each drifter has been used to calculate the mean surface velocity field in the North Atlantic. The basin has been divided into a $0.5^\circ \times 0.5^\circ$ grid and the mean vector velocity associated to each grid box is the ensemble average of all the velocity data in the box. The robustness of such binned mean technique has been studied in the past. Garraffo et al. (2001b), comparing the true Eulerian mean with binned mean of simulated Lagrangian observation with the MICOM model, showed that in regions characterized by major currents the binned mean overestimates the Eulerian mean, but the difference is not significant with respect to the sampling error. Lumpkin (2003) compared the binned mean with the Gauss-Markov (GM) derived mean, demonstrating that both methods agree well in the Atlantic basin, although the Gauss-Markov method shows higher values of the mean velocity in the Gulf Stream.

Despite the imprecision of the binned mean in western boundary currents, we consider the estimates of the mean velocity satisfactory, in particular considering that the focus of this study is not a detailed description of the intensity of the currents in the North Atlantic, but rather the tracks of individual drifters.

2.3.3 Ekman velocity

The drifter velocity, which is measured at 15 m, can be decomposed into an Ekman component, a geostrophic component, a residual ageostrophic

component, and slippage due to the wind.

$$\mathbf{U}(t)_d = \mathbf{U}(t)_e + \mathbf{U}(t)_{geo} + \mathbf{U}(t)_{ageo} + \mathbf{U}(t)_{slip} \tag{2.1}$$

where $\mathbf{U}(t)_d$ is the velocity measured from the drifter, $\mathbf{U}(t)_e$ is the Ekman component, $\mathbf{U}(t)_{geo}$ is the geostrophic component, $\mathbf{U}(t)_{ageo}$ is the residual ageostrophic component and $\mathbf{U}(t)_{slip}$ is the slippage due to the wind. As mentioned in section 2.1, the slippage velocity due to the wind was quantified by Niiler (1995). The Ekman component is computed using the 6-hourly wind data provided in the drifter dataset. After subtracting these from the drifter velocity, the residual velocity includes the geostrophic component, a remaining ageostrophic part and errors related to uncertainties in the Ekman computation and in the wind data.

The Ekman component was calculated for each 6-hourly interval position along each drifter track using the complex-notation formula from Ralph and Niiler (1999) :

$$\mathbf{U}_e = \beta e^{-i\theta} u_\circ \frac{\tau}{|\tau|} f^{-1/2} \tag{2.2}$$

In (2.2), $\mathbf{U}_e = U_e + iV_e$, β=0.065, $\theta = 55°$is the rotation of the Ekman current to the right of the wind, f is the Coriolis parameter, and $u_\circ^2 = \frac{|\tau|}{\rho}$ is the friction velocity, where the wind stress τ is computed using the 10m NCEP wind reanalysis interpolated at the same 6-hourly interval locations along the drifter tracks. Once the Ralph-Niiler model has been applied, the resulting Ekman velocity is binned and averaged in 0.5°$\times$ 0.5°grid boxes to produce the mean Ekman velocity field (Fig. 2.8).

This method of producing an Ekman velocity field in conjunction with

drifter data analysis, from the wind data following the drifters and the Ralph and Niiler (1999) model, was used by Flatau et al. (2003); Niiler et al. (2003); Lumpkin and Garzoli (2005) for basin and global-scale analysis of the Ekman and non-Ekman components of the velocity. In contrast, O'Connor et al. (2002) used the surface drifters and an estimate of the geostrophic velocity from climatological hydrographic data to construct an Ekman velocity field. As described in O'Connor et al. (2002), the comparison between the Ekman velocity field obtained in this manner agrees with the Ekman velocity expected from the regional wind stress.

2.3.4 Synthetic drifters

In order to address the impact on the surface drifter trajectories of possible undersampling, short drifter lifetimes, and the effect of the Ekman and turbulent velocity components, we have created a synthetic drifter data set based on various assumed flow fields constructed from the surface drifter mean field. The trajectories of the synthetic drifters are obtained by advecting artificial particles through the surface velocity field. As opposed to the observed drifters, the synthetic drifters have the advantage of an indefinite lifetime, and the density of the particles can be as large as desired. Furthermore, computing the synthetic drifter trajectories, it is possible to use individual components of the mean velocity field (e.g. total, Ekman and residual) through which the particles are advected to test the impact of each on the trajectories. Noise can also be added to simulate

eddies or rms error in the mean velocities.

Two kinds of advection model are used to calculate the trajectory of synthetic drifters. The first is based on simple advection of particles through the mean velocity fields computed from the drifter observations, considering the velocity of the particle at each time step to be completely uncorrelated with the velocity at the immediately previous and following time steps. The second model adds a turbulent component to the mean velocity to simulate eddy noise. The amplitude of the noise is based on the observed standard deviation ellipses from the drifters, to simulate the geographic variation in eddy amplitudes and hence spatial variation in drifter dispersion. The velocity at each time step is set to be partially correlated to the velocity at the previous time step. We refer to the two models as the "mean advection" and "turbulent advection" models.

a) MEAN ADVECTION

The "mean advection" model is

$$\mathbf{r}(t) = \mathbf{u}(t - dt, \mathbf{r}(t - dt))dt + \mathbf{r}(t - dt) \tag{2.3a}$$

$$\mathbf{u} = < \mathbf{U} >_m \tag{2.3b}$$

alternatively:

$$\mathbf{u} = < \mathbf{U} >_m - < \mathbf{U} >_e \tag{2.3c}$$

where $\mathbf{r}(t)$ is the position vector (longitude and latitude); dt is the time step; $< \mathbf{U} >_m$ is the mean velocity vector (ensemble average); $< \mathbf{U} >_e$ is the mean Ekman component (ensemble average) computed as described in section 2.3.3.

The mean velocity field and the mean Ekman velocity field are computed on a regular 0.5°× 0.5°grid. A velocity vector is associated with the center of each grid box. At each time step, the mean surface velocity and the mean Ekman velocity that appear in (2.3b,c) are calculated as the bilinear interpolation, in the location of the particles, of the gridded velocity vectors that surround the position of the particle.

For synthetic drifter runs through the mean field, deployment locations were either: (a) on a regular grid 1°× 1°in a confined region between 78°W-48°W, 35°N-47°N (305 drifters), or (b) at the actual surface drifter release locations (272). A three-year lifetime was assigned to all synthetic drifters.

b) TURBULENT ADVECTION

The second advection model is based on the advection of artificial particles through the observed mean velocity field with a superimposed turbulence field. The model belongs to the general class of "random flights" models (Thomson, 1987). It simulates the advection of independent particles through a mean velocity field on which is superimposed spatially homogeneous turbulence. This kind of model is commonly used in simulation of Lagrangian advection, e.g. Dutkiewicz et al. (1993), Falco et al. (2000), Ozgokmen et al. (2000), Castellari et al. (2001).

The turbulence is represented by random impulses based on the velocity variance at each grid point computed from the actual surface drifter observations. The model (Griffa, 1996) can be written for each component in incremental form as:

$$dx_{1,2} = (U_{1,2} + u'_{1,2})dt \tag{2.4a}$$

$$du'_{1,2} = -(\frac{1}{T_L})u'_{1,2}dt + \sqrt{(\frac{\sigma^2_{1,2}}{T_L})}dw_{1,2} \tag{2.4b}$$

where $U_{1,2}$ are the meridional and zonal mean velocity, $u'_{1,2}$ are the departure from the mean, $\sigma^2_{1,2}$ is the variance on the ensemble average in each grid box, T_L is the Lagrangian time scale, $dw_{1,2}$ is a random increment from a normal distribution of zero mean and second order - momentum $< dw_{1,2}(ti)dw_{1,2}(t_j) >= \delta_{ij}2dt$.

As explained in Griffa (1996), (2.4b) states that at each time step the particle loses a fraction of its momentum, $U(\frac{dt}{T_L})$, and on the other hand receives a random impulse dw. This can also be interpreted as memory of the particle's velocity during a finite time of order T_L.

In the application of the "turbulent advection" model, the time step dt is 6 hours and the total period during which the model runs is 3 years. T_L has been calculated from the drifter data to be 1.5 days for the meridional component and 2.5 days for the zonal component (section 2.A). The deployment locations of the artificial particles follow the same scheme as for the "mean-advection" model (section 2.3.4a).

2.4 Cross gyre exchange observed by surface drifters

In this section, we examine the 15-m velocity field given by the surface drifters. We consider the mean flow and individual Lagrangian trajectories. The mean field from surface drifters has been published by multiple authors (McClean et al., 2002; Flatau et al., 2003; Reverdin et al., 2003; Niiler et al., 2003), but the discrepancy between it and the Lagrangian trajectories has not been highlighted.

The surface mean velocity (Fig. 2.2), calculated as described in section 2.3.2, agrees with the surface mean velocity computed from the same surface drifter data set shown in the cited papers, and captures all the major features of the surface circulation in the North Atlantic. The strongest currents are the Gulf Stream, along the North American coast, the East and West Greenland Currents, and the Labrador Current along the eastern coast of Canada. Less strong, yet well defined, is the North Atlantic Current (NAC), which, after passing the northwest corner east of the Grand Banks region, crosses the North Atlantic and eventually splits in two branches. One branch passes through the Iceland Basin and the other through Rockall Trough. The mean velocity field also shows a strong Irminger Current, arising on the western flank of the Reykjanes Ridge and connecting to the East Greenland Current.

The mean speed of each surface current listed above has been computed from the drifter velocities and the observed mean surface velocity field (Table 2.1). For each current, it has been possible to estimate the mean direction of the flow and

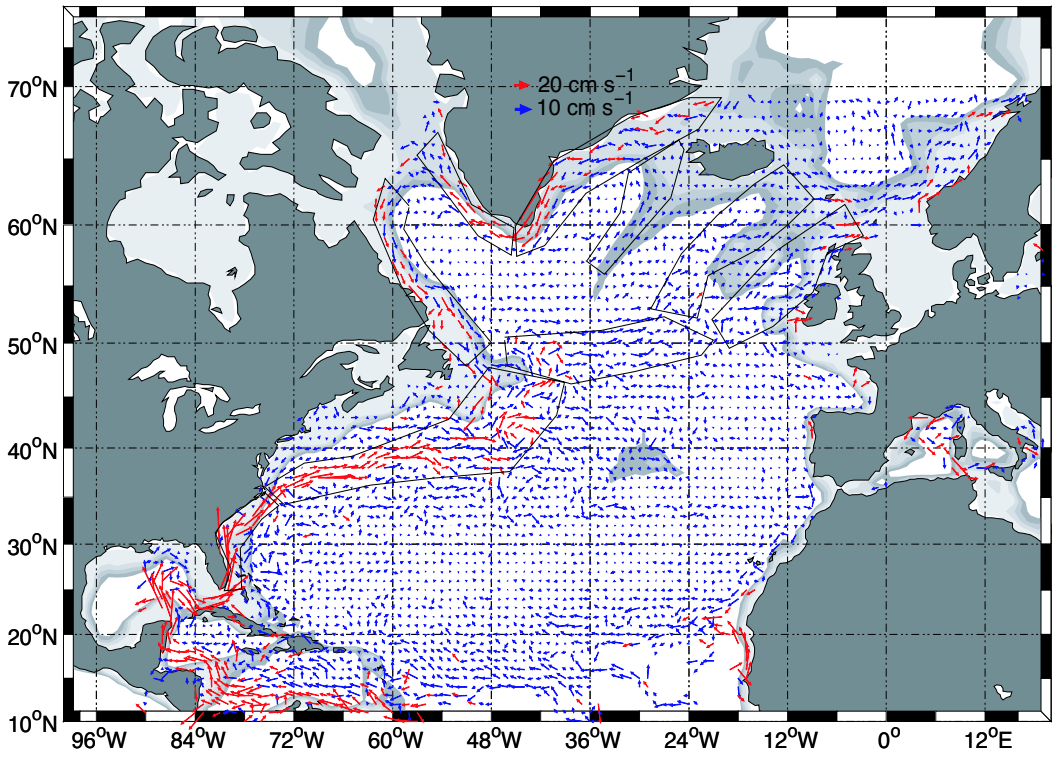

Figure 2.2: Mean velocity field based on drifter data on a 1°×1° grid, using a binning technique. The mean has been computed using 15-m drifters with drogues attached. The data cover the period from 1990 to 2002. Red arrows are velocity $>$ 20 cm/s. The black boxes identify each current in the North Atlantic. The mean speed of each current is computed averaging the speed inside the boxes. Topography is shaded in gray. The darkest contour is at 2000m. Contour interval is 500m.

the standard deviation from the mean. The mean speed for each current, then, is the ensemble average of all the 6-hourly drifter velocities that have direction included in the range provided by the mean direction of the current plus or minus its standard deviation.

Values of mean surface speed from the same Lagrangian drifters have been previously provided by Fratantoni (2001). Our estimates agree in the Gulf Stream, Labrador Current, and East and West Greenland Currents. We use a different division of the NAC (Eastward Branch, Iceland Basin Branch, and Rockall Trough Branch), and we add the Irminger Current mean speed. Our results are also consistent with the mean velocities shown by McClean et al. (2002), obtained using just four years (1993-97) of the same dataset.

The surface mean velocity field suggests a general tendency of a northward flow from subtropical to subpolar latitudes, through the Gulf Stream and the North Atlantic Current. The Gulf Stream Extension visually appears connected to the North Atlantic Current. As we see next, however, this appearance is misleading.

a) LAGRANGIAN TRAJECTORIES IN THE NORTH ATLANTIC

Based on the appearance of the mean velocity field, one might expect the surface drifters to track the apparent flow that carries water from the subtropical to the subpolar gyre. However, the drifter trajectories do not support this visual

Table 2.1: Speeds of the strongest currents in the North Atlantic based on the surface drifter data. Second column is the mean speed (cm/s) and the standard deviation from the mean. The mean speed are computed among the speed of the mean velocity vectors observed inside the black boxes superimposed to the mean velocity field. Just the vectors for which the distribution of the direction of the velocity is approximately Gaussian are considered. Third column is the swiftest drifter observation (cm/s).

	mean speed (cm/s)	max speed (cm/s)
Gulf Stream	66 ± 38	239
Labrador Current	20 ± 12	133
West Greenland Current	21 ± 13	147
East Greenland Current	23 ± 17	185
Irminger Current	6 ± 3	90
NAC (Eastward Branch)	11 ± 7	143
NAC (Iceland Basin Branch)	8 ± 5	82
NAC (Rockall Trough Branch)	10 ± 6	114

interpretation (Fig. 2.3). Of the drifters deployed south of 45°N, only one reached the subpolar gyre. This drifter had a lifetime of 495 days and had been deployed just south of Newfoundland. Its trajectory followed the edge of the continental shelf, was caught by the permanent Mann eddy east of Newfoundland, and escaped after just 1 loop. It then followed the branch of the NAC that passes through the Rockall Trough, reaching the Norwegian Current. Thus the only connection between the two gyres in the surface drifters is via the northwest corner of the NAC (Rossby, 1996) . This location is in agreement with that suggested by the mean velocity field, but the solitary drifter that reached the Norwegian Current cannot represent the expected full intergyre exchange.

For later comparison with synthetic drifter experiments in which we explore the connection of the Gulf Stream extension with the subpolar gyre, we narrow our focus to a rectangular box across the Gulf Stream extension of the following dimensions: 78°W-48°W, 35°N-47°N (hereinafter, Gulf Stream box or GS box) (Fig. 2.4A). 273 drifters flow through this box. Among these, just one reaches the Iceland Basin, which is the same drifter seen in Fig. 2.3.

Drifter deployment within the GS box was not uniform. There was a large concentration of deployments south of Georges Bank, of which about half were lost to the coast while the others were entrained in the Gulf Stream (Lozier and Gawarkiewicz, 2001). This deployment bias could change (reduce) the percentage of GS box drifters that cross to the subpolar gyre, but we would not expect it to reduce the number to just one. Moreover, although the box extends westward including the southward flow of the Middle Atlantic Bight, it is representative

of the northward flow since the Middle Atlantic Bight shelf water is eventually entrained in the Gulf Stream (Churchill and Berger, 1998). We explore the issue of deployment bias in section 3b using synthetic drifters and conclude that it only affects the precise percentages rather than the general picture, and therefore the use of the box region is a reasonable tool.

On the other hand, of the many drifters that reached the Iceland Basin-Rockall Trough region, most originated in the western part of the subpolar gyre (Labrador and Irminger Seas) (Fig. 2.4B). Again, we cannot conclude that these drifters are tracking water parcels. A simple check of the temperatures recorded by these drifters (with an annual temperature cycle removed) shows a large increase from the Labrador Sea to the northeastern subpolar gyre, which cannot be supported by local air-sea heat fluxes which are neutral or cooling in the annual mean (not shown). Thus we see that drifters constrained to remain at the sea surface clearly cannot represent the three-dimensionality of convecting flow within the Labrador Sea or subducting flow as the currents exit this region of dense surface water.

The nearly complete separation between the gyres in terms of surface drifter trajectories contrasts with the certain connection in the upper ocean between the gyres, from decades of studies of dynamic topographies and meridional transport calculations based on hydrographic data, and with chemical tracers that suggest the connection. As noted in the introduction, the drifter separation is similar to the Lavender et al. (2000) result for subsurface floats at 1500 m in the Labrador Sea; floats exiting the Labrador Sea do not continue southward past

Flemish Cap to the Deep Western Boundary Current although tracers clearly show the connection.

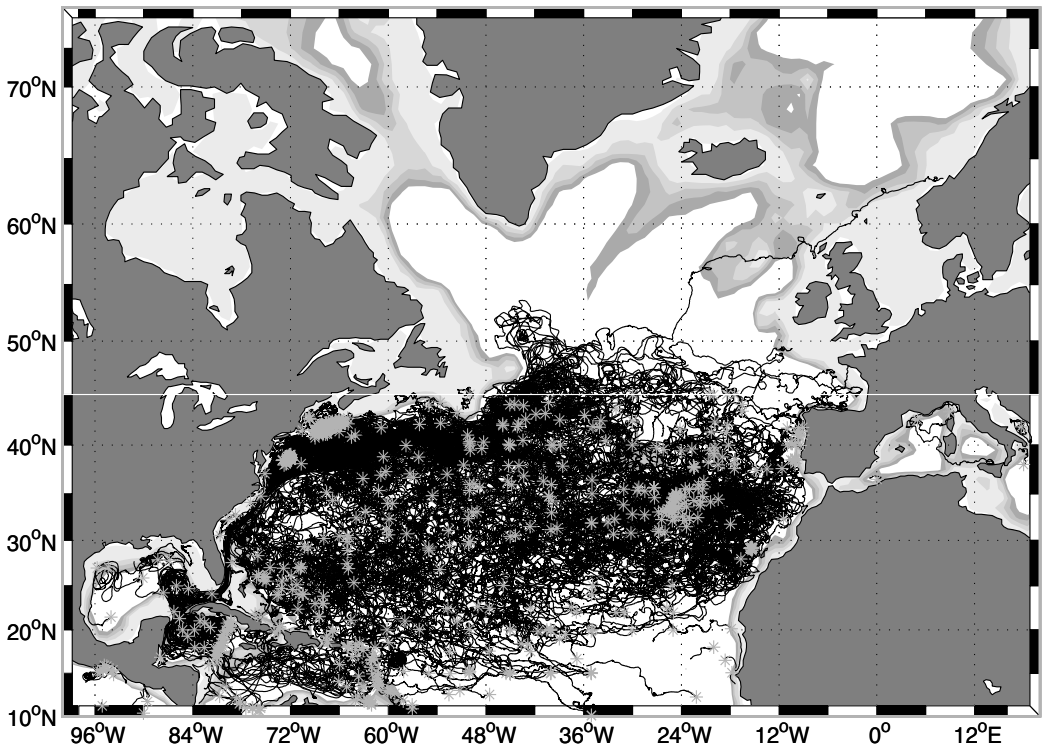

Figure 2.3: Trajectories of drifters deployed south of 45°N from 1990 to 2002. Gray asterisks are the deployment locations. The white line refers to 45°N. Topography is shaded in gray. The darkest contour is at 2000m. Contour interval is 500m.

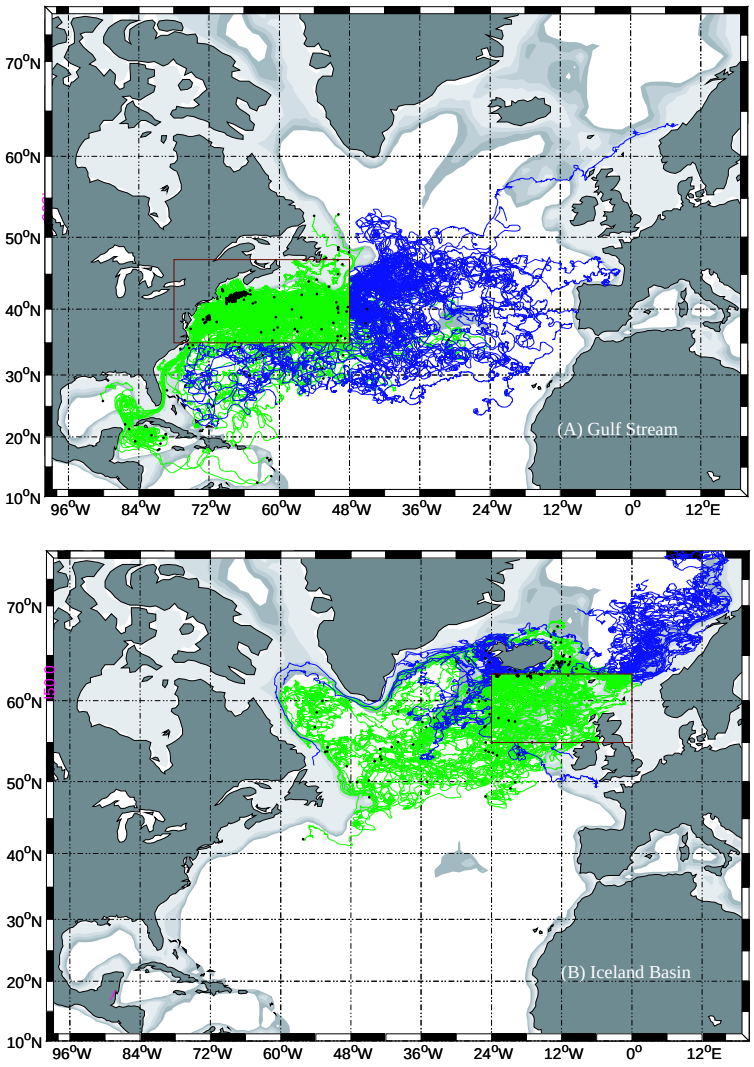

Figure 2.4: A) Surface drifter trajectories passing through the Gulf Stream-box (brown). B) Initial location of surface drifter trajectories passing through the Iceland Basin. Most of the drifters are coming from the west part of the subpolar gyre. For both panels, green trajectories are the drifters before and within the box; blue trajectories are the drifters after exiting the box. Black dots are the deployment locations. Topography is shaded in gray. The darkest contour is at 2000m. Contour interval is 500m.

b) LAGRANGIAN TRAJECTORIES USING SYNTHETIC DRIFTERS

Our observation of lack of connectivity of surface water from the subtropical to the subpolar gyre could be biased by the limited drifter lifetime of 271 days ± 260 days. Therefore, we conducted experiments with long-lived synthetic particles advected through the observed mean field (section 2.3.4) to test several potential sources of bias. Although the mean velocity field presented in Fig.2.2 suggests continuity between the Gulf Stream extension and the North Atlantic Current, artificial particles advected through the same mean do not reproduce the apparent continuity.

Of the 305 synthetic drifters (section 2.3.4) deployed in the Gulf Stream region on a regular grid with a 3-year lifetime, just 3 enter the subpolar gyre, while the rest remain in the subtropical gyre. When the synthetic drifters are deployed at the release locations of the actual drifters (272 drifters), 15 enter the subpolar gyre. (Results from the synthetic drifters advected through the observed mean velocity field and deployed at the release locations of the observed drifters are highly biased by the spatial inhomogeneity of their initial locations with respect to the coarse grid of the mean velocity field. Drifters deployed at very close locations will be advected by the same vector velocities; therefore the number of Lagrangian trajectories computed in this experiment overestimates the number of independent trajectories). Table 2.2 summarizes the number of the actual drifters and synthetic drifters, from the various runs, that enter the subpolar gyre.

We then added turbulent advection proportional to the observed error

ellipses to simulate the eddy field (section 2.3.4b), and conducted the same two synthetic drifter release experiments. Addition of the eddy field increased the number of synthetic drifters entering the subpolar gyre, to 18 (average) or 6% with a regular grid deployment in the GS box and to 7 (average) or 3% with a deployment at the actual drifter release locations in the GS box. This increase in connectivity was to be expected since eddies increase dispersion (Ozgokmen et al., 2000; Drijfhout et al., 2003; Tansley and Marshall, 2001), but the resulting gyre connectivity is still not overwhelming.

Thus, caution is necessary to interpret the appearance of the mean velocity field. In fact a northward flow between the two gyres, although indicated by northward transport from low to high latitudes observed using tracers, dynamic topographies and net transport calculations based on hydrography, is reflected in neither the observed nor the synthetic drifter trajectories, with and without eddy noise.

In the next section (2.5.2), we analyze the disagreement between the appearance of mean velocity field and the Lagrangian trajectories in terms of the Ekman velocity and eddies.

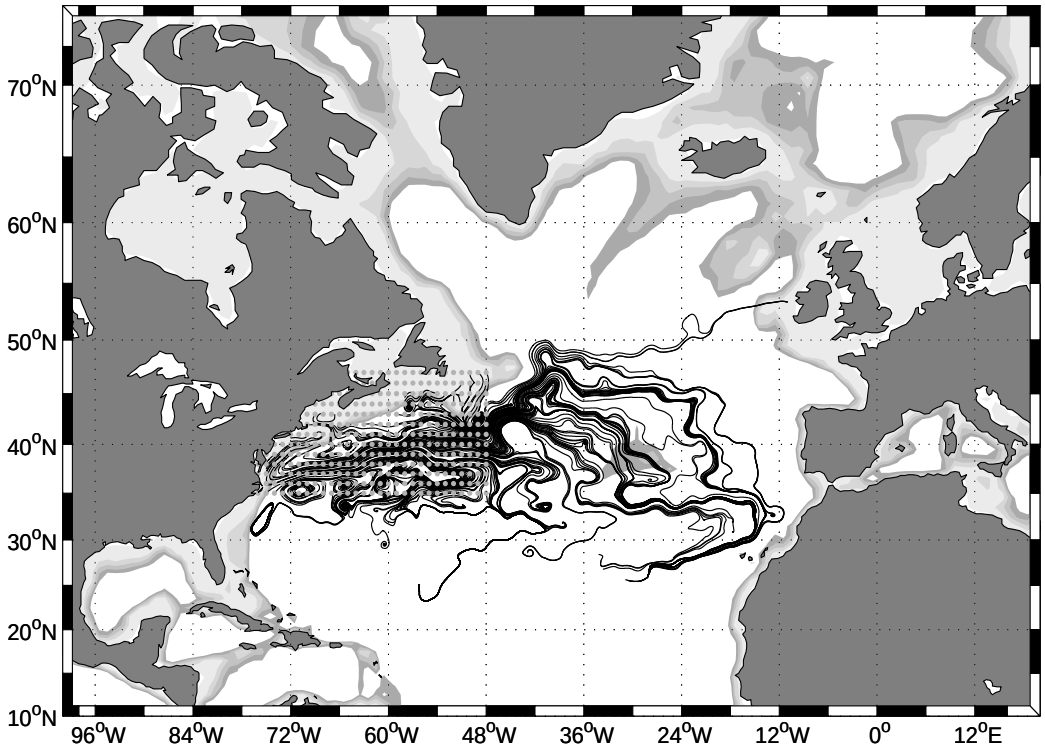

Figure 2.5: Advection of synthetic drifters through the observed total mean velocity field (Fig. 2.2). This allows an unlimited number of drifters and unlimited drifter lifetime. Total number of synthetic drifters: 305, with a life-time of 3 years. Drifters entering the subpolar gyre: 3. Gray dots are the deployment locations. Topography is shaded in gray. The darkest contour is at 2000m. Contour interval is 500m.

2.5 Causes for a low intergyre exchange experienced by drifters

To investigate possible causes for the low number of drifters that are crossing from the subtropical to the subpolar gyre, we check, first, if the drifter life time or the data set density bias the observations. We then examine how the Ekman velocity and eddies affect the drifter trajectories to see if their opposite impact can prevent the drifters from flowing northward. We reserve consideration of the three-dimensionality of the flow for a later study incorporating other data types and general circulation model results.

2.5.1 Sampling issues

We first examine the limitation of the drifter data in terms of the number of drifters available (drifter density space) and their life-time. The average drifter lifetimes are likely shorter than the time necessary to flow from the Gulf Stream region to the subpolar gyre.

a) DENSITY OF THE DATA SET

The spatial distribution is shown in Fig. 2.1 with density calculated in buoy-days per 0.5°squares; 296,365 total buoy-days are available from the drifters.

The spatial distribution of the drifters in the North Atlantic basin is not

Table 2.2: Summary of the actual drifters and all the synthetic drifter runs. The first column specifies the velocity field through which the artificial particles have been advected. The second column specifies the number of synthetic drifters that have been deployed and the scheme used for their release locations. The third column refers to the number of synthetic drifters and the respective percentage in the subpolar gyre. In all the advection experiments the drifter lifetime is 3 years. The high percentages of the synthetic drifters released in the deployment locations of the actual drifters advected through the observed mean velocity field (second and third row) are biases by the spatial inhomogeneity of their initial locations with respect to the coarse grid of the mean velocity field.

Velocity field	**Drifters released**	**Drifters enter the subpolar gyre**
Actual drifters	273	1 (0.3%)
Observed mean	272 (actual release location)	15 (6%)
Observed mean *without Ekman*	272 (actual release location)	24 (9%)
Observed mean *with turbulence*	272 (actual release location)	7 (3%)
Observed mean *with turbulence & without Ekman*	272 (actual release location)	23 (8%)
Observed mean	305 (regular grid)	3 (1%)
Observed mean *without Ekman*	305 (regular grid)	20 (6%)
Observed mean *with turbulence*	305 (regular grid)	18 (6%)
Observed mean *with turbulence & without Ekman*	305 (regular grid)	36 (12%)

homogeneous. Three locations have high density: the region just offshore of the west coast of Iceland, the region north of Cape Hatteras, and the region northwest of Africa. Many of the drifters were deployed in these regions, so high concentration is expected and is not related to any specific dynamic process. At 30°N there is another region where there is high drifter concentration, related to convergence in the basin (Garraffo et al., 2001a).

Poorly sampled regions are defined as those with less than 5 buoy-days inside the grid box, thus excluding grid boxes where drifter measurements are completely correlated. Fratantoni (2001) applied a similar criterion based on the correlation timescale to select for reliable data in his study, choosing a cutoff Lagrangian time scale of 10 days. However, five days exceeds the highest Lagrangian time scale (3.5 days) calculated for different subregions of the North Atlantic (section 2.A).

The regions of insufficient observations are shelf regions in the Nordic Seas, Labrador Sea, the water offshore Nova Scotia, and along the southeast coast of the U.S.; the shelf regions around France, Ireland, Britain and Norway; and some open ocean regions in the western Sargasso Sea, around 40°N-30°W, and along 50°N. The low drifter density south of 20°N is due to poor sampling, as noted by Lumpkin and Garzoli (2005). Since in this study we are focusing on the subtropical-subpolar flow, these undersampled regions are not a problem.

b) OBSERVED DRIFTER LIFE TIME

The other source of sampling error is drifter lifetime, as already discussed in section 2.4. The time necessary to flow from the Gulf Stream box to the Iceland Basin is order 400-500 days. This is based on the sole drifter that crossed the inter-gyre edge and on the average time that other drifters need to cover shorter distances. Drifters with shorter life time may not correctly represent the cross-gyre flow.

To estimate the impact of short drifter lifetime on our primary result, the actual drifter trajectories have been combined together into trajectories that last at least 600 days, slightly longer than the 400-500 days mentioned before. To obtain 600-day trajectories, we do the following: *a*) remove the seasonal cycle of temperature from each drifter's temperature record; *b*) assign a box of fixed dimension (connection area) for each drifter; *c*) identify the closest drifter to the center of the connection area and join it to the previous drifter if it satisfies the following temperature criteria.

We do not wish to join trajectories of drifters that are sampling very different water masses. As a crude criterion, we therefore require that the temperatures of the joined drifters not differ greatly from each other. We first remove the seasonal temperature cycle calculated at each geographical location of the drifters using the World Ocean Atlas 1994 (Levitus94). We then join the

"original drifter" to the "joining drifter" if:

$$|T_{orig} - T_{join}| < |\Delta T|_{max} \tag{2.5}$$

where T_{orig} is the temperature of the "original drifter" at its last known position, and T_{join} is the temperature of the "joining drifter" at the "joining location". $|\Delta T|_{max}$ is the maximum of the absolute value of temperature difference between the location of the two drifters calculated from the mean temperature field:

$$|\Delta T|_{max} = |(T_{mean} \pm \sigma)_{orig} - (T_{mean} \pm \sigma)_{join}|_{max} \tag{2.6}$$

where $(T_{mean} \pm \sigma)_{orig}$ is the mean temperature at the location of the "original drifter" with its standard deviation, and $(T_{mean} \pm \sigma)_{join}$ is the mean temperature at the location of the "joining drifter" with its standard deviation. The difference of temperature has been calculated from the mean temperature field (without the seasonal cycle) computed with the binning technique (1°× 1°and 0.5°× 0.5°) from the drifter dataset. The maximum takes into account the error associated with each mean temperature value.

In addition to this criterion, another constraint is applied in the drifter connection computation. The temperature distribution for the entire North Atlantic is bimodal (Fig. 2.6). The colder peak comes from the subpolar gyre and the warmer from the subtropical gyre. This suggests that criterion (2.5) could fail in some regions, since the mean might not be significant. This might be most evident where subtropical and subpolar waters meet, for instance in the region south and east of Newfoundland. To examine the temperature distribution in limited geographical areas, the region between 45°and 55°N has been divided into

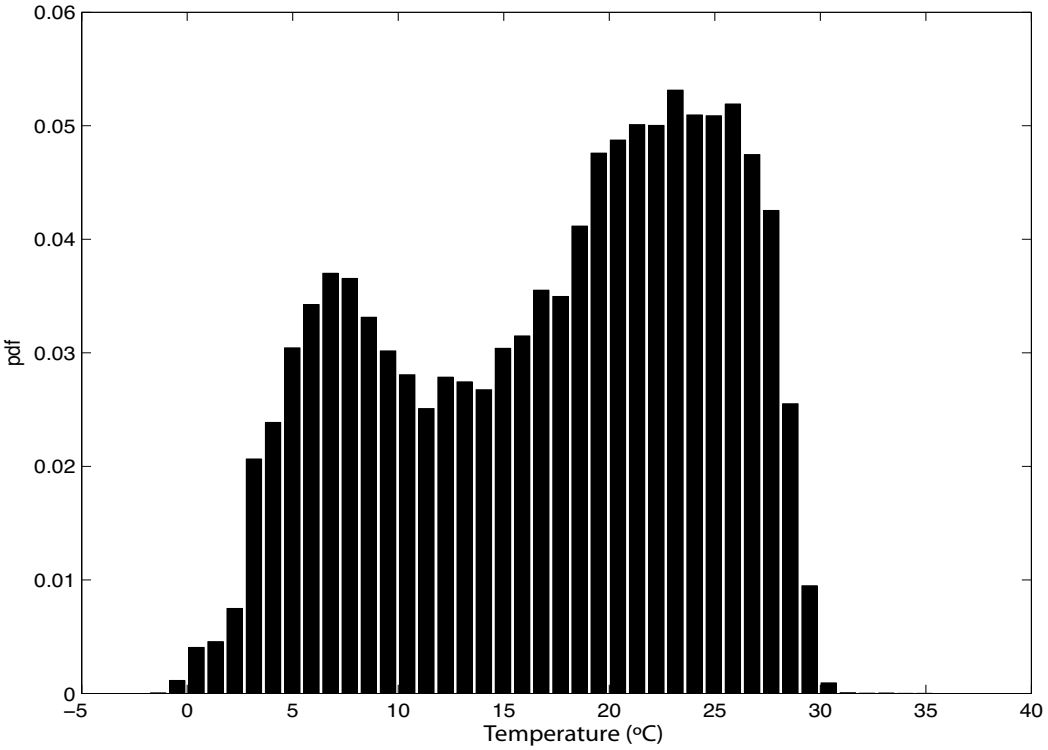

Figure 2.6: Probability density function of the surface temperature in the North Atlantic basin using drifter temperatures. The peak at lower temperature arises from the subpolar gyre; the peak at higher temperature arises from the subtropical gyre.

a regular 1°grid. In the event of bimodal distribution in a given grid box, the temperatures of the two peaks and their standard deviations have been noted. The two modes of the distribution are identified fitting an analytical function to the temperature distribution:

$$f(x)_{fit} = A_1 e^{-\frac{(x-a_1)^2}{2b_1^2}} + A_2 e^{-\frac{(x-a_2)^2}{2b_2^2}} \tag{2.7}$$

The two maxima and their standard deviations are obtained by the coefficient of the function ($a_{1,2}$,$b_{1,2}$). In case the last known position falls in a box with a bimodal temperature distribution, the following procedure is adopted: first the temperature of the last known position is noted to determine if the drifter comes from a warm or cold water mass. Then, the temperature of the "joining drifter" is required to belong to the same mode of the distribution.

Data sets with 600-day composite trajectories were formed for both 1°and 0.5°squares (size of connection area) (Fig. 2.7). For 1°squares, 60% of the Gulf Stream drifters could be extended to 600-day trajectories. For 0.5°squares, this percentage was 58%. The similarity between the percentage of 600-day trajectories with different size of connection area suggests that reduction to the 0.5°grid still provides adequate data density. For 1°(0.5°) squares, 15% (20%) could not be joined because there were no drifters passing through the connection area, while 20% (19%) could not be joined because of the temperature requirement. The other connection failure is due to drifters that exit the study domain.

With extended drifter trajectories joined in 0.5°squares the percentage of drifters that flow from the Gulf Stream-box to the subpolar gyre increases to 4%.

With 1°squares, 5% enter the subpolar gyre. This suggests that the solitary actual drifter that crossed the inter-gyre edge underestimates the total number of drifters that would be carried by the Gulf Stream to the subpolar gyre given much longer drifter lifetimes.

c) SYNTHETIC DRIFTER LIFE TIME

Synthetic drifter trajectories can also provide information on the importance of lifetime in biasing the observations of cross-gyre connections. In section 2.4b, synthetic tracks were computed using the observed mean velocity field and a "mean-advection" model (section 2.3.4a). Synthetic drifters calculated with the "mean-advection" model have been set to last 3 years (1095 days), which should be sufficient for cross-gyre flow. Despite the long life time, the number of drifters flowing into the subpolar gyre (Fig. 2.5) is very low: only 3 synthetic drifters cross the inter-gyre edge.

The low number of synthetic drifters in the subpolar gyre, despite the long lifetime, is confirmed by synthetic drifters advected through the mean velocity field with a turbulent component added to it (section 2.3.4b). When the synthetic drifters are released on a regular grid, an average of 18 (5%) reach the subpolar gyre. When the synthetic drifters are deployed at the release locations of the actual drifters, an average of 7 drifters (3%) flow north into the subpolar gyre. This confirms the result obtained in section 2.5.1b. Hence, drifter lifetime biases the observations, underestimating the Lagrangian trajectories that cross the intergyre

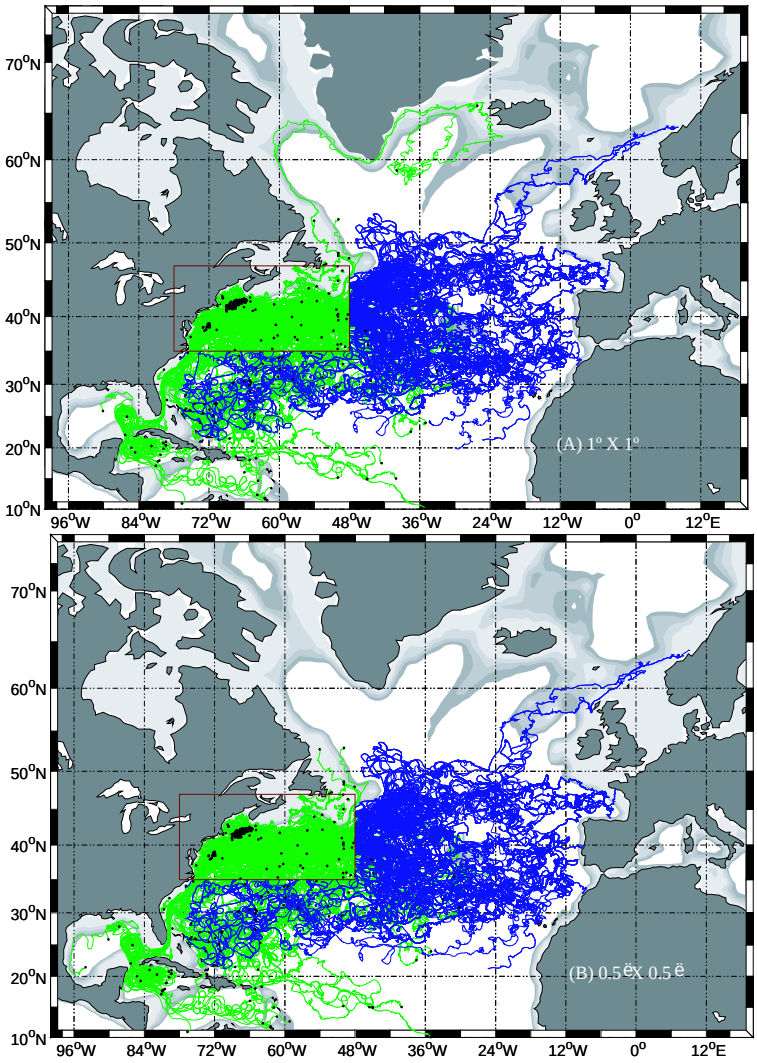

Figure 2.7: 600-day combined trajectories (section 2.5.1b). Green trajectories are the drifters before and within the Gulf Stream-box; blue trajectories are the drifters after exiting the box. Black dots are the deployment locations. Topography is shaded in gray. The darkest contour is at 2000m. Contour interval is 500m. (a) Using a connection area of 1°× 1°; 5% of the connected trajectories cross into the subpolar gyre. (b) Using a connection area of 0.5°× 0.5°; 4% enter the subpolar gyre.

boundary.

2.5.2 Ekman velocity bias and effects of eddies

The Ekman velocity is another possible source of bias for the representation of the cross-gyre flow by surface drifters. Figure 2.8 shows the mean Ekman velocity field in the North Atlantic from the winds observed simultaneously with the surface drifter observations, then using the Ralph-Niiler model (section 2.3.1). The computation presented here agrees with the mean Ekman velocity field described in Flatau et al. (2003). The average Ekman speed is order 1 cm/s, as reported in Flatau et al. (2003). Although Ekman is a small fraction of the total velocity of the drifters, it could still significantly affect the drifter trajectories, acting as a southward forcing that prevents the drifters from crossing to the north.

To address the effect of the Ekman component and eddies we use synthetic drifters (section 2.3.4) propagated through various components of the same observed mean velocity field. The Ekman component and the turbulent component are removed or added to the observed mean velocity field to obtain 4 different sets of synthetic drifters that are, then, compared.

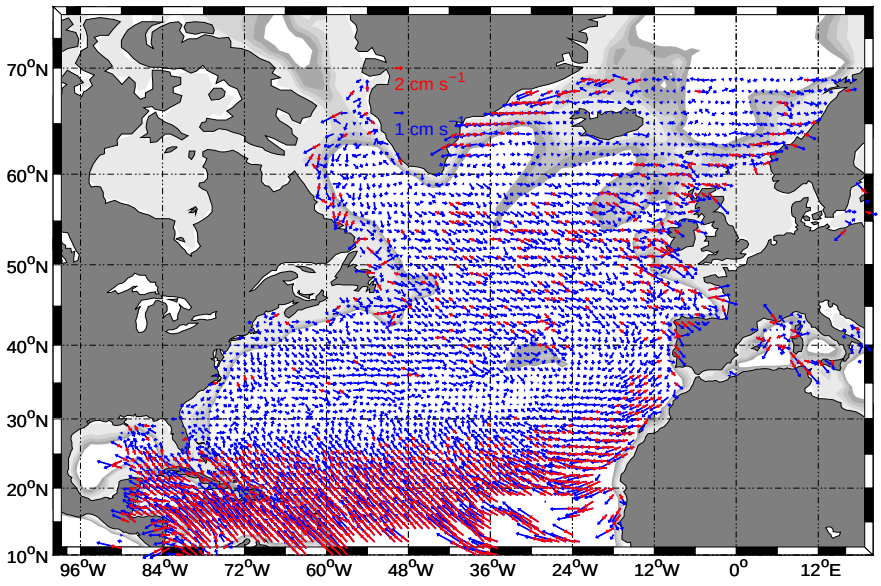

Figure 2.8: Mean Ekman velocity field in 1°×1° calculated from wind data. Red arrows are velocity > 2 cm/s. Topography is shaded in gray. The darkest contour is at 2000m. Contour interval is 500m.

a) ADVECTION EXPERIMENT THROUGH THE MEAN VELOCITY FIELD

Synthetic drifters advected through the simple observed mean velocity field were introduced in section 2.4a to highlight the visually misleading continuity between the subtropical and subpolar gyres and to consider the influence of limited drifter lifetime on the gyre connection.

Here, we compare synthetic trajectories advected through the mean velocity field in which the Ekman component is retained and synthetic trajectories computed through the same mean field from which the Ekman component has been removed (Fig.2.9). As shown previously (section 2.4b), only 3 synthetic drifters (1% of 305) cross into the subpolar gyre when we use the total mean which includes the Ekman component.

When Ekman is removed, more drifters move north in the North Atlantic Current with 20 (6%) reaching the subpolar gyre.

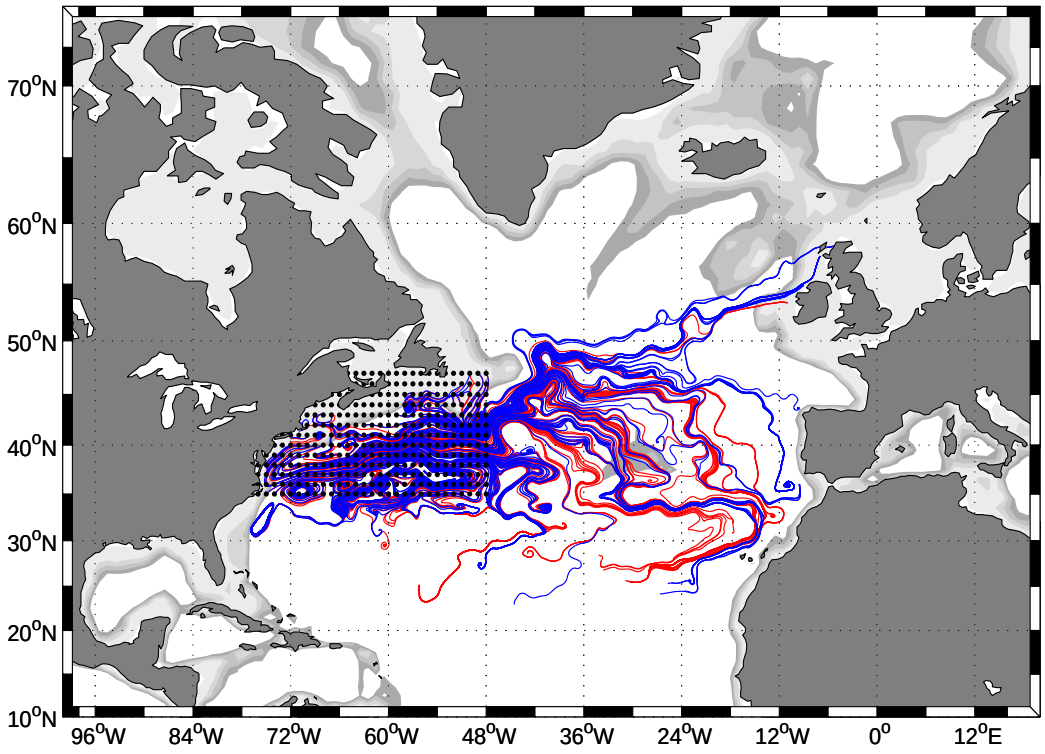

Figure 2.9: Advection of synthetic drifters through the observed mean velocity field. Red: trajectories advected through the total mean velocity field (already shown in fig. 2.5). Drifters entering the subpolar gyre = 3. Blue: trajectories advected through the mean velocity field without the Ekman component. Drifters entering the subpolar gyre = 20. In both cases (red and blue) the total number of synthetic drifters is 305, with a lifetime of 3 years. Black dots are the synthetic drifter deployment locations. Topography is shaded in gray. The darkest contour is at 2000m. Contour interval is 500m.

b) ADVECTION EXPERIMENT INCLUDING TURBULENCE

The actual oceanic velocity field includes an eddy field, which can be thought of as random turbulence added to the mean. Cross-gyre transport should be augmented by turbulence (Bower, 1991; Berloff et al., 2002), which is normally associated with dispersion about the mean.

As already described (section 2.3.4b), the turbulence is parameterized by a random value added at each time step based on the velocity variance at each grid box. Since the addition of a random impulse makes each model run unique, the numerical experiments have been repeated several times. We ran the "turbulent-advection" model 9 times retaining the Ekman component (Fig.2.5.2a), and 9 times removing Ekman (Fig.2.5.2b). The reported fraction of drifters that enter the subpolar gyre is the average of the runs.

The results are that 6% of the synthetic drifters in the "turbulent-advection" model with the total mean velocity reach the Iceland Basin-Rockall Trough region. When the Ekman component is removed, 12% of synthetic drifters flow northward.

These results lead to two separate conclusions. The synthetic drifter runs, with and without turbulence, show that removal of Ekman velocity increases by up to 5-6% the number of drifters crossing to the subpolar gyre. Likewise and separately, addition of a turbulent component, with and without Ekman, increases by up to 5-6% the number of drifters reaching the subpolar gyre.

Thus the Ekman velocity and eddies counteract each other in this region,

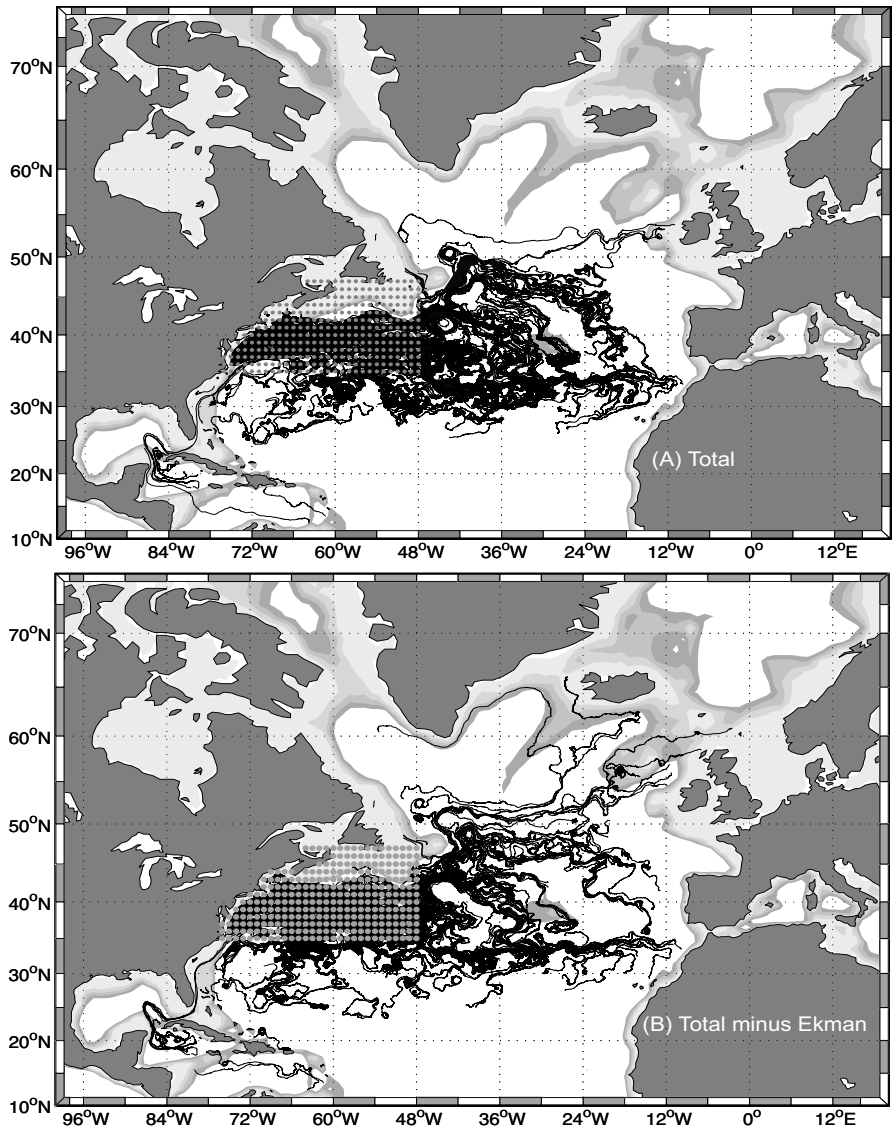

Figure 2.10: Synthetic drifters advected through the mean velocity field with random turbulence added to it. In both cases the number of synthetic drifters is 305 with a lifetime of 3 years. Gray dots are the deployment locations. Topography is shaded in gray. The darkest contour is at 2000m. Contour interval is 500m. (a) Synthetic drifters advected through the total mean with random turbulence. Average of drifters entering the subpolar gyre:18. (b) Synthetic drifters advected through the mean velocity field after removing the Ekman component. Random turbulence is added to the mean. Average of drifters entering the subpolar gyre: 36.

in agreement with the model study by Drijfhout et al. (2003). The opposite impact of the two processes is of course not dynamical, but is an artifact of the location of the study area in a region of southward Ekman transport. Eddy noise itself always increases dispersion, and therefore results in increased leakage to the subpolar gyre of drifters released in the subtropical gyre. It is though notable that in our study as well as in Drijfhout et al. (2003), the two effects are of the same order of magnitude.

2.6 Summary and conclusion

In this paper we described the surface drifter exchange between the subtropical and subpolar gyres in the North Atlantic. Surface drifters deployed in the subtropical gyre mostly recirculate within the gyre. Just one drifter in this twelve-year data set crossed from the subtropical gyre northward into the subpolar gyre, which was surprising given the known connectivity between the gyres based on many decades of hydrographic and tracer analyses.

The steps that we have taken to understand the observed separation between subtropical and subpolar drifters led us to the following conclusions. (1) Limited drifter lifetime results in an underestimate of the northward flux, based on constructing 600-day trajectories from the actual drifter data. With the extended trajectories the number of drifters from the GS area to the subpolar gyre increases from 1% to 5%. (Drifter density was judged to be sufficient based on the Lagrangian time scale of the drifters presented in section 2.A and in a number

of previous works.) (2) The mean flow observed by the surface drifters, which includes the Ekman component, does not produce synthetic drifter trajectories that cross from the subtropical to the subpolar gyre, even with long synthetic drifter lifetimes. (3) The Ekman component of the flow counteracts the turbulent component, preventing the drifters from crossing the inter-gyre edge. Using a basic advection model, the percentage of synthetic drifters flowing from the subtropical to the subpolar gyre increases by up 5-6% when the Ekman component is removed from the mean velocity field. On the other hand, the number of synthetic drifters in the subpolar gyre advected through the observed mean velocity field to which a turbulent component has been added increases by up 5-6%.

We conclude that sampling bias and Ekman velocity contribute to the drifter separation between the subtropical and subpolar gyre in the North Atlantic, while turbulent eddies act to increase the connectivity. The Ekman and turbulent contributions are of the same order of magnitude. Therefore, if one had Lagrangian drifters in the upper ocean but below the Ekman layer, one might expect somewhat more connectivity, on the order of 5-6% of the drifters. This is still well below the 20% or so of the upper Gulf Stream that should move to the subpolar gyre as part of the meridional overturning circulation. We are in the process of exploring the role of the three dimensionality of the flow using particle tracing in general circulation models; this is expected to yield the rest of the connecting flow.

Chapter 2, in full, is a reprint of the material as it appears in:

Brambilla, E., L. D. Talley (2006), Surface drifter exchange between the North Atlantic subtropical and subpolar gyres, J. Geophys. Res., 111, C07026, doi:10.1029/2005JC003146. The dissertation author was the primary investigator and author of this paper.

2.A Appendix: Lagrangian time scale

The computation of the Lagrangian time scale follows the procedure described in many previous studies (Garraffo et al., 2001a; Zhang et al., 2001; McClean et al., 2002; Lumpkin et al., 2002). The Lagrangian time scale in the North Atlantic from surface drifters represents the interval in time in which the velocity of the drifters are strongly correlated. In order to calculate it from the 15-m drogued drifters, we divided each drifter track in segments of 50 days, to exclude any correlation of drifter velocity over a time longer than 50 days. For each segment the autocorrelation function has been calculated

$$C_{1,2}(\tau) = \frac{1}{\sigma^2_{1,2}} R_{1,2}(\tau) \tag{2.A.1}$$

where $\sigma^2_{1,2}$ is the variance and $R_{1,2}$ is the Lagrangian temporal autocovariance function, computed for each component as :

$$R_{1,2}(\tau) =< (u_{1,2}(t) - \overline{u_{1,2}}(t))(u_{1,2}(t+\tau) - \overline{u_{1,2}}(t) > \tag{2.A.2}$$

where $<>$ indicates expected values, $\overline{u}$ is the mean velocity component in the drifter segment and τ is the time lag. The indices 1,2 refer to the meridional and zonal components. After calculating the average of the autocorrelation function

from the segments, the Lagrangian time scale is :

$$T_{L1,2} = \int_0^{\infty} C_{1,2}(\tau) d\tau \tag{2.A.3}$$

where $C(\tau)$ is the autocorrelation function. Due to the impossibility of extending the integral in (2.A.3) to ∞, following the general practice suggested by other calculations (Böning, 1988), (2.A.3) is simplified to:

$$T_{L1,2} = \int_0^{\tau_0} C_{1,2}(\tau) d\tau \tag{2.A.4}$$

where τ_0 is the first zero crossing of the autocorrelation function. The choice of the first zero crossing is also justified by the fact that the autocorrelation function tends to be dominated by noise for large lags (Lumpkin et al., 2002).

Although the Lagrangian time scale from surface drifters has been calculated in different subregions of the North Atlantic, the value T_L that has been used to calculate the trajectory of the synthetic drifters is constant in space and corresponds to the T_L in the Gulf Stream and North Atlantic Current region. For the meridional component we found $T_L = 1.5$ days; for the zonal component we found $T_L = 2.5$. These are consistent with the previous studies here cited.

References

Berloff, P. S., McWilliams, J. C., and Bracco, A., 2002: Material transport in oceanic gyres. Part I: Phenomenology. *J. Phys. Oceanogr.*, **32**(3), 764–796.

Böning, C., 1988: Characteristics of particle dispersion in the North Atlantic: An alternative interpretation of SOFAR float results. *Deep-Sea Res.*, **35**, 1379–1385.

Bower, A. S., 1991: A simple kinematic mechanics for mixing fluid particles across a meandering jet. *J. Phys. Oceanogr.*, **21**, 173–180.

Bower, A. S., and Rossby, H. T., 1989: Evidence of cross-frontal exchange processes in the gulf stream based on isopycnal rafos float data. *J. Phys. Oceanogr.*, **19**, 1177–1190.

Castellari, S., Griffa, A., Ozgokmen, T. M., and Poulain, P.-M., 2001: Prediction of particle trajectories in the Adriatic Sea using Lagrangian data assimilation. *J. Mar. Sys.*, **29**, 33–57.

Churchill, J. H., and Berger, T. J., 1998: Transport of Middle Atlantic Bight shelf water to the Gulf Stream near Cape Hatteras. *J. Geophys. Res.*, **103**(C13), 30605–30621.

Drijfhout, S. S., de Vries, P., Döös, K., and Coward, A. C., 2003: Impact of eddy-induced transport on the Lagrangian structure of the upper branch of the thermohaline circulation. *J. Phys. Oceanogr.*, **33**, 2141–2155.

Dutkiewicz, S., Griffa, A., and Olson, D. B., 1993: Particle diffusion in a meandering jet. *J. Geophys. Res.*, **98**, 16487–16500.

Falco, P., Griffa, A., Poulain, A., Poulain, P.-M., and Zambianchi, E., 2000: Transport properties in the Adriatic Sea deduced from drifter data. *J. Phys. Oceanogr.*, **30**, 2055–2071.

Flatau, M. K., Talley, L. D., and Niiler, P. P., 2003: The North Atlantic Oscillation, surface current velocities and SST changes in the subpolar North Atlantic. *J. Clim,*, **16**, 2355–2369.

Fratantoni, D. M., 2001: North Atlantic surface circulation during the 1990s observed with satellite-tracked drifters. *J. Geophys. Res.*, **106**(C10), 22067–22093.

Ganachaud, A., 2003: Large-scale mass transports, water mass formation, and diffusivities estimated from World Ocean Circulation Experiment (WOCE) hydrographic data. *J. Geophys. Res.*, **108**(C7), 3213. doi: 10.1029/2002JC001565.

Ganachaud, A., and Wunsch, C., 2003: Large-scale ocean heat and freshwater transports during the World Ocean Circulation Experiment. *J. Clim,*, **16**, 696–705.

Garraffo, Z. D., Mariano, A. J., Griffa, A., Veneziani, C., and Chasignet, E. P., 2001a: Lagrangian data in a high-resolution numerical simulation of the North Atlantic I. Comparison with in situ drifter data. *J. Mar. System*, **29**, 157–176.

Garraffo, Z. D., Mariano, A. J., Griffa, A., Veneziani, C., and Chasignet, E. P., 2001b: Lagrangian data in a high-resolution numerical simulation of the North Atlantic II. On the pseudo-Eulerian averaging of Lagrangian data. *J. Mar. System*, **29**, 177–200.

Gordon, A. L., 1986: Interocean exchange of thermocline water. *J. Geophys. Res.*, **91**, 5037–5046.

Griffa, A., 1996: Applications of stochastic particle models to oceanographic problems. *Stochastic Modelling in Physical Oceanography*, **24**, 467pp. R. Adler, P. Muller, and B. Rozovskii, Eds., Birkhauser.

Hall, M. M., and Bryden, H. L., 1982: Direct estimates and mechanism of ocean heat transport. *Deep-Sea Res.*, **29**, 339–359.

Koltermann, K. P., Sokov, A. V., Tereschenkov, V. P., Dobroliubov, S. A., Lorbacher, K., and Sy, A., 1999: Decadal changes in the thermohaline circulation of the North Atlantic. *Deep- Sea Res.*, **46**, 109–138.

Lavender, K. L., Davis, R. E., and Owens, W. B., 2000: Mid-depth recirculation observed in the interior Labrador and Irminger seas by direct velocity measurements. *Nature*, **407**, 66–69.

Liu, Z., and Yang, H., 1994: The intergyre chaotic transport. *J. Phys. Oceanogr.*, **24**, 1768–1782.

Lozier, M. S., and Gawarkiewicz, G., 2001: Cross-frontal exchange in the Middle Atlantic Bight as evidenced by surface drifters. *J. Phys. Oceanogr.*, **31**, 2498–2510.

Lozier, M. S., and Riser, S. C., 1990: Potential vorticity sources and sinks in a quasi-geostrophic ocean: beyond western boundary currents. *J. Phys. Oceanogr.*, **20**, 1608–1627.

Lumpkin, R., 2003: Decomposition of surface drifter observations in the Atlantic Ocean. *Geophys. Res. Lett.*, **30**(14), 1753. doi:10.1029/2003GL017519.

Lumpkin, R., and Garzoli, S., 2005: Near surface circulation in the Tropical Atlantic Ocean. *Deep-Sea Res. I*, **52**, 495–518.

Lumpkin, R., and Speer, K., 2003: Large-scale vertical and horizontal circulation in the North Atlantic Ocean. *J. Phys. Oceanogr.*, **33**, 1902–1920.

Lumpkin, R., Treguier, A. M., and Speer, K., 2002: Lagrangian eddy scales in the North Atlantic Ocean. *J. Phys. Oceanogr.*, **32**, 2425–2440.

Macdonald, A. M., 1998: The global ocean circulation: A hydrographic estimate and regional analysis. *Prog. Oceanogr.*, **41**, 281–382.

McCartney, M. S., and Talley, L. D., 1982: The Subpolar Mode Water of the North Atlantic. *J. Phys. Oceanogr.*, **12**, 1169–1188.

McClean, J. L., Poulain, P.-M., Pelton, J. W., and Maltrud, M. E., 2002: Eulerian and Lagrangian statistics from surface drifters and a high-resolution POP simulation in the North Atlantic. *J. Phys. Oceanogr.*, **32**, 2472–2491.

Niiler, P. P., 1995: Measurements of the water-following capability of holey-sock and TRISTAR drifters. *Deep-Sea Res I*, **42**, 1951–1964.

Niiler, P. P., Maximenko, N. A., and McWilliams, J. C., 2003: Dynamically balanced absolute sea level of the global ocean derived from near-surface velocity observations. *Geophys. Res. Lett.*, **30**(22), 2168. doi:10.1029/2003GL018628.

O'Connor, B. M., Fine, R. A., Maillet, K. A., and Olson, D. B., 2002: Formation rates of subtropical underwater in the Pacific Ocean. *Deep-Sea Res. I*, **49**, 1571–1590.

Owens, W. B., 1984: A synoptic and statistical description of the Gulf Stream and subtropical gyre using SOFAR floats. *J. Phys. Oceanogr.*, **14**, 104–113.

Ozgokmen, T. M., Griffa, A., Mariano, A. J., and Piterbarg, L. I., 2000: On the predictability of Lagrangian trajectories in the ocean. *J. Atms. Oceanic Technol.*, **17**, 366–383.

Pazan, S. E., and Niiler, P. P., 2001: Recovery of near-surface velocity from undrogued drifters. *J. Atmos. Technol.*, **18**, 476–489.

Poulain, P. M., Warn-Varnas, A., and Niiler, P. P., 1996: Near-surface circulation of the Nordic seas as measured by Lagrangian drifters. *J. Geophys. Res.*, **101**, 18,237–18,258.

Pratt, J. L., Lozier, M. S., and Beliakova, N., 1995: Parcel trajectories in quasigeostrophic jets: Neutral models. *J. Phys. Oceanogr.*, **22**, 431–440.

Qiu, B., and Huang, R. X., 1995: Ventilation of the North Atlantic and North Pacific: Subduction versus obduction. *J. Phys. Oceanogr.*, **8**, 2374–2390.

Ralph, E., and Niiler, P. P., 1999: Wind-driven currents in the tropical Pacific. *J. Phys. Oceanogr.*, **29**, 2121–2129.

Reid, J. L., 1994: On the total geostrophic circulation of the North Atlantic Ocean: Flow patterns, tracers and transports. *Prog. Oceanogr.*, **33**, 1–92.

Reverdin, G., Niiler, P. P., and Valdimarsson, H., 2003: North Atlantic Ocean surface currents. *J. Geophys. Res.*, **108**(C1), 3002. doi:10.1029/2001JC00102.

Richardson, P. L., and Schmitz, W. J., 1993: Deep cross-equatorial flow in the Atlantic measured with SOFAR floats. *J. Geophys. Res.*, **98**(C5), 8371–8387.

Roemmich, D., and Wunsch, C., 1985: Two translatantic sections: meridional circulation and heat flux in the subtropical North Atlantic Ocean. *Deep-Sea Res.*, **32**, 619–664.

Rossby, T., 1996: The North Atlantic Current and surrounding waters: at the crossroads. *Rev. Geophys.*, **34**, 463–481.

Schmitz, W. J., and McCartney, M. S., 1993: On the North Atlantic circulation. *Rev. Geophys.*, **31**, 29–49.

Sybrandy, A. L., and Niiler, P. P., 1991: WOCE/TOGA Lagrangian drifter constructin manual. *SIO Ref. 9/16, WOCE Rep. 63*, 58pp.

Talley, L. D., Reid, J. L., and Robbins, P. E., 2003: Data-based meridional overturning streamfunctions for the global ocean. *J. Clim.*, **16**, 3213–3226.

Tansley, C. E., and Marshall, D. P., 2001: On the dynamics of wind-driven circumpolar currents. *J. Phys. Oceanogr.*, **31**, 3258–3273.

Thomson, D. J., 1987: Criteria for the selection of stochastic models of particle trajectories in turbulent flows. *J. Fluid Mech.*, **180**, 529–556.

Yang, H., 1996: The subtropical/subpolar gyre exchange in the presence of annually migrating wind and a meandering jet: water mass exchange. *J. Phys. Oceanogr.*, **26**, 115–130.

Zhang, H. M., Prater, M. D., and Rossby, T., 2001: Isopycnal Lagrangian statistics from the North Atlantic Current RAFOS float observations. *J. Geophys. Res.*, **106**, 13817–13836.

3

Subpolar Mode Water in the northeastern Atlantic. Part I: properties and circulation

3.1 Conspectus

Subpolar Mode Waters (SPMW) in the eastern North Atlantic subpolar gyre are investigated with hydrographic and Lagrangian data (surface drifters and isopycnal floats). Using historical hydrographic data from 1900 to 1990 and 6 hydrographic sections from the World Ocean Circulation Experiment (WOCE), we observe that SPMWs are surface water masses with nearly uniform properties that remain confined between the ocean surface and the permanent pycnocline. SPMWs represented by densities $27.3\sigma_\theta$, $27.4\sigma_\theta$, and $27.5\sigma_\theta$ are present in the eastern subpolar gyre and are influenced by the topography and the circulation

of the region. Construction of an absolute surface streamfunction from surface drifters shows that SPMWs are found along each of the several branches of the NAC, and their density increases gradually downstream along each branch. The Iceland Basin and Rockall Trough branches of the NAC are both characterized by the $27.3\sigma_\theta$, $27.4\sigma_\theta$, and $27.5\sigma_\theta$ SPMWs. A large pool of $27.5\sigma_\theta$ SPMW is also found on the eastern flank of the Reykjanes Ridge, with temperature and salinity that indicates that it is separated from $27.5\sigma_\theta$ SPMW found on the Iceland-Faroe Ridge. Since the branches of the NAC have a dominant northeastward direction, the newly observed distribution of SPMW combined with the new streamfunction calculation modify the original hypothesis of McCartney and Talley (1982) of a smooth cyclonic pathway for SPMW advection and density increase around the subpolar gyre.

3.2 Introduction

Subpolar Mode Waters are the near surface water masses of the subpolar North Atlantic characterized by thick layers of nearly uniform properties (temperature, salinity, density) (McCartney and Talley, 1982). Masuzawa (1969) first defined mode waters in the context of the North Pacific Subtropical Mode Water with its large volume of water with nearly uniform temperature of 16°-18°C. "Mode Water" is now broadly used to describe a large number of water masses with nearly uniform properties (density, temperature, salinity) (Hanawa

and Talley, 2001). The original description of SPMW by McCartney and Talley (1982) has been partially revised by more recent studies (e.g. Talley, 1999; Read, 2001). Here and in an accompanying paper (Brambilla and Talley, submitted), we present a new analysis of SPMW in the northeastern Atlantic, highlighting the link between the SPMWs and the predominantly northeastward circulation of the region. The most significant addition to the earlier studies is an analysis of the circulation, using Lagrangian data in conjunction with hydrographic data.

SPMWs have long been the object of particular attention due to their important role in the transfer of warm and salty North Atlantic water from the subtropical gyre to the Nordic Seas and Labrador Sea. McCartney and Talley (1982), in their original description of SPMWs, suggested that SPMWs, formed during late winter convection, follow the cyclonic circulation of the subpolar gyre, gradually increasing their density due to buoyancy loss caused by cooling along the path. The final products of this gradual transformation are the Labrador Sea Water and the dense water masses formed in the Nordic Seas. Thus, SPMWs are the primary water masses that participate in the upper flow of the overturning circulation and provide the water that is eventually transformed into the several components of North Atlantic Deep Water (NADW) (e.g. McCartney and Talley, 1982; McCartney and Talley, 1984; Schmitz and McCartney, 1993; McCartney and Mauritzen, 2001).

The interest in SPMW studies is also driven by the fact that these particular water masses may play a crucial role in the still-unresolved controversy about feedback between the subpolar gyre and the atmosphere (Hanawa and Talley,

2001). Because of their large volume and their nearly uniform temperature, mode waters represent in general a near-surface reservoir of heat that is slowly released back to the atmosphere and might influence the global atmospheric circulation (Kwon and Riser, 2004).

Schmitz and McCartney (1993) synthesized prior studies, reporting that SPMWs carry 5 Sv (1 $Sv = 10^6 m^3 s^{-1}$) into the Nordic Seas across the Iceland-Faroe Ridge and the Denmark Strait. In addition, 7 Sv of dense water sinks in the Labrador Sea that is replenished by the SPMW from the subpolar gyre. Bersch (1995), calculating the volume transport across a hydrographic section (WOCE A1/AR7E) from Cape Farvel (southern tip of Greenland) to Porcupine Bank (offshore Ireland), computed a similar balance between the SPMW that circulates in the upper layer of the subpolar gyre and the LSW formed in the Labrador Sea.

Talley (1999), on the other hand, raised some doubts about the concept of a complete cyclonic flow of SPMWs around the subpolar gyre feeding the LSW. The Subarctic Front flows northward east of Iceland, feeding the Iceland-Faroe Front and the Norwegian Current (e.g Flatau et al., 2003). SPMWs east of the Subarctic Front do not appear to connect to SPMWs west of the front, contrary to McCartney and Talley's 1982) hypothesis. The lighter SPMWs are located in the southeastern part of the basin (Rockall Trough) where the surface circulation is directed northeastward, connecting the Atlantic water to the Norwegian Current (Orvik and Niiler, 2002; Orvik and Skagseth, 2003), hence making difficult the link between this mode water and denser ones on the Reykjanes Ridge (Perez-Brunius et al., 2004). On the other hand, at subsurface depths, the circulation is cyclonic on

shoaling isopycnals (Bower et al., 2002), possibly permitting a connection between water from the Subarctic Front and the denser SPMW on the Reykjanes Ridge.

Read (2001) identified SPMWs in the eastern subpolar gyre from hydrographic data collected during the CONVEX-91 survey (2 hydrographic sections between Greenland and Ireland). Light SPMW was found in the eastern part of the subpolar gyre (Rockall Trough), while denser SPMW was found on the Reykjanes Ridge. These SPMWs are separated horizontally by highly stratified water masses not belonging to any SPMW class, confirming the previous observation by Talley (1999). Therefore, observations along those hydrographic sections do not support the smooth progression of SPMW hypothesized by McCartney and Talley (1982).

This paper and the accompanying paper (Brambilla and Talley, submitted) aim to clarify the controversy related to the location and progressive connection of SPMWs. Historical hydrographic data are used to track the SPMWs based on the their hydrographic (potential temperature, potential density, salinity, pressure) and dynamical (potential vorticity) properties. Lagrangian data are used to describe the circulation in the subpolar gyre and to study the presence of SPMWs with respect to the currents of the region. Hydrographic data are used to compute geostrophic flow at levels not sampled by drifters and floats, using the Lagrangian streamfunction as a reference.

We confirm that SPMWs are part of the surface layer that roughly extends vertically from the ocean surface to the permanent pycnocline. Thus SPMWs are the water masses through which the shallow circulation carries warm and salty

water to the sites of dense water formation (McCartney and Talley, 1982; Talley, 2003).

Since the original analysis of McCartney and Talley (1982), it has become clear that the subpolar circulation consists of three separate intense northeastward currents, the Rockall Trough and Iceland Basin branches of the North Atlantic Current (NAC) and the Irminger Current (Fratantoni, 2001; Flatau et al., 2003; Reverdin et al., 2003). We show that SPMW is associated with each of these intense currents. Along each current, the SPMW potential density increases gradually. The various currents and hence thir SPMWs however are not obviously connected by cyclonic flow. This supports the progressive density increase following the circulation suggested by McCartney and Talley (1982), but also the horizontal separation between SPMWs observed by Talley (1999) and Read (2001). These previous studies, which relied exclusively on a hydrographic description of the SPMWs, could not adequately link the SPMW and the intense currents.

The paper is organized as follows. Section 3.3 describes the data and the methods. Section 3.4 discusses the depth of the SPMWs relative to the depth of the winter mixed layer. In section 3.5, we detail the characteristics of the SPMWs in the eastern subpolar gyre and the seasonal variation of the location of SPMWs. In section 3.6, we analyze the circulation of the eastern subpolar gyre using Lagrangian observation to reference the geostrophic flow. In section 3.7, we summarize the main results of this study.

3.3 Data and methods

Hydrographic and Lagrangian data sets are used. Historical hydrographic bottle data from the National Oceanographic Data Center (NODC) (Fig. 3.1), organized in the "Hydrosearch" data base at the Scripps Institution of Oceanography (Reid, personal communication), are used to describe the water mass properties (potential density, salinity, potential temperature, depth) and to compute the depth of the winter mixed layer (Fig. 3.2), described in section 3.4. The historical data set covers the period from 1900 to 1990. To these we add hydrographic data from 6 cruises during the World Ocean Circulation Experiment (WOCE): A16 in July- August 1988, AR12 in September-November 1996, AR24-147 in November-December 1996, A24 in May-July 1997, AR24-154 in October-November 1997, and AR16 in June-August 2003.

The conclusions from hydrographic observations are combined with results from Lagrangian data. We use surface drifters drogued at 15 m to compute the streamfunction of the currents at the surface, as in Niiler et al. (2003), and isopycnal floats targeted on the $27.5\sigma_\theta$ isopycnal to compute the streamfunction on the corresponding potential density surface, as in Bower et al. (2002).

The surface drifters are part of the global drifter data set from the Global Drifter Program at the National Oceanographic and Atmospheric Administration's (NOAA) Atlantic Oceanographic and Meteorological Laboratory (AOML). They cover the period from 1990 to 2002. They were designed with a submerged cylindrical drogued centered at 15 m below the surface, to reduce the slippage

due to the wind (Niiler, 1995). Each drifter continuously transmits to the Argo satellite system. This data set has been used in several studies to track surface circulation (Fratantoni, 2001; McClean et al., 2002; Reverdin et al., 2003; Niiler et al., 2003; Flatau et al., 2003; Brambilla and Talley, 2006).

Isopycnal floats (Ranging and Fixing of Sound, RAFOS) were deployed as part of the US Atlantic Climate Change Experiment (ACCE). They cover the period 1996-1997 (Bower et al., 2002). They were ballasted for $\sigma_\theta = 27.5\ kg/m^3$. They were acoustically tracked during their mission and collected measurements of temperature and pressure (Rossby et al., 1986).

Finally, to complete the analysis of the circulation in the northeastern Atlantic, we use the annual mean hydrographic data objectively mapped on a $1^\circ \times 1^\circ$grid from the World Ocean Atlas 2001 (WOA01) (Conkright et al., 2002) to compute the absolute streamfunction on the $27.3\sigma_\theta$, $27.4\sigma_\theta$ and $27.5\sigma_\theta$ isopycnal surfaces, referenced to both the surface streamfunction from drifters and to the $27.5\sigma_\theta$ streamfunction derived from the floats. Results from the two separate reference streamfunctions are compared in section 3.6.

3.3.1 SPMW definition

Subpolar Mode Water is identified in this study, as in previous studies (e.g. Talley, 1999; Read, 2001), by a minimum of isopycnic potential vorticity (PV), ignoring relative vorticity. The Ertel definition of potential vorticity can be

written in terms of the vertical gradient of potential density :

$$PV = \left| \frac{f}{\rho} \frac{\partial \rho}{\partial z} \right| \tag{3.1}$$

where f is the Coriolis parameter and ρ is the density referenced to the mid-point of the depth interval (Talley and McCartney, 1982). McCartney and Talley (1982) used the Brunt-Vaisala frequency $N^2 = -\frac{g}{\rho}\frac{\partial \rho}{\partial z}$; results are identical in terms of locating the minimum in the vertical density gradient, identified as the SPMW.

The minimum of potential vorticity corresponds to a low vertical gradient of density, therefore to high vertical homogeneity of the water mass. Since mode waters are defined as water masses with nearly uniform vertical properties, it is appropriate to use potential vorticity as a tracer for these particular masses of water. Furthermore, in the absence of mixing, PV is conserved along the flow, hence it is the most appropriate dynamical property for tracing water masses horizontally (Talley and McCartney, 1982).

To identify the surface SPMW, we first computed the potential vorticity profile at each station of the historical hydrographic data set and secondly we located the vertical minimum of PV with density lower than $27.7\sigma_\theta$. The density constraint masks the PV minimum associated with the LSW, which, at $27.78\sigma_\theta$, lies below the gyre SPMWs (Talley and McCartney, 1982). The properties (PV, potential temperature, potential density, depth, salinity) at the minimum of the potential vorticity profile are then bin-averaged on a regular $0.5° \times 0.5°$grid and objectively mapped (Fig. 3.3, described in section 3.5.1). (The objective mapping

method is discussed in section 3.6 and Appendix 3.A.)

To further study the properties and the connection of the eastern SPMWs with each other, we found it useful to characterize SPMWs based on potential density. The potential density of SPMW varies from approximately $27\sigma_\theta$ to $27.6\sigma_\theta$ (Fig. 3.3). The northeastern Atlantic is dominated by SPMW in the density range $27.3\sigma_\theta$ to $27.5\sigma_\theta$. Therefore we choose to analyze properties on the $27.3\sigma_\theta$, $27.4\sigma_\theta$, and $27.5\sigma_\theta$ isopycnal surfaces. On each of these isopycnals, we first use low potential vorticity to identify the location of the SPMW. Within the region of low PV on each isopycnal, we then plot the potential temperature, salinity and pressure (Figs. 3.4, 3.5, and 3.6, described in section 3.5.2).

We focus here on the northeastern Atlantic (40°W - 0°E, 50°N - 70°N). The topographic features that confine the region (Fig. 3.1) are the Reykjanes Ridge in the west; Iceland in the north; the Iceland-Faroe Ridge on the northeastern - eastern edge; and the continental shelf of Great Britain in the east. Figure 3.1 also shows the historical hydrographic data and WOCE cruise transects.

3.3.2 Computation of the winter mixed layer

A question to address is whether the winter mixed layer is identical to SPMW in most of the subpolar gyre, as hypothesized by McCartney and Talley (1982). Similarly to McCartney and Talley (1982), profiles at each hydrographic station can be used to evaluate the approximate winter mixed layer depth and

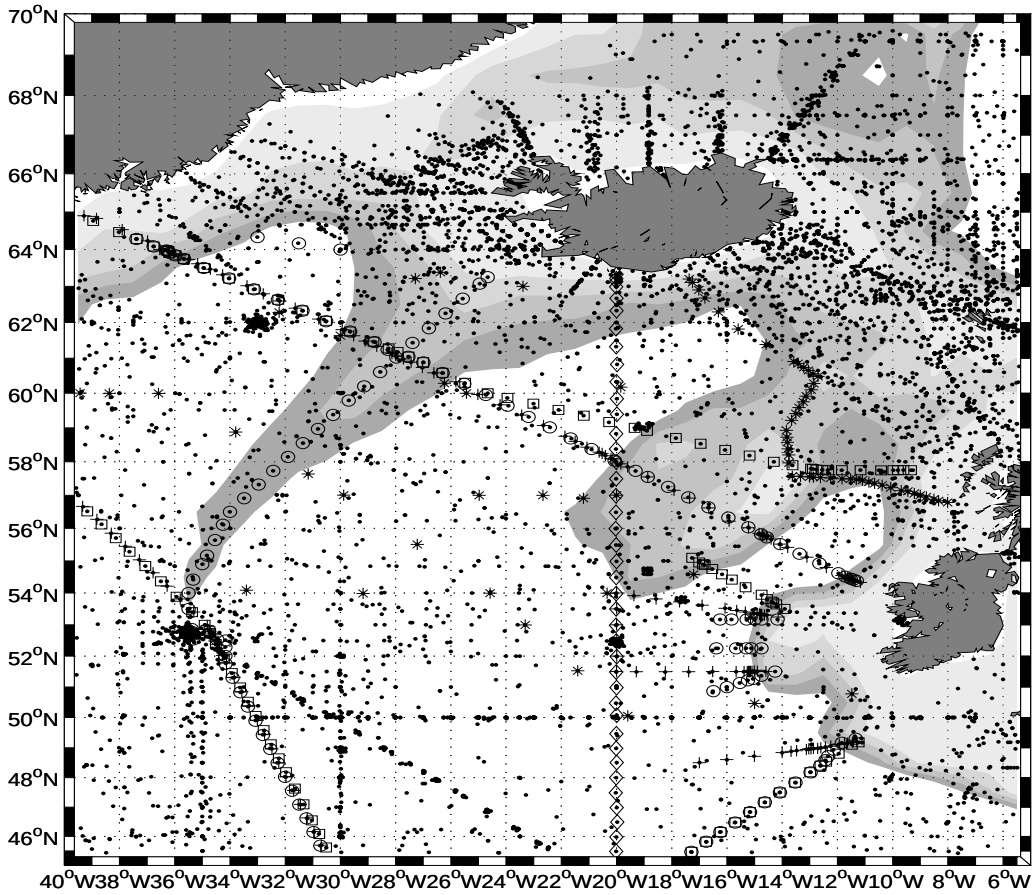

Figure 3.1: Study area. Topography is shaded; the darkest contour is 2000, the lightest is 10m, contour interval is 500m. The round dots correspond to the historical hydrographic stations and the symbols correspond to the WOCE cruises: AR12 1996 Sep-Nov (asterisk); AR24-147 1996 Nov-Dec (circle); A24 1997 May-Jul (square); AR24-154 1997 Oct-Nov (plus); A16 1988 Jul-Aug & AR16 2003 Jun-Aug (diamond).

its properties. Operationally, we use the temperature profiles of the historical hydrographic data to estimate the depth of the thermocline marking the base of the winter mixed layer. All profiles are used, without any distinction based on the month in which they were collected.

The winter stations clearly show a thermocline with depth greater than 200 m associated with the base of the winter mixed layer (McCartney and Talley, 1982), while late spring or summer stations have a surface thermocline associated with the summer stratification. However, in addition to the shallow thermocline, the stations collected in the warm months are characterized by another deeper thermocline, which identifies the base of the remnant of the winter mixed layer (McCartney and Talley, 1982). To obtain an approximate winter mixed layer depth, we therefore locate the deeper thermocline, between 200 and 1000 m, for each temperature profile (January through December). This depth range excludes the shallow summer stratification and reduces the possible bias due to poor sampling for depths larger than 1000m. The thermocline is identified as the largest maximum in the vertical temperature gradient between 200 and 1000 m. This method is equivalent to the computation of the Brunt-Vaisala frequency, using temperature rather than density. The thermocline depth is a first order approximation of the depth of the base of the winter mixed layer. In our computation, in fact, the largest maximum peak associated with the thermocline is biased toward the center of the thermocline, therefore it estimates a slightly greater depth than the actual winter mixed layer base.

The depth of the base of the winter mixed layer from all individual

hydrographic stations has then been objectively mapped on a uniform 1°× 1°grid (Bretherton et al., 1976) (sections 3.3.3 and 3.6, and Appendix 3.A).

3.3.3 Absolute Streamfunctions

The computation of the streamfunction of the flow in the eastern subpolar gyre allows us to investigate how SPMWs participate in the subpolar circulation.

The streamfunction at the ocean surface is computed first, using velocity measurements from surface drifters drogued at 15-m. Secondly, using the hydrographic data from the WOA01, we compute the streamfunction on the $27.3\sigma_\theta$, $27.4\sigma_\theta$ and $27.5\sigma_\theta$ isopycnal surfaces, using the surface drifter streamfunction as a reference. An independent reference streamfunction is also calculated from isopycnal floats on the $27.5\sigma_\theta$ isopycnal (Bower et al., 2002).

The streamfunction computation follows the methods described by Bretherton et al. (1976), Davis (1998, 2005), and Gille (2003), using an objective mapping technique to obtain a nondivergent streamfunction field from velocity data.

As described by Bretherton et al. (1976), the streamfunction is a scalar quantity defined by a linear operator on the measured velocity field. The objective analysis applied to the computation of the streamfunction ψ leads to the best estimate of $\hat{\psi}$, defined as the estimate with the least error. The estimates of the

velocity components

$$u = -\frac{1}{f}\frac{\partial \psi}{\partial y} \quad and \quad v = \frac{1}{f}\frac{\partial \psi}{\partial x} \tag{3.2}$$

are optimized and automatically nondivergent. In (3.2) f is the Coriolis parameter. A detailed summary of the the specific procedure followed in this paper is given in Appendix 3.A.

Surface drifter velocities are bin-averaged to form a mean velocity field, as in Brambilla and Talley (2006). In order to obtain an estimate of the geostrophic surface mean velocity field, the drifter measurements have been previously adjusted removing the Ekman component, calculated using the Ralph and Niiler (1999) model, as in Flatau et al. (2003) and Brambilla and Talley (2006). The entire data set has been used without applying any correction due to time variability or seasonality. The procedure to compute the mean velocity field from float data differs from the surface drifter procedure (see Appendix 3.B).

After the computation of the mean velocity field, we calculate the streamfunction ψ using a covariance function $C(\rho) =< \psi(x,y)\psi(x+r,y+s) >$ that has been assumed to be a priori (Appendix 3.A):

$$C(\rho) = [1 + \frac{d}{d_0}]e^{(-\frac{d}{d_0})} \tag{3.3}$$

where d is the radial distance, $d^2 = r^2 + s^2$. d_0 has been chosen to be 100 km.

The absolute streamfunctions on the $27.3\sigma_\theta$, $27.4\sigma_\theta$ and $27.5\sigma_\theta$ isopycnal surfaces are obtained by computing the pressure anomaly streamfunction (Zhang and Hogg, 1992) with respect to the ocean surface and then adding the surface streamfunction values estimated from the surface drifters. The pressure anomaly

streamfunction, valid for specific volume anomaly surfaces, is a good approximation of the streamfunction on isopycnals (Zhang and Hogg, 1992; Gille, 1997). The pressure anomaly streamfunction of ψ_1 on the isopycnal surface σ_1 with respect to ψ_2 on the isobaric surface p_2 is:

$$\psi_1 - \psi_2 = \int_{\overline{p_1}}^{p_2} \delta dp - \delta_1 p_1' \tag{3.4}$$

where $\overline{p_1}$ is the mean pressure of the isopycnal surface, $p_1' = p_1 - \overline{p_1}$ is the pressure anomaly with respect to the mean pressure on the isopycnal surface, p_2 is the pressure of the isobaric reference surface and δ_1 is the specific volume anomaly or steric anomaly defined by

$$\delta = \frac{1}{\rho(S,T,p)} - \frac{1}{\rho(\overline{S},\overline{T},p)} \tag{3.5}$$

where $\overline{S}$ and $\overline{T}$ are the mean salinity and temperature on the reference isopycnal surface, and ρ is the in situ density.

When the estimate of the surface streamfunction from the surface drifters is added to the pressure anomaly streamfunction (3.4), we obtain the absolute streamfunction on isopycnal surfaces:

$$\psi_\sigma = \int_{\overline{p_1}}^{p_2} \delta dp - \delta_1 p_1' + \psi_{15m} \tag{3.6}$$

where ψ_{15m} is the surface drifter streamfunction.

It can be argued that the surface drifters are not the proper tool to measure and reference the geostrophic velocity. Although we corrected the drifter velocity measurements by subtracting the Ekman component (Ralph and Niiler, 1999), we cannot exclude the possibility of a residual ageostrophic velocity and

errors related to uncertainties in wind correction (Brambilla and Talley, 2006). Isopycnal floats, on the other hand, directly measure the geostrophic velocity and could theoretically provide a more adequate reference. In Bower et al. (2002), floats were successfully used to calculate the streamfunction on the $27.5\sigma_\theta$, identified as the geostrophic circulation. However, the float data set has much poorer spatial distribution than the surface drifters in the eastern subpolar gyre (Bower et al., 2002; Brambilla and Talley, 2006). Hence the absolute streamfunction from the floats has gaps in some important areas of the SPMW study region, especially in Rockall Trough and over the Iceland-Faroe Ridge. The gaps cause error in the absolute streamfunctions at $27.3\sigma_\theta$ and $27.4\sigma_\theta$. Thus, their better spatial distribution led us to use the surface drifters as the primary reference. Comparison of the results obtained using the two different reference surfaces in section 3.6 confirms the validity of our choice.

The procedure to compute the absolute streamfunction on isopycnal surfaces with respect to the $27.5\sigma_\theta$ isopycnal floats is similar to that for the surface drifter reference. First, following Bower et al. (2002), the absolute streamfunction on the $27.5\sigma_\theta$ isopycnal surface was computed from the observed mean velocity field (Appendix B). Secondly, this mean was used as the reference streamfunction for the $27.3\sigma_\theta$ and $27.4\sigma_\theta$ isopycnals as in Zhang and Hogg (1992):

$$\psi_\sigma = \int_{\overline{p_i}}^{\overline{p_{27.5}}} \delta dp - \delta_i p'_i + \delta_{27.5} p'_{27.5} + \psi_{27.5} \tag{3.7}$$

where $p'_{i,27.5} = p_{i,27.5} - \overline{p_{i,27.5}}$ is the pressure anomaly with respect to the mean pressure on the isopycnal surfaces $\sigma_{i,27.5}$, $\delta_{i,27.5}$ is the specific volume anomaly on

the two isopycnal surfaces $\sigma_{i,27.5}$, and $\psi_{27.5}$ is the absolute streamfunction on the $27.5\sigma_\theta$ isopycnal surface.

3.4 Northeastern Atlantic mixed layer

The deep vertical convection that occurs during the winter leads to the formation of a well-mixed surface layer with nearly uniform properties in the vertical (Fig. 3.2). Consequently, this process has been considered one of the major causes for the formation of SPMW (McCartney and Talley, 1982). Thus, we first present the winter mixed layer to compare it with the SPMW, which is identified by regions of low PV. This permits us to investigate whether SPMW is subducted anywhere in this domain. (Based on the prevalence of positive wind-stress curl in this region, we do not expect to find classical subduction. Nevertheless, it is important to evaluate this possibility, especially in light of the results described in the companion paper (Brambilla and Talley, 2007).)

Figure 3.2 is the depth of the thermocline just below the winter mixed layer, calculated as described in section 3.3.2, taken to represent the base of the winter mixed layer. The deepest values are in Rockall Trough ($\sim$ 600 m) and on the northeastern edge of the Iceland Basin, where the winter mixed layer reaches $\sim$ 650 m. The depth decreases toward the topographic features. On the eastern flank of the Reykjanes Ridge it is 450-500 m; on the Iceland-Faroe Ridge it is $\sim$400 m. The base of the mixed layer in the center of the Iceland basin is $\sim$500

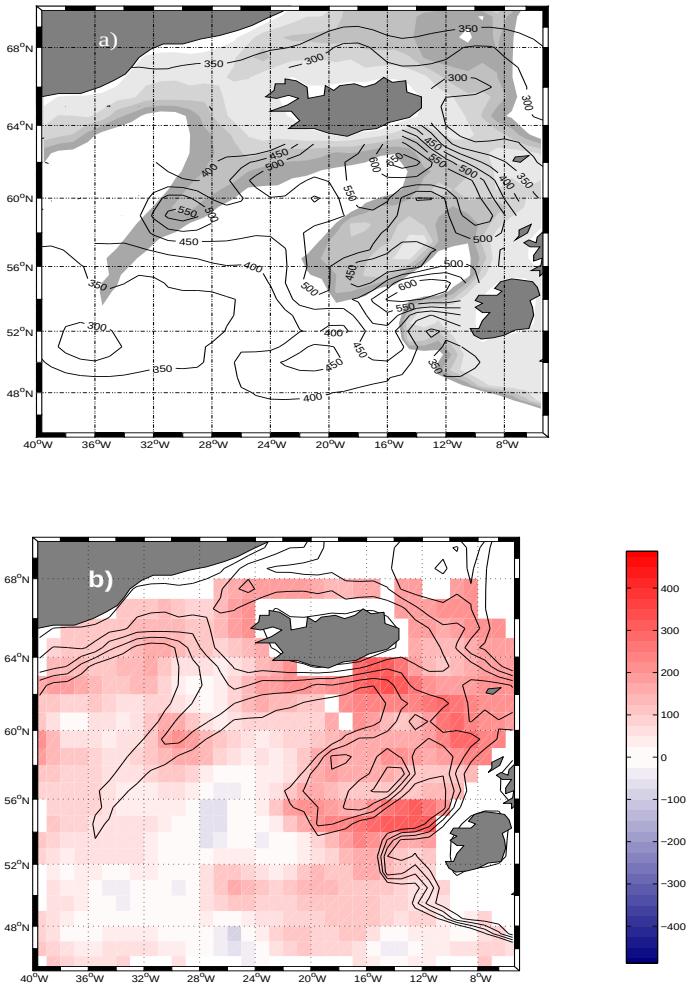

Figure 3.2: a) Depth of the winter mixed layer (m) The data have been objectively mapped on a 1°× 1°grid. Topography is shaded, the darkest contour is 2000 m, the lightest is 10m, contour interval is 500m. b) Difference between the winter mixed layer depth and the SPMW depth (m). Contour lines represent the topography. Contour values and interval are as in (a).

m. (Depths are not mapped in the Irminger Sea because of large error due to the difficulty in locating the winter thermocline in the temperature profiles of this region.) These values are consistent with the older mixed layer depth estimates from McCartney and Talley (1982), Qiu and Huang (1995), and with the recent estimates from Kara (2003) and de Boyer Montégut et al. (2004).

We then compare the depth of the winter thermocline to the depth of the SPMW. The latter has been evaluated at each hydrographic station by looking at the depth of the minimum of potential vorticity in the water column that excludes densities larger than $27.7\sigma_\theta$ (Fig. 3.3e), following the definition of section 3.3.1. For a simple mixed layer that is identical with SPMW, the PV minimum will always be shallower than the thermocline depth used to estimate the base of the winter mixed layer.

The difference between the base of the winter mixed layer and the SPMW pycnostad depth is shown in Fig. 3.2b. For positive values (red) the base of the winter mixed layer is greater than the SPMW PV minimum. The values are predominantly positive in the entire eastern subpolar gyre. Thus, there is no indication of subduction of SPMW below the base of the winter mixed layer, which agrees with McCartney and Talley's (1982) conclusion. (The negative values in the southern Iceland basin and south of 52°N, of the order of 25 m, are within the uncertainty of the computation.)

This confirmation of the lack of visible subduction of SPMW is important because the air-sea flux calculation presented in the accompanying paper (Brambilla and Talley, 2007) shows large regions of "formation" which

is interpreted typically as "subduction". Since the PV minimum SPMWs do not subduct (unlike Subtropical Mode Water), the net formation of SPMW is interpreted in that paper as loss by entrainment to the interior layers (e.g. at the Nordic Seas overflows and into Labrador Sea Water).

3.5 SPMW distribution

The original description of SPMW by McCartney and Talley (1982) emphasizes the cyclonic arrangement of SPMWs of increasing density around the subpolar gyre with the implication of a continuous cyclonic flow connecting them sequentially. More recent studies (Talley, 1999; Read, 2001) suggest that patches of SPMW are horizontally separated by stratified water masses. Here, taking advantage of a larger data set than the one used in the past studies, we further investigate the SPMW distribution and properties. We then interpret SPMW in terms of the streamfunction (section 3.6).

3.5.1 SPMW properties

The SPMW studied here is identified as the vertical PV minimum at densities lower than $27.7\sigma_\theta$ (Fig. 3.3). (This therefore eliminates LSW and might also eliminate the densest SPMW precursor to LSW.) As described in section 3.3.1, the properties of the vertical PV minimum at each hydrographic station

are first bin-averaged and then objectively-mapped. The vertical minimum of PV is characterized by large mean values of potential vorticity along the strongest currents of the region: the NAC that flows eastward into the study domain, the northern side of the Iceland-Faroe Front, and the East Greenland Current, none of which are characterized by SPMW (Talley, 1999). Patches of low potential vorticity at the PV minimum are identified as SPMW. These are detected southwest of Porcupine Bank, on the southern Rockall Plateau, and over the northwestern Reykjanes Ridge.

In the Iceland Basin, Talley (1999), using synoptic data, showed that the NAC (Subarctic front) is characterized by large potential vorticity and therefore by the absence of SPMW. This high potential vorticity region is not present in Fig. 3.3a. Instead, the mean potential vorticity is quite low in the entire Iceland Basin. The difference is likely due to our use of an average field that smooths out the NAC front, whose location and intensity vary in time and space (Flatau et al., 2003).

In the Irminger Sea, we expected to find very low potential vorticity associated with the SPMW precursor of LSW (Talley, 1999; Pickart et al., 2003). The high PV found there is most likely due to the density cutoff we used to separate SPMW and LSW. Since the density of the SPMW in the Irminger Sea is very close to $27.7\sigma_\theta$, such a cutoff does not allow a proper mapping of the actual potential vorticity values. The unrealistically shallow depth of the PV minimum in the Irminger Sea also confirms this.

The density of the PV minimum in the eastern subpolar gyre increases

smoothly following two main pathways: northeastward, in the Rockall Trough and Iceland Basin, and westward, from the Reykjanes Ridge to the Irminger Sea. In the Rockall Trough, the potential density varies from $27.28\sigma_\theta$ to $27.38\sigma_\theta$; in the Iceland Basin, from $27.38\sigma_\theta$ to $27.48\sigma_\theta$; on the Reykjanes Ridge, from $27.42\sigma_\theta$ to $27.56\sigma_\theta$. (SPMW properties are patchy when mapped synoptically but still appear to increase downstream (Talley, 1999; Read, 2001).) The connection between the mean properties of the SPMWs and the subpolar gyre circulation is usefully explored in section 3.6.

3.5.2 SPMW on isopycnal surfaces

A different way to illustrate the properties of SPMW, more convenient to investigate its connecting pathways, is to look at isopycnals that intersect the SPMW. Here, we identify SPMWs by low potential vorticity along the desired isopycnal, and describe the associated potential temperature, salinity and depth in the low potential vorticity region. We show results for the $27.3\sigma_\theta$, $27.4\sigma_\theta$, and $27.5\sigma_\theta$ isopycnals (Fig. 3.9).

At $27.3\sigma_\theta$, there are three main regions of low PV: west of Porcupine Bank, in the southern Rockall Trough, and on the southwestern flank of Rockall Plateau. The $27.4\sigma_\theta$ SPMW is located on both the western flank of Rockall Plateau and in the northern part of Rockall Trough. The $27.5\sigma_\theta$ SPMW is located on both the Iceland-Faroe Ridge and on the eastern and southern flank of the Reykjanes

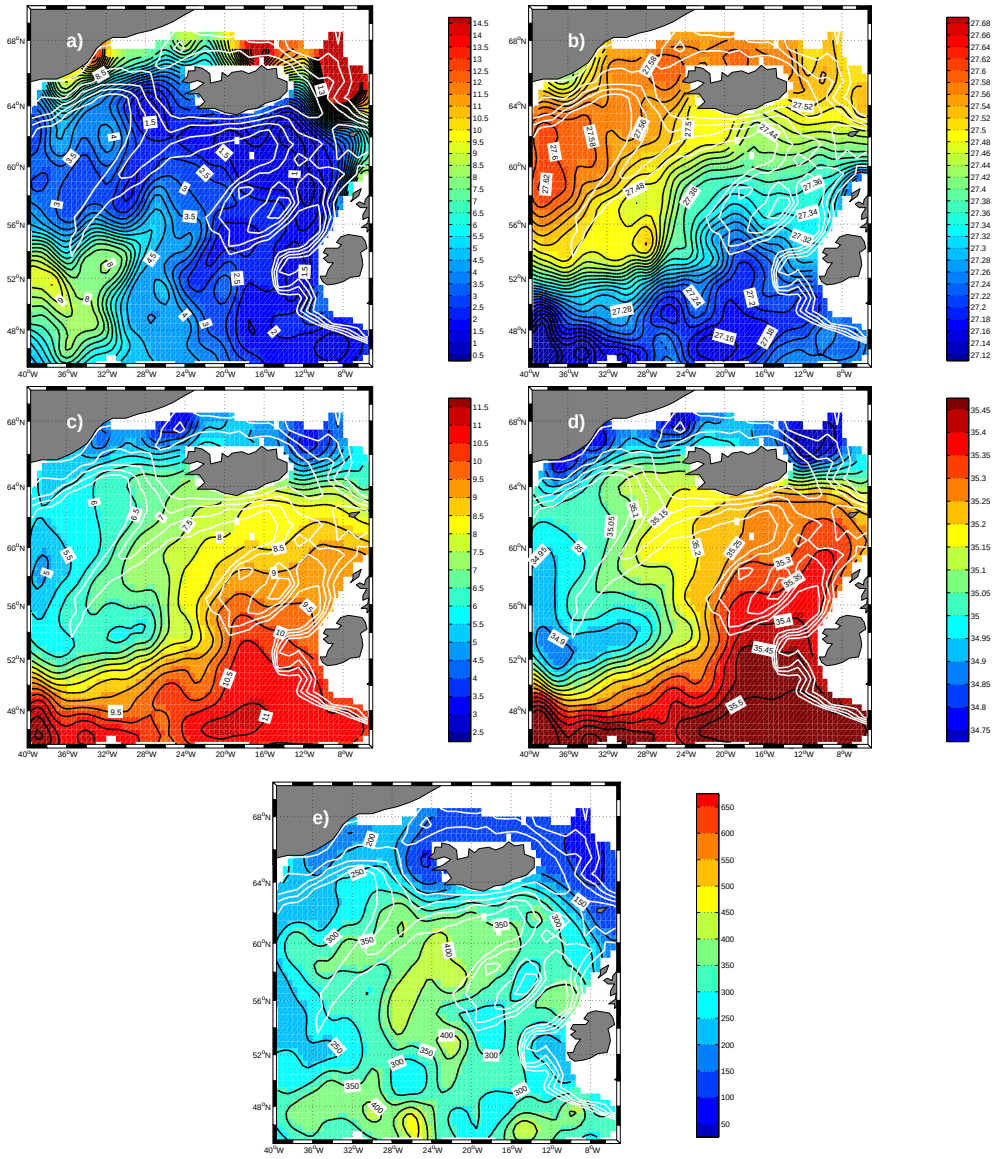

Figure 3.3: Properties at the PV minimum with density lower than $27.7\sigma_\theta$. The property maps are obtained by bin-averaging the historical hydrographic measurements and objectively mapping the mean field on a uniform $0.5° \times 0.5$ °grid. White contours are the topography from 2000 m to 10 m; the contour interval is 500 m. a) Potential vorticity $10^{-13} cm^{-1} s^{-1}$. b) Potential density ($\sigma_\theta - 1000$), contour interval $0.02 kg/m^3$. b) Potential temperature (°C), contour interval 0.5 °C. c) Salinity (psu), contour interval 0.05 psu. d) Depth (m), contour interval 50m.

Ridge.

The location of the $27.3\sigma_\theta$ and $27.4\sigma_\theta$ SPMW agrees with the isopycnic potential vorticity maps shown in Talley (1999), based on a sparser historical data set. The location of the $27.5\sigma_\theta$ SPMW exhibits some differences. In Talley (1999), the $27.5\sigma_\theta$ SPMW is shown only on the Reykjanes Ridge, while here we identify $27.5\sigma_\theta$ SPMW on both the Reykjanes and the Iceland-Faroe Ridges. The much larger hydrographic data set used here is the cause of this discrepancy. Only a few stations on the Iceland-Faroe Ridge were used in Talley's (1999) study, as opposed to the large number in the present study (Fig. 3.1).

From these three isopycnals, the low PV visually proceeds northeastward with increasing potential density, in both the Iceland Basin and the Rockall Trough, while it veers westward-southwestward along the Reykjanes Ridge passing from $27.4\sigma_\theta$ to $27.5\sigma_\theta$. As discussed in section 3.6, the gradual densification of the low PV regions in each basin is due to the link between the subpolar gyre circulation, which is strongly influenced by the topography, and the SPMW (see section 3.6.1).

Potential temperature, salinity, and depth of the SPMW on each isopycnal ($27.3\sigma_\theta$, $27.4\sigma_\theta$, $27.5\sigma_\theta$) are shown in Figs. 3.4, 3.5, and 3.6 with mean values listed in Table 1. The filled colors are the values limited to regions of potential vorticity lower than $10\times10^{-13}cm^{-1}s^{-1}$ at $27.3\sigma_\theta$, and lower than $8\times10^{-13}cm^{-1}s^{-1}$ at $27.4\sigma_\theta$ and $27.5\sigma_\theta$, while the contours represent the property values elsewhere. Figs. 3.4, 3.5, and 3.6 confirm a smooth progression of SPMW properties northeastward through the Iceland Basin and Rockall Trough, and westward-southwestward along the Reykjanes Ridge. On each isopycnal,

the SPMW potential temperature, salinity, and depth tend to decrease in these directions. This is likely associated with heat loss in the subpolar gyre that drives the temperature decrease and shoaling of the isopycnals (Brambilla and Talley, submitted).

In addition to the regional distribution of the properties of the $27.3\sigma_\theta$, $27.4\sigma_\theta$, and $27.5\sigma_\theta$ SPMW, we also show the temperature probability distribution of the same SPMWs (Figs. 3.4d, 3.5d, 3.6d) to better described the nearly homogeneity of the SPMW properties (in this case temperature). The probability distribution of temperature is computed from the hydrographic station measurements, without averaging the data. The $27.3\sigma_\theta$ and $27.4\sigma_\theta$ SPMW are characterized by a nearly Gaussian distribution suggesting that these SPMWs are nearly homogeneous around a mean value. (In both the $27.3\sigma_\theta$ and $27.4\sigma_\theta$ SPMW, the tail toward colder temperature is due to few stations sparse in the southern Iceland Basin.) In contrast, the temperature probability distribution of the $27.5\sigma_\theta$ SPMW is bimodal (Fig. 3.6d), indicating that two separate types of the same density SPMW occupy different regions: the Reykjanes Ridge and the Iceland-Faroe Ridge. The $27.5\sigma_\theta$ SPMW on the Reykjanes Ridge is colder and fresher compared with the $27.5\sigma_\theta$ SPMW on the Iceland-Faroe Ridge. This suggests that the $27.5\sigma_\theta$ SPMW on the Reykjanes Ridge might not simply originate from lighter SPMWs in the Iceland Basin, as is most likely for the $27.5\sigma_\theta$ SPMW on the Iceland-Faroe Ridge, but that other sources might be necessary (see section 3.6.1).

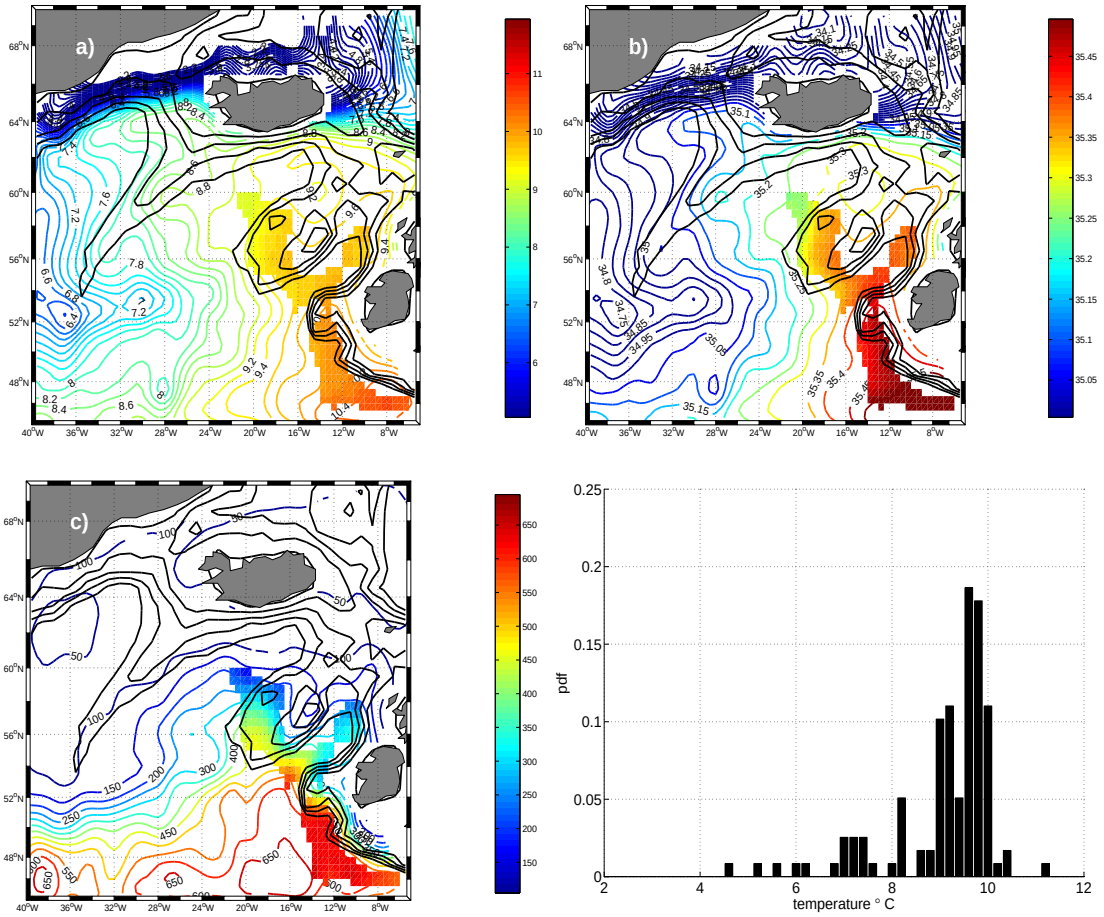

Figure 3.4: Properties at $27.3\sigma_\theta$. Colored contours are the values on the entire isopycnal surface; the filled colors are the property values limited to the areas where the potential vorticity is less that $10\times10^{-13}cm^{-1}s^{-1}$. Black contours represent the topography. The deepest contour is at 2000m, the shallowest 10m, the contour interval 500 m. a) Potential temperature (°C), contour interval 0.02 °C; b) salinity (psu), contour interval 0.05 psu; c) depth (m), contour interval 50 m. d) Pdf of temperature values collected at each historical hydrographic station with a PV minimum at $27.3\sigma_\theta$ possibly biases by the limited number of data.

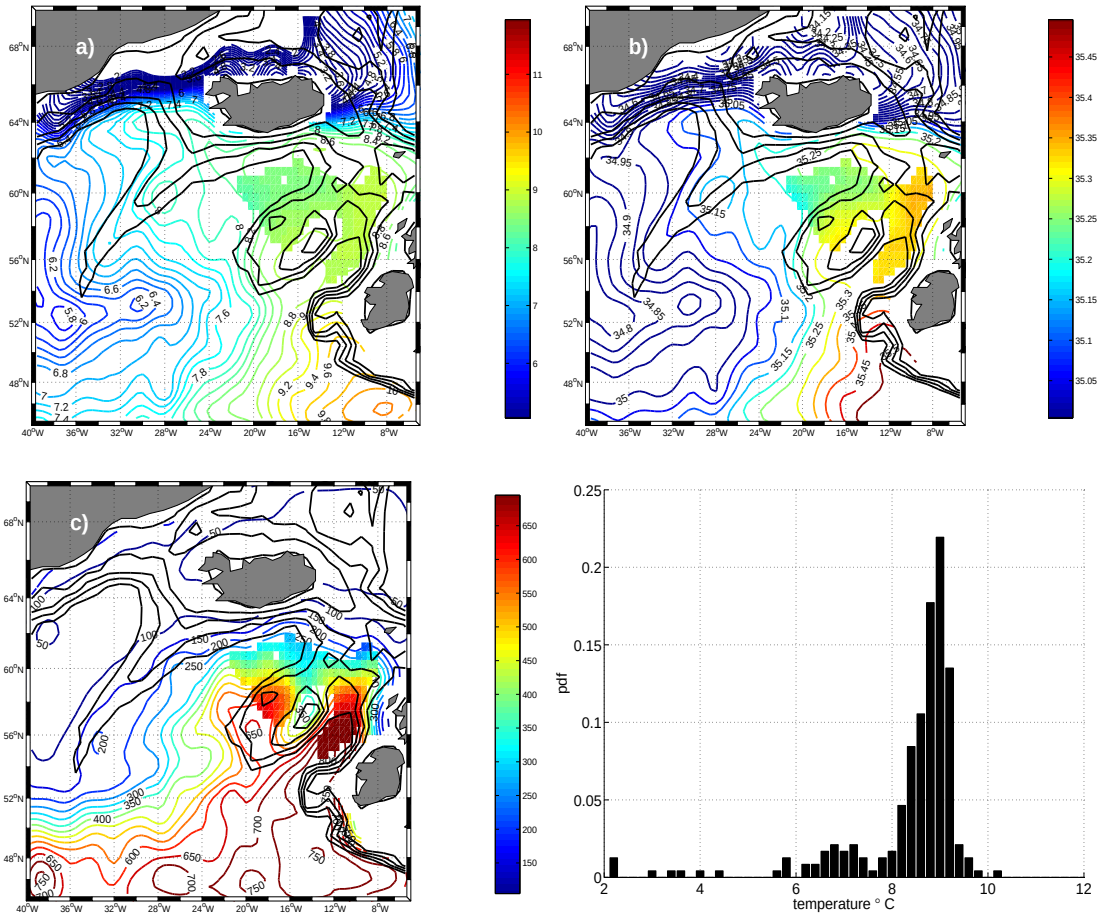

Figure 3.5: Properties at $27.4\sigma_\theta$. Colored contours are the values on the entire isopycnal surface; the filled colors are the property values limited to the areas where the potential vorticity is less that $8{\times}10^{-13}cm^{-1}s^{-1}$. Black contours represent the topography. The deepest contour is at 2000m, the shallowest 10m, the contour interval 500 m. a) Potential temperature (°C), contour interval 0.02 °C; b) salinity (psu), contour interval 0.05 psu; c) depth (m), contour interval 50 m. d) Pdf of temperature values collected at each historical hydrographic station with a PV at $27.4\sigma_\theta$.

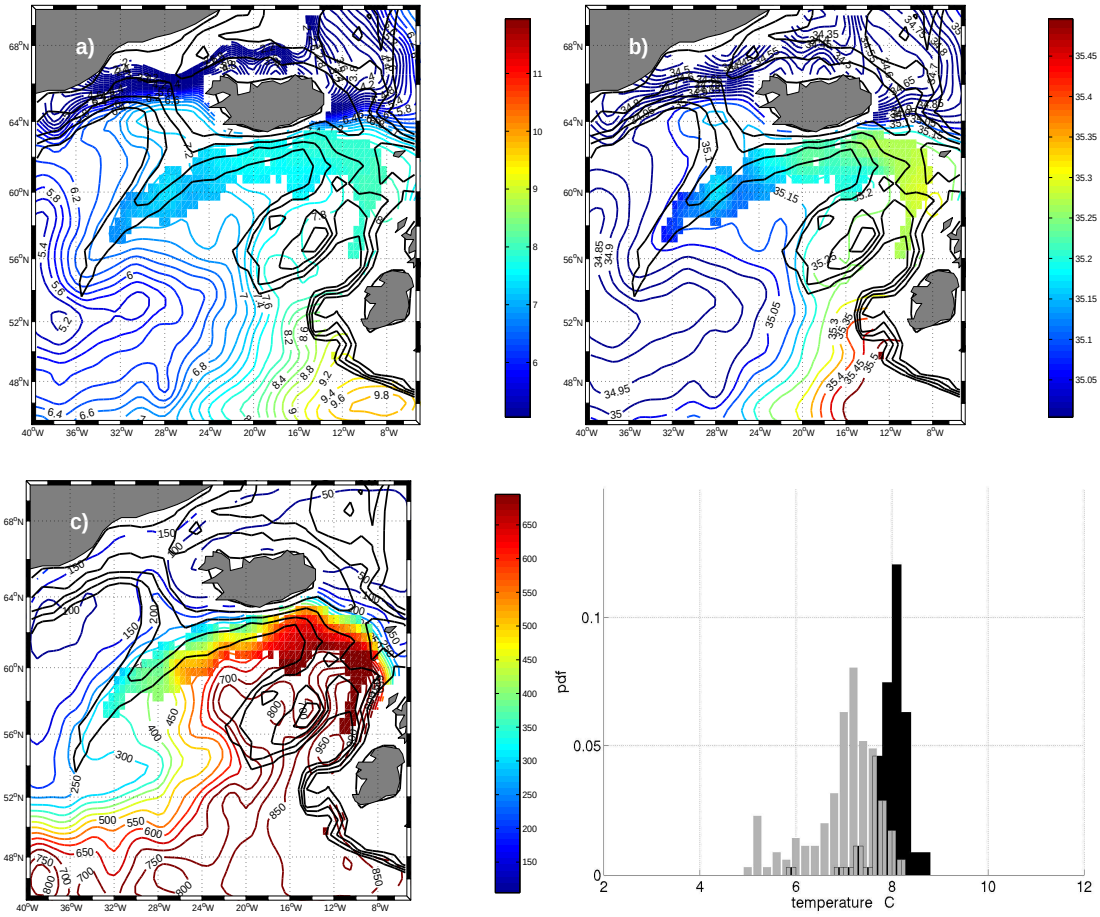

Figure 3.6: Properties at $27.5\sigma_\theta$. Colored contours are the property values on the entire isopycnal surface; the filled colors are the property values limited to the areas where the potential vorticity is less that $8\times10^{-13}cm^{-1}s^{-1}$. Black contours represent the topography. The deepest contour is at 2000m, the shallowest 10m, the contour interval 500 m. a) Potential temperature (°C), contour interval 0.02 °C; b) salinity (psu), contour interval 0.05 psu; c) depth (m), contour interval 50 m. d) Pdf of temperature values collected at each historical hydrographic station with a PV minimum at $27.5\sigma_\theta$. In gray is the temperature pdf of the $27.5\sigma_\theta$ on the Reykjanes Ridge, in black on the Iceland-Faroe Ridge.

Table 3.1: Mean and standard deviation of potential temperature, salinity and depth for each SPMW.

	Θ (°C)	S(psu)	D(m)
27.3 σ_θ	9.82 ± 0.37	35.41 ± 0.083	453 ± 145
27.4 σ_θ	8.64 ± 0.20	35.29 ± 0.04	481 ± 143
27.5 σ_θ - Iceland-Faroe Ridge	7.81 ± 0.21	35.25 ± 0.04	670 ± 143
27.5 σ_θ - Reykjanes Ridge	7.28 ± 0.24	35.15 ± 0.04	435 ± 86

3.5.3 Seasonal variation of SPMW location

Seasonal variability of SPMW has not been examined previously. Since SPMW proprieties are set in the winter, a zero-order description will not be expected to have much seasonal variability. However, the circulation that advects the SPMW continues through all seasons. Thus, SPMW for a given winter should move downstream and thus yield a seasonal cycle of SPMW at each location. The historical hydrographic data set has enough data in spring (AMJ), summer (JAS), and fall (OND) to examine this possibility (Fig. 3.7). Winter (JFM) coverage is not adequate. The mean potential vorticity field for the three seasons on the three isopycnals 27.3σ_θ, 27.4σ_θ, 27.5σ_θ is bin-average and objectively mapped on a regular 0.5°× 0.5°grid (Fig. 3.8).

At 27.3σ_θ and 27.4σ_θ, the location of the lowest potential vorticity (i.e. the location of the corresponding SPMW) moves northeastward with advancing seasons along the Iceland Basin and the Rockall Trough, suggesting advection of these SPMWs following formation in late winter. At 27.5σ_θ, the bin-average potential vorticity field does not show an annual progression, probably because of the poor seasonal spatial distribution of the data. However, annual advection is suggested by the hydrographic stations identifying the 27.5σ_θ SPMW. These

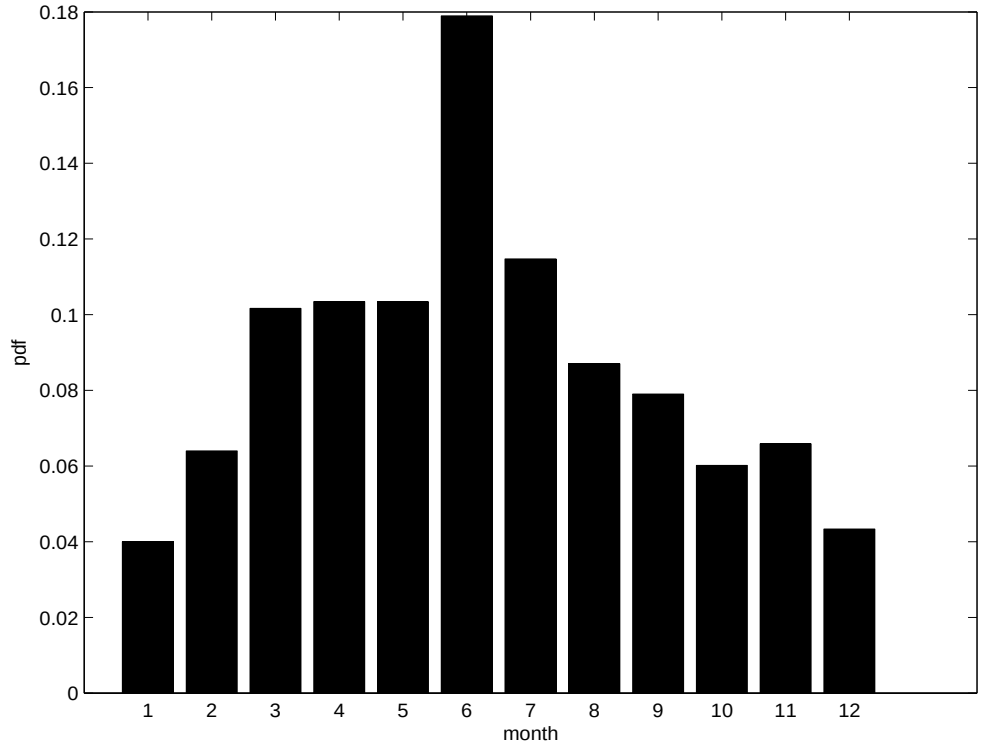

Figure 3.7: Monthly distribution of the hydrographic data.

stations proceed northeastward along the Irminger Current passing from spring to summer.

3.6 Circulation in the eastern subpolar gyre

Mode waters are generally associated closely with the warm side of major currents (e.g. McCartney and Talley, 1982; Hanawa and Talley, 2001). New understanding of the strength of the several branches of the NAC in the northeastern Atlantic (Orvik and Niiler, 2002; Niiler et al., 2003; Flatau et al., 2003) suggests that we re-examine the relation of SPMW to the circulation in

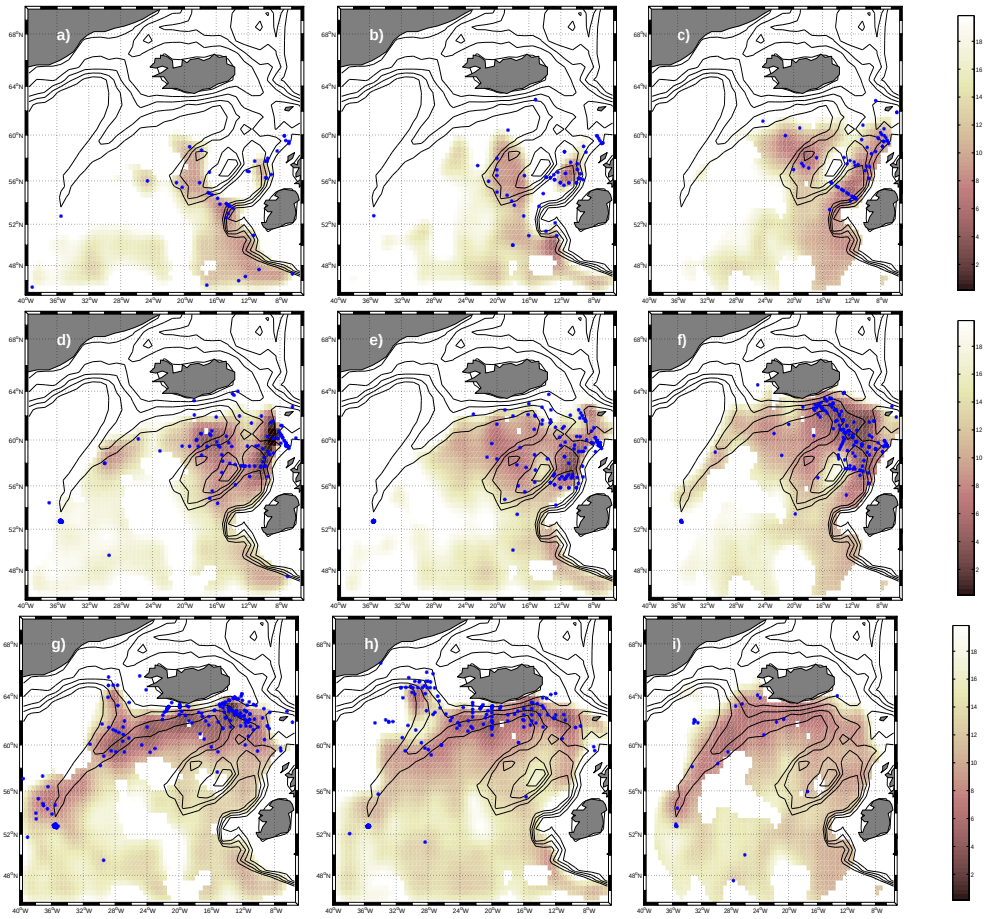

Figure 3.8: Seasonal potential vorticity values ($10^{-13} cm^{-1} s^{-1}$) objectively mapped on a uniform 0.5°× 0.5 °grid. Black contours represent the topography. The deepest contour is at 2000m, the shallowest 10m, contour interval is 500m. On each panel the blue asterisks refer to the hydrographic stations with PV values less than $4{\times}10^{-13} cm^{-1} s^{-1}$, on the corresponding isopycnal and during the corresponding season. a) PV mapped at $27.3\sigma_\theta$, spring; b) PV mapped at $27.3\sigma_\theta$, summer; c) PV mapped at $27.3\sigma_\theta$, fall; d) PV mapped at $27.4\sigma_\theta$, spring; e) PV mapped at $27.4\sigma_\theta$, summer; f) PV mapped at $27.4\sigma_\theta$, fall; g) PV mapped at $27.5\sigma_\theta$, spring; h) PV mapped at $27.5\sigma_\theta$, summer; i) PV mapped at $27.5\sigma_\theta$, fall.

the region. The downstream SPMW evolution coincides with the directions of the branches of the NAC in Rockall Trough and the Iceland Basin (section 3.5.2). Here, we show the visual correspondence between the surface streamfunction and the direction in which the SPMW density increases. Then, to better quantify the association between the SPMW and the NAC branches, we compute the joint probability density function between the potential vorticity on each isopycnal and the estimated values of the surface streamfunction.

3.6.1 Surface circulation

The surface streamfunction computed from surface drifters drogued at 15 m (black contours in Figs. 3.9) reproduces previous results (Fratantoni, 2001; Orvik and Niiler, 2002; Reverdin et al., 2003; Niiler et al., 2003; Flatau et al., 2003). From the northwestern corner at ∼50°N, 50°W (Rossby, 1996), the NAC flows eastward at ∼50°N, crossing the North Atlantic basin. On the southeastern side of the subpolar gyre, it divides into two branches, one passing into the Rockall Trough (Rockall Trough Branch of the NAC) and the other passing into the Iceland Basin (Iceland Basin Branch of the NAC). The latter then splits into a northeastward branch, toward the Iceland-Faroe Ridge, and a southwestward branch along the eastern flank of the Reykjanes Ridge (East Reykjanes Ridge Current) (Orvik and Niiler, 2002).

To identify the location of the SPMW with respect to the NAC branches,

we superimpose the surface streamfunction on the potential vorticity field at $27.3\sigma_\theta$, $27.4\sigma_\theta$ and $27.5\sigma_\theta$ (Fig. 3.9). As mentioned in section 3.5, low potential vorticity indicates the presence of SPMW.

As described earlier (section 3.5.1), Talley (1999), using synoptic data, showed that the property front associated with the Iceland Basin branch of the NAC (Subarctic Front) was characterized by the absence of SPMW at each station within the front, while SPMW was detected in the stations next to the front. Hence, our association of SPMW with a branch of the NAC (Fig. 3.9) refers to SPMW located next to the property front. Because of the spatial and temporal averaging of the hydrographic data used to identify SPMW and of the data used for the streamfunctions, the precise relationship of SPMW to the precise current cores is necessarily smeared out. In the following, we describe the general correspondence between particular SPMWs and the currents.

The $27.3\sigma_\theta$ SPMW in Rockall Trough is located along the Rockall Trough branch of the NAC. The $27.3\sigma_\theta$ SPMW located along the western flank of the Rockall Plateau is associated with the Iceland Basin branch of the NAC (Fig. 3.9a). The minimum of PV at the western edge of the British continental shelf is marginally associated with the southern part of the Rockall Trough branch of the NAC. However here the error in the computation of the surface streamfunction is quite large (50%) and therefore might bias the direction of the streamlines.

The $27.4\sigma_\theta$ SPMW (Fig. 3.9b) is also located along the Iceland Basin and the Rockall Trough branches of the NAC. Moreover, the position of the $27.4\sigma_\theta$ SPMW is slightly downstream of the lighter $27.3\sigma_\theta$ SPMW, suggesting that the

former is derived from the latter.

The densest SPMW considered ($27.5\sigma_\theta$) (Fig. 3.9c) is associated with the Iceland-Faroe Front and the East Reykjanes Ridge Current. The $27.5\sigma_\theta$ SPMW along the Iceland-Faroe Ridge is probably derived from two distinct branches of the $27.4\sigma_\theta$ SPMW (Iceland Basin and Rockall Trough) that eventually converge on the Ridge. In contrast, the $27.5\sigma_\theta$ SPMW located along the East Reykjanes Ridge Current seems to be connected to the lighter density SPMW along the weak cyclonic circulation of the western Iceland Basin that connects the Iceland Basin branch to the East Reykjanes Ridge Current and eventually to the Irminger Current.

The joint probability density function (pdf) computed along each isopycnal ($27.3\sigma_\theta$, $27.4\sigma_\theta$, $27.5\sigma_\theta$) between the PV and the surface streamfunction values confirms the visual link proposed based on Fig. 3.9. The largest values of the joint pdf for low values of PV correspond to the streamfunction values that characterize the surface currents along which SPMWs have been visually tracked (Fig. 3.10).

Thus, in contrast to the description of McCartney and Talley (1982), who hypothesized that all SPMWs are connected by a continuous cyclonic flow, we have shown that the surface eastern subpolar circulation is characterized by two strong northeastward flows that transport SPMW to the Norwegian Current and a weaker cyclonic circulation that joins part of the Iceland Basin branch of the NAC to the East Reykjanes Ridge Current. Each of the two NAC branches in the eastern subpolar gyre is characterized by progression of SPMWs with gradually

increasing density (from $27.3\sigma_\theta$ to $27.5\sigma_\theta$). Hence, the smooth SPMW connection concluded by McCartney and Talley (1982) is valid as long as we consider SPMWs belonging to each specific current. However, a broad connection of, say, the $27.3\sigma_\theta$ SPMW in the Rockall Trough with the $27.5\sigma_\theta$ SPMW of the Reykjanes Ridge (and hence the Irminger Sea) is unlikely.

The progressive sequence of SPMW along the cyclonic circulation of the Iceland Basin does not completely address the connection between the $27.5\sigma_\theta$ SPMW on the Reykjanes Ridge and the $27.4\sigma_\theta$ SPMW in the Iceland Basin. As said earlier, the presence of averaged SPMW following streamlines associated with a strong current most likely reflects synoptic SPMW located next to the front, while the synoptic front itself is characterized by absence of SPMW (Talley, 1999). Thus, the SPMWs that follow the streamlines of the Iceland basin branch up to the Iceland-Faroe Ridge are probably located on the eastern side of the NAC front. This can connect easily with the Iceland-Faroe Front SPMW, but its connection to the Reykjanse Ridge seems more problematic since the NAC front acts as property barrier. The Iceland Basin branch of the NAC bifurcates near the southeast coast of Iceland, with a lot of temporal variability (Flatau et al., 2003). Perhaps this allows an intermittent connection between the eastern and western SPMWs of the Iceland Basin.

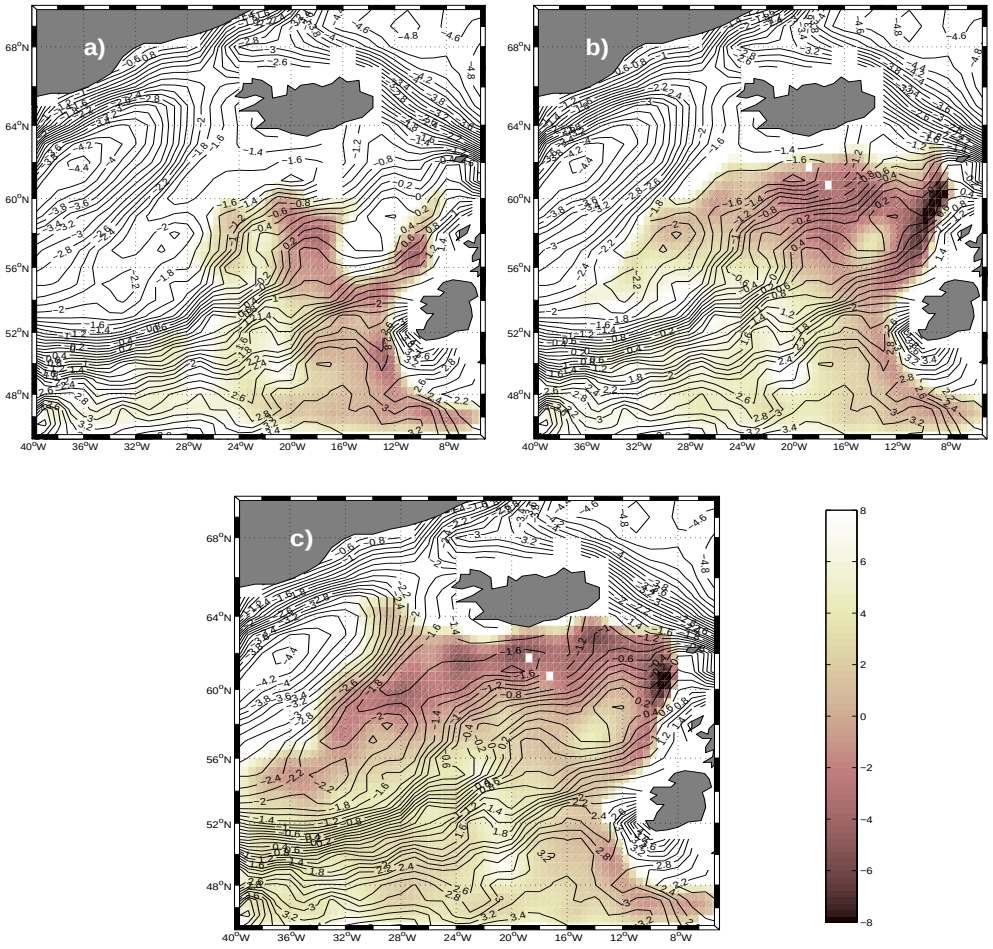

Figure 3.9: Absolute surface streamfunction (cm) based on surface drifters with Ekman removed, superimposed on the potential vorticity field ($10^{-13} cm^{-1} s^{-1}$). a) Surface streamfunction (cm), contour interval 0.2 cm, superimposed on the PV field at the $27.3\sigma_\theta$; b) Surface streamfunction (cm), contour interval 0.2 cm, superimposed on the PV field at the $27.4\sigma_\theta$; c) Surface streamfunction (cm), contour interval 0.2 cm, superimposed on the PV field at the $27.5\sigma_\theta$.

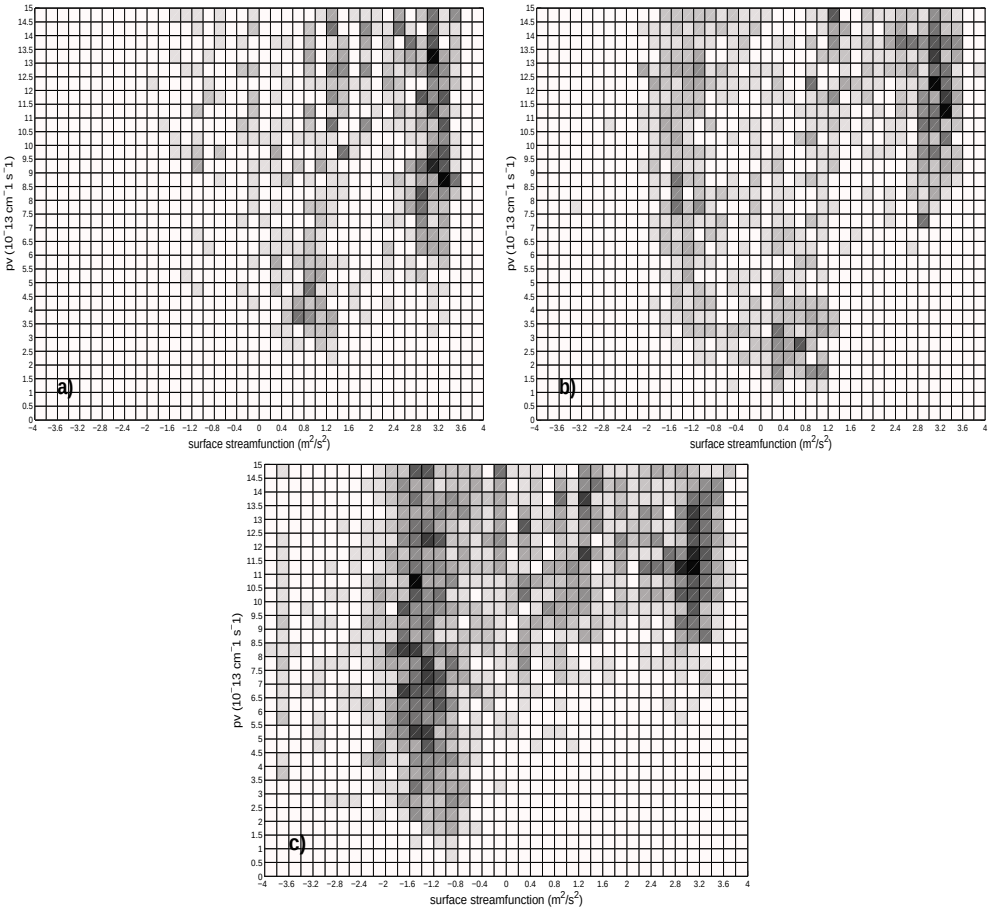

Figure 3.10: Joint probability density function (pdf) between the surface streamfunction and the potential vorticity values. The results are shown for a smaller domain than the actual computation domain, in order to focus on the lowest values of potential vorticity. a) PV at $27.3\sigma_\theta$; b) PV at $27.4\sigma_\theta$; c) PV at $27.5\sigma_\theta$.

3.6.2 Streamfunctions on isopycnal surfaces

The surface absolute streamfunction (section 3.6.1) shows that the surface flow is predominantly northeastward, with a weak cyclonic circulation that connects the Iceland Basin branch of the NAC to the East Reykjanes Ridge Current. It could be argued that the westward diapycnal flux that departs from the Iceland Basin branch is not sufficient to provide the water mass that is part of the extended $27.5\sigma_\theta$ SPMW located on the Reykjanes Ridge. Thus, we provide a qualitative description of the subsurface circulation on the $27.3\sigma_\theta$, $27.4\sigma_\theta$, and $27.5\sigma_\theta$ to identify the isopycnal pathways and their possible contribution to SPMWs. (In Brambilla and Talley (submitted), we present a quantitative discussion.)

The hypothesis that cyclonic flow could play an important role in along-isopycnal advection is suggested by the shear that exists between the surface circulation and the circulation on the $27.5\sigma_\theta$ isopycnal (Bower et al., 2002). While the surface is dominated by northeastward flow, the $27.5\sigma_\theta$ isopycnal is characterized by a cyclonic path, with no apparent northeastward flow, that could provide water to the SPMW on the Reykjanes Ridge.

As mentioned in section 3.3.3, because of the good spatial distribution of the surface drifters, we used them as the primary reference velocity for streamfunctions on underlying isopycnals (Fig. 3.11). The isopycnal streamfunctions thus obtained are then also compared with the absolute streamfunction computed using the $27.5\sigma_\theta$ floats as the reference velocity.

The circulation at $27.3\sigma_\theta$ relative to the surface drifters (Fig. 3.11a) is mostly northeastward, resembling the surface circulation since this isopycnal is quite shallow. The northeastward Rockall Trough and Iceland Basin branches of the NAC, where the $27.3\sigma_\theta$ SPMW is present, are well represented. The isopycnal outcrops before reaching the Irminger Sea. The streamfunction referenced to the $27.5\sigma_\theta$ floats shows similar features in the Iceland Basin; however, due to the lack of data, it does not show the Rockall Trough branch of the NAC (Fig. 3.11b).

The streamfunction at $27.4\sigma_\theta$ relative to surface drifters (Fig. 3.11c) tracks the Rockall Trough branch of the NAC, the Iceland Basin branch of the NAC, and the flow over the Iceland-Faroe Ridge, corresponding well with the location of the $27.4\sigma_\theta$ SPMW. The absence of streamlines on the Rockall Plateau is due to intersection of this isopycnal with this topographic features. Streamlines appear also in the Irminger Sea. One continuous streamline runs cyclonically connecting the western flank of the Rockall Plateau to the eastern flank of the Reykjanes Ridge.

On the $27.5\sigma_\theta$ surface, the connection between the Rockall Trough and the Iceland Basin branches of the NAC with the Iceland-Faroe Front is less evident, while the cyclonic circulation in the Iceland Basin is more clearly represented. Moreover, we observe that the depth of this isopycnal is large in the center of the Iceland Basin, and then shoals westward toward the Reykjanes Ridge. On the Reykjanes Ridge, this isopycnal is shallower than the depth of the remnant winter mixed layer (Fig. 3.2a), suggesting that the $27.5\sigma_\theta$ isopycnal outcrops in this region.

Thus, we have shown that the surface northeastward flow tends to weaken on denser isopycnal ($27.5\sigma_\theta$), while the cyclonic flow in the Iceland Basin appears to be stronger. The cyclonic flow along the $27.5\sigma_\theta$ isopycnal, therefore, might play an important role in providing the water forming the $27.5\sigma_\theta$ SPMW on the Reykjanes Ridge, but it cannot be considered fully responsible for the connection between the SPMW along the Iceland Basin branch of the NAC and the SPMW on the Reykjanes Ridge (see section 3.6.1).

Figure 3.11: Absolute streamfunction (gray contour, cm) at: a),b) $27.3\sigma_\theta$; c),d) $27.4\sigma_\theta$; e),f) $27.5\sigma_\theta$. On each panel the background is the depth (m) of the corresponding isopycnal. White dots correspond to the location of the SPMW identified as low potential vorticity. In the left panels, the absolute streamfunction is the pressure anomaly streamfunction computed with respect to the surface drifter streamfunction; in the right panels, the absolute streamfunction is the pressure anomaly streamfunction computed with respect to the $27.5\sigma_\theta$ float streamfunction.

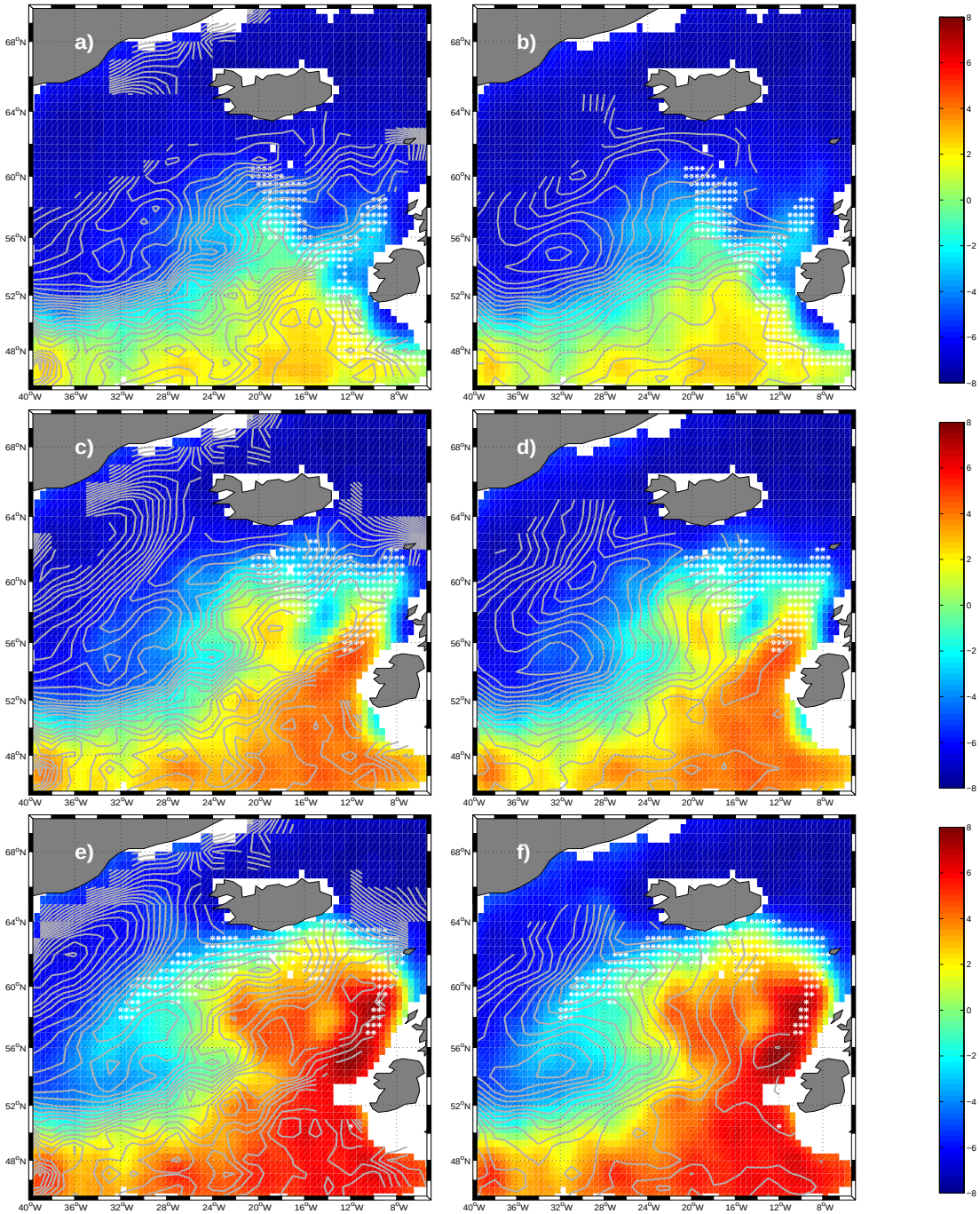
a)
b)
c)
d)
e)
f)
68°N
64°N
60°N
56°N
52°N
48°N
40°W
36°W
32°W
28°W
24°W
20°W
16°W
12°W
8°W
8
6
4
2
0
−2
−4
−6
−8

3.7 Summary and conclusions

In this first part of our two-part study of eastern North Atlantic Subpolar Mode Waters, we focus on properties, relation to the winter mixed layer, locations, and links with the major currents, including two branches of the NAC. We conclude that 1) SPMWs are surface water masses confined between the ocean surface and the permanent pycnocline; 2) they can be tracked along each of the various branches of the NAC in the eastern subpolar gyre; 3) the NAC branches of the northeastern Atlantic do not create a cyclonic pathway connecting the lightest to the densest SPMW, in contrast to the hypothesis of McCartney and Talley (1982); 4) the SPMWs continuously increase in density as long as we restrict the SPMWs to those of the same current branch; 5) the $27.5\sigma_\theta$ SPMW located on the Reykjanes Ridge has different properties from the $27.5\sigma_\theta$ SPMW on the Iceland-Faroe Ridge. While the latter can result from the progressive densification of the $27.3\sigma_\theta$ and $27.4\sigma_\theta$ SPMW along the Iceland Basin branch of the NAC, the $27.5\sigma_\theta$ SPMW is unlikely connected with the SPMWs along the Iceland Basin branch of the NAC because of the property barrier that this front could cause.

With respect to (1), SPMWs in the eastern subpolar gyre remain within the remnant of the winter mixed layer, unlikely STMW. This is expected from general upwelling driven by wind-stress curl in the subpolar gyre. However, since in the accompanying paper (Brambilla and Talley, submitted) the subpolar gyre appears to be a region of water mass "subduction" as estimated from convergence of diapycnal volume flux, it is necessary to state this basic observation of the

vertical distribution of SPMW.

With respect to (2), identifying SPMW with the minimum of PV, the regions of the eastern subpolar gyre where SPMW is present (Rockall Plateau, southern Iceland-Faroe Ridge, northwestern Reykjanes Ridge) and absent (NAC, northern side of the Iceland-Faroe Front, East Greenland Current) have been located.

On isopycnals that intersect the eastern SPMWs ($27.3\sigma_\theta$, $27.4\sigma_\theta$, and $27.5\sigma_\theta$), the absolute streamfunction and potential vorticity field show how SPMWs are associated with the subpolar gyre currents. (SPMW is not present at the actual property front associated with the currents, but just next to it (Talley, 1999).)

A primary conclusion is that SPMWs are not distributed along a cyclonic flow around the subpolar gyre but instead proceed mainly northeastward, following the Iceland Basin and Rockall Trough branches of NAC. Each of the several branches of the NAC is characterized by SPMW with density increasing smoothly downstream. Along the Iceland Basin branch of the NAC, a progression from $27.3\sigma_\theta$ SPMW to $27.4\sigma_\theta$ SPMW and then $27.5\sigma_\theta$ is found, ultimately feeding the SPMW at the Iceland-Faroe Front. The same sequence is found along the Rockall Trough branch of the NAC.

The surface streamfunction also shows a weaker cyclonic circulation in the Iceland Basin that connects the Iceland Basin branch of the NAC to the East Reykjanes Ridge Current. This path is characterized by a sequence of $27.3\sigma_\theta$ and $27.4\sigma_\theta$ SPMW along the Iceland Basin branch of the NAC, however the connection between these two lighter SPMWs and the $27.5\sigma_\theta$ SPMW on the Reykjanes Ridge

is unlikely because of the property barrier provided by the Iceland Basin branch of the NAC (Talley, 1999). On the other hand, the variability in time and intensity of the Iceland Basin branch front and its bifurcation at Iceland (Flatau et al., 2003) might permit a connection between the SPMW of the Iceland Basin branch of the NAC and SPMW on the Reykjanes Ridge. In addition, the subsurface flow, which becomes increasingly cyclonic as density increases from $27.3\sigma_\theta$ to $27.5\sigma_\theta$ (as also shown by Bower et al. (2002)) might also play an important role in supplying the water that forms the Reykjanes Ridge SPMW (McCarney, personal communication). A detailed discussion of the transformation and formation of SPMWs that addresses this and other issues is presented in the accompanying paper (Brambilla and Talley, submitted).

3.A Appendix: Objective mapping

The objective mapping technique allows the computation of a regular spaced field from irregularly spaced measurements (Bretherton et al., 1976). Each irregularly spaced measurement is proportional to the regularly spaced estimate multiplied by an assigned weight that minimizes the error between the true field and the regularly spaced field:

$$\widehat{y} = \alpha^T x \tag{3.A.1}$$

where $\widehat{y}$ is the vector of estimated regularly spaced data, x is the vector of real measurements, α is the factor of proportionality and the upper symbol ^{T} indicates

the transpose matrix. The mean square error between the estimated field and the true one can be written as

$$< \epsilon^2 >=< (\widehat{y} - y)^2 >=< (\alpha^T x - y)^2 > . \tag{3.A.2}$$

From (3.A.2) the minimum of the mean square error is computed

$$\frac{\partial}{\partial \alpha} < \epsilon^2 >= 2 < xx^T > \alpha - 2 < 2xy >, \tag{3.A.3}$$

and using (3.A.3), we can obtain the proportionality factor:

$$\alpha =< xx^T >^{-1} \cdot < xy > . \tag{3.A.4}$$

In addition to the computation of regularly spaced fields for scalar quantities (density, depth, etc.), in this study we applied the objective method to compute the streamfunction of the flow from velocity measurements (Bretherton et al., 1976; Davis, 1998, 2005; Gille, 2003). We rewrite (3.A.1) changing the name of the variables

$$\widehat{\psi} = \alpha^T \Phi \tag{3.A.5}$$

where $\widehat{\psi}$ is the estimated streamfunction field $\widehat{\psi} = [\widehat{\psi_1}.....\widehat{\psi_M}]$, α is the factor of proportionality, Φ is the velocity vector that includes both u and v components, $\Phi = [u_1.....u_N v_1.....v_N]$. The equation for α becomes:

$$\alpha = (< \Phi\Phi^T >)^{-1} \cdot < \Phi\widehat{\psi} > \tag{3.A.6}$$

where $< \Phi\Phi^T >$ is the covariance matrix of the velocity vectors dimensioned 2N by 2N, and $< \Phi\widehat{\psi} >$ is the covariance matrix of the streamfunction and the velocity vector dimensioned 2N by M.

From (3.A.5) it appears clear that, by computing the covariance matrix for the velocity vectors and the covariance matrix for the streamfunction and the velocity vector, we can obtain the estimate of the streamfunction field that minimizes the mean square error between $\widehat{\psi}$ and ψ_{true}.

The covariance matrices used in (3.A.6) can be derived assuming that the covariance matrix for the streamfunction $< \widehat{\psi(x,y)}\psi(x+\widehat{r,}y+s) >= C(\rho)$, where $\rho^2 = r^2 + s^2$ is the radial distance, is known; and that the velocity field is nondivergent so that:

$$u = -\frac{1}{f}\frac{\partial \psi}{\partial y} \quad and \quad v = \frac{1}{f}\frac{\partial \psi}{\partial x}. \tag{3.A.7}$$

Using (3.A.7)

$$\begin{aligned} < \Phi\Phi^T > &= \frac{1}{f^2}\begin{bmatrix} < u,u > & < u,v > \\ < v,u > & < v,v > \end{bmatrix} = \\ &= \frac{1}{f^2}\begin{bmatrix} < -\frac{\partial\widehat{\psi}(x,y)}{\partial y}, -\frac{\partial\widehat{\psi}(x+r,y+s)}{\partial y} > & < -\frac{\partial\widehat{\psi}(x,y)}{\partial y}, \frac{\partial\widehat{\psi}(x+r,y+s)}{\partial x} > \\ < \frac{\partial\widehat{\psi}(x,y)}{\partial x}, -\frac{\partial\widehat{\psi}(x+r,y+s)}{\partial y} > & < \frac{\partial\widehat{\psi}(x,y)}{\partial x}, \frac{\partial\widehat{\psi}(x+r,y+s)}{\partial x} > \end{bmatrix} = \\ &= \frac{1}{f^2}\begin{bmatrix} -\frac{\partial^2}{\partial s^2}C(\rho) & \frac{\partial^2}{\partial s\partial r}C(\rho) \\ \frac{\partial^2}{\partial r\partial s}C(\rho) & \frac{\partial^2}{\partial r^2}C(\rho) \end{bmatrix} \end{aligned} \tag{3.A.8}$$

Accordingly,

$$< \Phi\widehat{\psi} >= \frac{1}{f}\begin{bmatrix} < u,\widehat{\psi} > \\ < v,\widehat{\psi} > \end{bmatrix} = \frac{1}{f}\begin{bmatrix} < -\frac{\partial\widehat{\psi}(x,y)}{\partial y},\widehat{\psi} > \\ < \frac{\partial\widehat{\psi}(x,y)}{\partial x},\widehat{\psi} > \end{bmatrix} = \frac{1}{f}\begin{bmatrix} -\frac{\partial}{\partial s}C(\rho) \\ \frac{\partial}{\partial r}C(\rho) \end{bmatrix} \tag{3.A.9}$$

The observed velocity field most likely does not respect the assumption of nondivergence on which this method is based. However, if the divergent component

is small and randomly distributed in the domain, we can consider the divergent component simply as the noise on the non-divergent field and we can still apply this technique. Including the noise due to the divergent component, (3.A.6) becomes

$$\alpha = (< \Phi\Phi^T > -\epsilon I)^{-1} \cdot < \Phi\widehat{\psi} > \tag{3.A.10}$$

where ϵ is the noise and I is the identity matrix.

Finally, we compute the square error in $\widehat{\psi}$

$$\frac{(\widehat{\psi} - \psi)^2}{\psi^2} = 1 - \frac{< \Phi\widehat{\psi} > (< \Phi\Phi^T > -\epsilon I) < \Phi\widehat{\psi} >^T}{diag(\Phi\widehat{\psi})}. \tag{3.A.11}$$

In the calculation of the streamfunction described in this paper we used the mean velocity field from drifter and float measurements and we apply the following covariance function

$$C(\rho) = [1 + \frac{\rho}{\rho_0}]e^{(-\frac{\rho}{\rho_0})}. \tag{3.A.12}$$

3.B Appendix: Mean velocity field from float measurements

The mean velocity field from subsurface float measurements is computed taking into account the steering effects of the topography on the flow (Davis, 1998; Gille, 2003) as opposed to the calculation of the mean velocity field from drifter data, where this effect has been neglected (section 3.3.3 and Brambilla and Talley (2006)).

Each float velocity is assigned to the closest point on a 1°× 1°grid (Davis,

1998; Lavender et al., 2005), but with the distance between the float measurements and the grid points defined as in Davis (1998):

$$D^2 = [(x_g - x_d)^2 + (y_g - y_d)^2] + [3\lambda \frac{H_g - H_d}{H_g + H_d}]^2 \tag{3.B.1}$$

where (x_g, y_g) are the grid coordinates and (x_d, y_d) are the observation coordinates; H_g and H_d are, respectively, the water depth at the grid point and at the observation point. $\lambda = 100km$ and acts to minimize the across-bathymetry correlation where the topographic effect is strong. The mean velocity vector at each grid point is defined as the average of the velocity measurements associated to that grid point.

References

Bersch, M., 1995: On the circulation of the northeastern North Atlantic. *Deep-Sea Res. I*, **42**, 1583–1607.

Bower, A. S., Le Cann, B., Rossby, T., Zenk, W., Gould, J., Speer, K., Richardson, P. L., Prater, M. D., and Zhang, H.-M., 2002: Directly measured mid-depth circulation in the northeastern North Atlantic Ocean. *Nature*, **419**, 603–607.

Brambilla, E., and Talley, L. D., 2006: Surface drifter exchange between the North Atlantic subtropical and subpolar gyres. *J. Geophys. Res.*, **111**, C07026. doi: 10.1029/2005JC003146.

Brambilla, E., and Talley, L. D., 2007: Subpolar Mode Water in the northeastern Atlantic. Part II: transformation and formation. Submitted.

Bretherton, F. P., Davis, R. D., and Fandry, C. B., 1976: A technique for objective analysis and design of oceanographic experiments applied to MODE-73. *Deep-Sea Res.*, **23**, 559–582.

Conkright, M. E., Antonov, J. I., Baranova, O., Boyer, T. P., Garcia, H. E., Gelfeld, R., Johnson, D., Locarnini, R. A., Murphy, P. P., O'Brien, T. D., Smolyar, I., and Stephens, C., 2002: World ocean database 2001, volume 1: Introduction. U.S. Gov. Printing Office, Wash., D.C. 167 pp.

Davis, R., 1998: Preliminary results from directly measuring middepth circulation in the tropical and South Pacific. *J. Geophys. Res.*, **103**, 24619 – 24639.

Davis, R., 2005: Intermediate-depth circulation of the Indian and South Pacific oceans measured by autonomous floats. *J. Phys. Oceanogr.*, **35**, 683–707.

de Boyer Montégut, C., Madec, G., Fisher, A., Lazar, A., and Iudicone, D., 2004: Mixed layer depth over the global ocean: An examination of profile data and profile based climatology. *J. Geophys. Res.*, **109**, C12003. doi: 10.1029/2004JC002378.

Flatau, M. K., Talley, L. D., and Niiler, P. P., 2003: The North Atlantic Oscillation, surface current velocities and SST changes in the subpolar North Atlantic. *J. Clim,*, **16**, 2355–2369.

Fratantoni, D. M., 2001: North Atlantic surface circulation during the 1990s observed with satellite-tracked drifters. *J. Geophys. Res.*, **106**(C10), 22067–22093.

Gille, S. T., 1997: Why potential vorticity is not conserved along mean streamlines in a numerical Southern Ocean. *J. Phys. Oceanogr.*, **27**, 1286–1299.

Gille, S. T., 2003: Float observations of the Southern Ocean. Part I: estimating mean fields, bottom velocities, and topographic steering. *J. Phys. Oceanogr.*, **33**, 1167–1181.

Hanawa, K., and Talley, L. D., 2001: Mode Waters. In *Ocean Circulation and Climate - Observing and Modelling the Global Ocean*, editors J. C. G. Siedler, and J. Gould, 372–386. Academic Press edition.

Kara, A. B., 2003: Mixed layer depth variability over the global ocean. *J. Geophys. Res.*, **108**(C3), 3079. doi:10.1029/2000JC000736.

Kwon, Y.-O., and Riser, S., 2004: North Atlantic Subtropical Mode Water: A history of ocean-atmosphere interaction 1961-2000. *Geophys. Res. Lett.*, **31**, L19307. doi:10.1029/2004GL021116.

Lavender, K. L., Owens, W. B., and Davis, R. E., 2005: The mid-depth circulation of the subpolar North Atlantic Ocean as measured by surface flaots. *Deep-Sea Res. I*, **52**, 767–785.

Masuzawa, J., 1969: Subtropical mode water. *Deep-Sea Res.*, **16**, 463–471.

McCartney, M. S., and Mauritzen, C., 2001: On the origin of the warm inflow to the Nordic Seas. *Prog. Oceanogr.*, **51**, 125–214.

McCartney, M. S., and Talley, L. D., 1982: The Subpolar Mode Water of the North Atlantic. *J. Phys. Oceanogr.*, **12**, 1169–1188.

McCartney, M. S., and Talley, L. D., 1984: Warm-to-cold water conversion in the northern North Atlantic. *J. Phys. Oceanogr.*, **14**, 922–935.

McClean, J. L., Poulain, P.-M., Pelton, J. W., and Maltrud, M. E., 2002: Eulerian and Lagrangian statistics from surface drifters and a high-resolution POP simulation in the North Atlantic. *J. Phys. Oceanogr.*, **32**, 2472–2491.

Niiler, P. P., 1995: Measurements of the water-following capability of holey-sock and TRISTAR drifters. *Deep-Sea Res I*, **42**, 1951–1964.

Niiler, P. P., Maximenko, N. A., and McWilliams, J. C., 2003: Dynamically balanced absolute sea level of the global ocean derived from near-surface velocity observations. *Geophys. Res. Lett.*, **30**(22), 2168. doi:10.1029/2003GL018628.

Orvik, K. A., and Niiler, P. P., 2002: Major pathways of Atlantic water in the northern North Atlantic and Nordic Seas toward Artic. *Geophys. Res. Lett.*, **29**(19), 1896. doi:10.1029/2002GL015002.

Orvik, K. A., and Skagseth, O., 2003: The impact of the wind stress curl in the North Atlantic on the Atlantic inflow to the Norwegian Sea toward the Arctic. *Geophys. Res. Lett.*, **30**(17), 1884. doi:10.1029/2003GL017932.

Perez-Brunius, P., Rossby, T., and Watts, D. R., 2004: Transformation of the warm waters of the North Atlantic from a geostrophic streamfunction perspective. *J. Phys. Oceanogr.*, **34**, 2238–2256.

Qiu, B., and Huang, R. X., 1995: Ventilation of the North Atlantic and North Pacific: Subduction versus obduction. *J. Phys. Oceanogr.*, **8**, 2374–2390.

Ralph, E., and Niiler, P. P., 1999: Wind-driven currents in the tropical Pacific. *J. Phys. Oceanogr.*, **29**, 2121–2129.

Read, J. F., 2001: CONVEX-91: Water masses and circulation of the Northeast Atlantic subpolar gyre. *Prog. Oceanogr.*, **48**, 461–510.

Reverdin, G., Niiler, P. P., and Valdimarsson, H., 2003: North Atlantic Ocean surface currents. *J. Geophys. Res.*, **108**(C1), 3002. doi:10.1029/2001JC00102.

Rossby, T., 1996: The North Atlantic Current and surrounding waters: at the crossroads. *Rev. Geophys.*, **34**, 463–481.

Rossby, T., Dorson, D., and Fontaine, J., 1986: The RAFOS system. *J. Atms. Oceanic Technol.*, **3**, 672–679.

Schmitz, W. J., and McCartney, M. S., 1993: On the North Atlantic circulation. *Rev. Geophys.*, **31**, 29–49.

Talley, L. D., 1999: Mode waters in the subpolar North Atlantic in historical data and during the WOCE period. *WOCE Newsletter*, **37**, 3–6.

Talley, L. D., 2003: Shallow, intermediate, and deep overturning components of the global heat budget. *J. Phys. Oceanogr.*, **33**, 530–559.

Talley, L. D., and McCartney, M. S., 1982: Distribution and circulation of Labrador Sea Water. *J. Phys. Oceanogr.*, **12**, 1189–1205.

Zhang, H., and Hogg, N. G., 1992: Circulation and water mass balance in the Brazil Basin. *J. Mar. Res.*, **50**, 385–420.

4

Subpolar Mode Water in the northeastern Atlantic. Part II: origin and transformation

4.1 Conspectus

The processes that lead to the transformation and formation of the eastern North Atlantic Subpolar Mode Waters (SPMW) are investigated from observational data. Air-sea flux data from the National Oceanography Center (NOC), Southampton, and hydrographic data from the A24 cruise collected during the World Ocean Circulation Experiment (WOCE) are used to estimate the contribution of diapycnal and isopycnal fluxes to SPMW transport. The surface diapycnal volume flux is the dominant source of SPMW. In the North Atlantic subpolar gyre the diapycnal volume flux occurs along the main branches

of the North Atlantic Current (NAC) and it has an average transport of 14 ± 6.5 Sv, with a maximum of 21.5 Sv across the $23.35\sigma_\theta$ isopycnal. The regional distribution of the diapycnal flux on isopycnal surfaces identifies the areas with the largest flux. These regions coincide with to the location of SPMW with corresponding density. It is also shown that the surface diapycnal flux is associated with obduction and subduction through the permanent pycnocline. Therefore, the water involved in the transformation of SPMWs is continuously exchanged with the ocean interior. The isopycnal component of the SPMW throughput is estimated from the geostrophic transport across the A24 section from Greenland to Scotland and is 10% to 40% of the diapycnal flux.

4.2 Introduction

Mode waters are water masses characterized by thick layers of nearly vertically uniform properties (potential temperature, salinity, potential density) that extend over a relatively large horizontal area (Hanawa and Talley, 2001). Masuzawa (1969) first introduced the term "Subtropical Mode Water" to refer to a thick layer of water with nearly uniform temperature (16°-18°C) in the northwestern North Pacific subtropical gyre. McCartney and Talley (1982) introduced the term "Subpolar Mode Water" to describe the mode water masses confined in the North Atlantic subpolar gyre.

SPMW constitutes the main transport of warm and salty water from low

latitudes to the dense water formation sites in the North Atlantic (e.g. McCartney and Talley, 1982; McCartney and Talley, 1984; Schmitz and McCartney, 1993; McCartney and Mauritzen, 2001). For this reason, great attention has been given to the study of these particular water masses. In the first part of our SPMW study (Brambilla and Talley, submitted), we detailed the hydrographic properties, the vertical and horizontal sites occupied by SPMWs, and the link between SPMW and the branches of the North Atlantic Current (NAC) in the subpolar gyre. Here, we investigate the major sources, processes and locations for SPMW formation.

McCartney and Talley (1982) hypothesized that SPMWs, formed during winter deep convection events, were advected by a cyclonic flow in the subpolar gyre, increasing their density along the path due to heat loss. Therefore they hypothesized that each SPMW is the source of SPMW of higher density. The hypothesis of smooth, cyclonic progression has been partially revised (e.g. Talley, 1999; Read, 2001; Perez-Brunius et al., 2004).

In Brambilla and Talley (submitted), we showed that SPMWs constitute the surface layer along each of the several branches of the North Atlantic Current (NAC). We showed that the separate Rockall Trough and Iceland Basin branches of the NAC are characterized by their own sequence of SPMWs of increasing density following the flow downstream. Since these NAC branches flow northeastward, carrying water from the Atlantic to the Norwegian Current, McCartney and Talley's (1982) concept of overall cyclonic circulation of SPMWs around the subpolar gyre is not accurate. Hence, we concluded that the origin of an SPMW with a certain density is most likely the lighter SPMW upstream as long as the

two water masses are associated with the same current.

Here, we focus on the contribution of isopycnal and diapycnal fluxes to the SPMW throughput. The isopcynal flux is simply measured in terms of geostrophic transport. The diapycnal flux is examined using the water mass transformation driven by air-sea interaction. SPMWs are the water masses that occupy the upper layer from the ocean surface to the permanent pycnocline (McCartney and Talley, 1982; Brambilla and Talley, submitted). Within this surface layer, the water masses (e.g. SPMW) are transformed by air-sea interaction (Walin, 1982). Therefore, the surface diapycnal volume flux (Walin, 1982) can be interpreted as a measurement of the SPMW transformation rate.

Estimates of water mass transformation rates in the North Atlantic have been the subject of many studies (e.g. Tziperman, 1986; Garrett et al., 1995; Garrett and Tandon, 1997; Nurser et al., 1999). Hydrographic measurements and air-sea flux data have been used to compute both the annual mean, zonally integrated meridional streamfunction (Marsh, 2000) and the basin-integrated water mass formation (Speer and Tziperman, 1992; Speer et al., 1995; Speer, 1997). Model output data (Marshall et al., 1999; Gulev et al., 2003; Valdivieso Da Costa et al., 2005) or hydrographic data combined in an inverse model method (Lumpkin and Speer, 2003) have been used for the same purpose.

In the mentioned papers, the water mass transformation rate in the North Atlantic subpolar gyre is included in the global basin-scale analysis (e.g Speer, 1997; Marsh, 2000), or it is partially represented because of data limitation at northern latitudes ($\phi > 65°$N) (e.g. Speer and Tziperman, 1992; Valdivieso

Da Costa et al., 2005). Here, we focus on the subpolar North Atlantic and the southern Nordic Seas to 75°N and compute the transformation rates for water masses characterized by potential density greater than $27\sigma_\theta$. Moreover, in addition to the basin-integrated annual mean transformation, we examine the regional distribution of the annual mean transformation for each potential density. This allows us to identify the specific areas where the transformations are more intense. Then, combining the annual mean regional distribution of the water mass transformation rates with the surface circulation based on surface drifters (Brambilla and Talley, submitted), we identify the currents that provide water to the intense transformation regions.

These estimates of water mass transformation represent the diapycnal contribution to the SPMW throughput. However isopycnal flux might also be relevant. Therefore we roughly estimate the contribution of the isopycnal flux by examining the baroclinic component of the geostrophic flow across a hydrographic transect that crosses the eastern subpolar gyre (Greenland-Scotland).

Section 4.3 describes the data and the methods used. In section 4.4, we discuss the surface water mass transformation due to air-sea fluxes. Section 4.5 describes the formation and obduction areas for specific isopycnal surfaces. In section 4.6, we examine the contribution of the isopycnal flux to SPMW transport. Section 4.7 summarizes the results.

4.3 Data and methods

4.3.1 Data

Air-sea flux and hydrographic data, along with streamfunction calculated in Brambilla and Talley (submitted). are used to investigate the water masses and the currents involved in the origin of SPMW in the northeastern Atlantic.

The air-sea flux data are from the "adjusted" air-sea flux climatology from the National Oceanography Center (NOC), Southampton. This data set represents an improved version of the original heat flux climatology from NOC (Grist and Josey, 2003). In the adjusted data set, the data have been constrained to hydrographic measurements using a mathematical inverse method to reduce the imbalance of the global mean net ocean heat flux to -5 W/m^2 (Grist and Josey, 2003). The data used in this research are monthly mean heat flux and monthly mean evaporation minus precipitation in the region 10°N - 75°N, 100°W - 20°E. Both data types are located on a regular 1°$\times$ 1°grid.

Monthly mean climatological hydrographic data are used, objectively mapped on a regular 1°$\times$ 1°grid, from the World Ocean Atlas 2001 (WOA01) (Conkright et al., 2002). Synoptic hydrographic data from the A24 cruise (May-July 1997) during the World Ocean Circulation Experiment (WOCE) are used. The WOA01 data are used in the computation of the water mass transformation rates (section 4.3.2) while the cruise data are used to compute geostrophic transport across the hydrographic section.

4.3.2 Computation of the water mass transformation and formation

a) BACKGROUND

Water mass formation in a certain density class can be computed using either a dynamic or a thermodynamic method (Marshall et al., 1999). The former measures the rate at which the water mass crosses from the surface mixed layer into the permanent pycnocline. It depends on the time variability of the mixed layer depth and the horizontal transport through the mixed layer (Marshall et al., 1993). In contrast, the thermodynamic method, used here, is based on the relation derived by Walin (1982) between water mass formation and heat fluxes. Combining heat and volume budgets, he showed that the diapycnal volume flux across an outcropping isopycnal is equivalent to the transformation of surface water mass from one certain surface density class to another density class. The convergence (divergence) of this transformation yields the water mass formation (obduction) rate.

As pointed out by Garrett et al. (1995), and later by Marshall et al. (1999), the equivalence between the diapycnal volume flux and the air-sea transformation is valid only with specific a priori assumptions. They showed that air-sea fluxes are not the only forcing involved in the water mass transformation; indeed vertical mixing processes across the base of the mixed layer act to reduce the density changes related to air-sea interaction. Because light water tends to

spread over dense water, and therefore requires a poleward diapycnal volume flux (Walin, 1982), vertical mixing is particularly important at subtropical latitudes to counteract air-sea flux that transforms water toward lighter density (Marshall et al., 1999). In the subpolar gyre, in contrast, since most of the mixing occurs by lateral flux through the almost vertical isopycnals of the mixed layer, vertical mixing can be neglected at these latitudes and the relation between diapycnal volume flux and the air-sea flux can still be applied (Nurser et al., 1999; Marsh, 2000; Valdivieso Da Costa et al., 2005; Tandon and Zhao, 2004).

As described by Tziperman (1986), surface buoyancy loss over the outcrop area of isopycnal $\sigma_\theta^{[1]}$ (where σ_θ is the mean potential density of the outcrop, and the superscript is an index of the outcrop density of the isopycnal) increases the density to a new value $\sigma_\theta^{[2]}$ ($\sigma_\theta^{[1]} > \sigma_\theta^{[2]}$). If there is also buoyancy loss within the $\sigma_\theta^{[2]}$ outcrop area, the surface water mass continues increasing its density, e.g. to a new density $\sigma_\theta^{[3]}$. If the volume leaving the $\sigma_\theta^{[1]}$ outcrop area is larger than the volume leaving the $\sigma_\theta^{[2]}$ area, there is a convergence that leads to subduction, or "formation", of the water mass with density $\sigma_\theta^{[2]}$. Following Speer and Tziperman (1992) the word "transformation" refers to the diapycnal flux at the ocean surface from one density to the next density class and so on. Given the equivalence between diapycnal volume flux and water mass transformation, the two expressions are used interchangeably. The term "formation" (obduction) is used to refer to convergence (divergence) of the water mass transformation (diapycnal flux).

Mathematically, the proportionality between air-sea flux and water mass transformation, integrated in time and space, can be written (Speer and

Tziperman, 1992):

$$\overline{F(\sigma_\theta)} = \int_{year} dt \int\int_{area} dA\delta(\sigma'_\theta(x,y,t) - \sigma_\theta) f(x,y,t). \tag{4.1}$$

$\overline{F(\sigma_\theta)}$ is the annual mean water mass transformation function (diapycnal volume flux); overbar is the annual average. The annual mean water mass transformation is a function only of the potential density. The double integral is the integral of the surface density flux $f(x,y,t)$ in the outcropping area where $\sigma_\theta = \sigma'_\theta$; δ is the delta function, where $\delta = 1$ if $\sigma_\theta = \sigma'_\theta$, otherwise $\delta = 0$. The surface density flux, $f(x,y,t)$, is defined as

$$f(x,y,t) = -\frac{\alpha H}{C_p} + \sigma_\theta(0,T)\frac{\beta(W \cdot S)}{1-S}. \tag{4.2}$$

In (4.2), $f(x,y,t)$ and all the other terms on the right hand side are functions of time and space; α and β are the thermal expansion and saline contraction coefficients ($\alpha = -\frac{\partial\rho}{\rho\partial T}$; $\beta = \frac{\partial\rho}{\rho\partial S}$); $\sigma_\theta(S,T)$ is the surface density; T and S are respectively the surface temperature and surface salinity; H is the heat flux and W is evaporation minus precipitation.

From the area-integrated annual mean transformation function, it is possible to estimate the annual mean formation function (Speer and Tziperman, 1992; Marshall et al., 1999)

$$\overline{M(\sigma_\theta)} = -\frac{\partial\overline{F}}{\partial\sigma_\theta}. \tag{4.3}$$

Note that $\overline{M(\sigma_\theta)}$ refers to the annual mean (overbar is the time mean) convergence and divergence of the transformation function integrated over the entire basin.

b) COMPUTATION

Using the data described in section 4.3.1, we first computed the surface density flux $f_{i,j,k}$ (4.2). The subscripts i, j, represent the spatial grid points, while k refers to the time dimension. To reduce the uncertainties related to the discretization in time of the data, at each grid point the monthly values of the density flux $f(x, y, t)$ have been linearly interpolated in time, with a time step $\Delta t = 1.5 days$.

Secondly, applying (4.1), we computed the annual mean transformation $\overline{F(\sigma_\theta)}$ for densities $27.05\sigma_\theta$ - $27.95\sigma_\theta$ in steps of $0.1\sigma_\theta$. These isopycnal densities outcrop in winter in our study domain (10°N- 75°N, 100°W - 20°W). Values of $\overline{F(\sigma_\theta)}$ computed for the entire North Atlantic have been shown, using different data, in several previous studies (Speer and Tziperman, 1992; Speer, 1997; Marshall et al., 1999; Valdivieso Da Costa et al., 2005).

Third, differently from the other papers, in addition to the space and time integral of the transformation function $\overline{F(\sigma_\theta)}$, we also show the regional distribution of the annual mean transformation function, $\overline{F(x, y, \sigma_\theta)}$ or $\overline{F_{i,j}(\sigma_\theta)}$. (When the annual mean transformation function is integrated over the study domain, the (x, y) variables or the (i, j) indices are omitted.) The regional distribution $\overline{F(x, y, \sigma_\theta)}$ is computed as

$$\overline{F(x, y, \sigma_\theta)} \cong \overline{F_{i,j}(\sigma_\theta)} = \frac{1}{\Delta\sigma\Delta T} \sum_{k=1}^{240} \Delta t f_{i,j,k} A_{i,j} \Pi_{i,j} (\sigma_{\theta,i,j,k} - \sigma'_\theta) \qquad (4.4)$$

where $f_{i,j,k}$ is the density flux at time k in the grid box (i, j). $A_{i,j}$ is the area of the corresponding grid box in which we are computing $\overline{F_{i,j}(\sigma_\theta)}$. $\Pi_{i,j,k}$ is the boxcar function; $\Pi_{i,j,k}$ =1 if $\sigma_{\theta,i,j,k}$ is equal to the outcrop density σ'_θ, $\Pi_{i,j,k}$ =0 otherwise. The time stepis $\Delta t = 1.5 days$. The time period over which we compute the average is $\Delta T = 1 year$. The density bin width is $\Delta\sigma = 0.1\ kg/m^3$.

The annual mean transformation function integrated over the study domain is shown in Fig. 4.1. The regional distribution of the annual mean transformation function, mapped on a regular 1°× 1°grid, is shown in Fig. 4.2. The time series of the transformation values integrated over the study domain is shown in Fig 4.5.

Finally, it is useful to visualize the spatial distribution of formation as well as transformation. The definition of formation (4.3) eliminates any spatial information because it is based on spatial integrals of transformation. However, since formation is associated with density classes and these classes have well-defined outcrops, it is useful to visualize the spatial pattern of formation based on the outcropping regions. (Discrete estimates of the formation rate calculated at each grid point, computing the derivative of the local transformation, has not been considered an adequate approach because this method is biased by the dependence of the transformation on the outcropping region. Transformation rates, by definition (4.1), are different from zero just in the outcropping region, thus the local derivative is meaningful only if two different isopycnals outcrop at the same location and at the same time, which is impossible.)

To visualize the spatial pattern of formation (Fig. 4.7 described in section

4.5), we first compute the basin-integral transformation at each time time step k:

$$M_k(\sigma'_\theta) = -[F_k(\sigma_\theta^{[2]}) - F_k(\sigma_\theta^{[1]})] \tag{4.5}$$

where $F_k(\sigma_\theta^{[1],[2]})$ refers to the basin integral transformation values at time k for $\sigma_\theta^{[1],[2]}$ and $\sigma_\theta^{[1]} < \sigma'_\theta < \sigma_\theta^{[2]}$. Then, we identify the outcropping region ($R_k(\sigma'_\theta)$) for the isopycnal σ'_θ at time k. Hence, the average value of formation (obduction) (4.5) at each grid point in the outcropping region is

$$S_{i,j,k}(\sigma'_\theta) = \frac{M_k(\sigma_{\theta'})}{R_k(\sigma'_\theta)}, \quad \forall i, j \quad \exists \quad R_k(\sigma'_\theta) \tag{4.6}$$

A map of annual formation (obduction) for each isopycnal σ'_θ is then obtained as

$$\overline{S_{i,j}(\sigma'_\theta)} = \sum_{k=1}^{240} S_{i,j,k}(\sigma'_\theta). \tag{4.7}$$

4.4 Surface water mass transformation

In McCartney and Talley (1982), updated by Brambilla and Talley (submitted), it was shown that SPMWs dominate the layer between the ocean surface and the permanent pycnocline. This surface layer is obviously affected by the air-sea fluxes (Walin, 1982; Speer and Tziperman, 1992; Marshall et al., 1999) that cause a diapycnal flux that primarily transforms SPMW from lower to lighter densities.

To estimate the diapycnal volume flux involved in the SPMW transformation and to identify the time and space frame in which SPMWs are transformed, we first show the estimates of the annual mean transformation

function $\overline{F(\sigma_\theta)}$ integrated over the study domain (10°N- 75°N, 100°W - 20°W) for densities from $27.05\sigma_\theta$ to $27.95\sigma_\theta$. Then we provide maps of the regional distribution of the annual mean transformation function $\overline{F_{i,j}(\sigma_\theta)}$. Third, we discuss the time variability of the transformation estimates, again integrated over the study domain.

4.4.1 Annual mean transformation rates

The annual mean transformation function integrated in the study domain, for densities in the range $27.05\sigma_\theta$ to $27.95\sigma_\theta$ with a density bin width of $\Delta\sigma_\theta = 0.1kg/m^3$, is shown in Fig. 4.1. The transformation values are consistent and comparable with the geostrophic transport associated with the upper limb of the meridional overturning circulation (McCartney and Talley, 1984; Krauss, 1986; Schmitz and McCartney, 1993; Schmitz, 1995; Ganachaud, 2003; Talley, 2003), confirming that diapycnal volume flux plays a dominant role in the shallow thermohaline transport (Marsh, 2000; Lumpkin and Speer, 2003). The transformation varies from a minimum of 3 Sv crossing the $27.95\sigma_\theta$ isopycnal to a maximum of 21.5 Sv crossing the $27.35\sigma_\theta$ and has an average value of 14 ± 6.5 Sv. Thus, SPMWs carry much of the transport of the diapycnal component of the shallow thermohaline circulation.

We then observe that the transformation (Fig. 4.1) is characterized by increasing transport from $27.05\sigma_\theta$ to $27.35\sigma_\theta$ and decreasing transport from

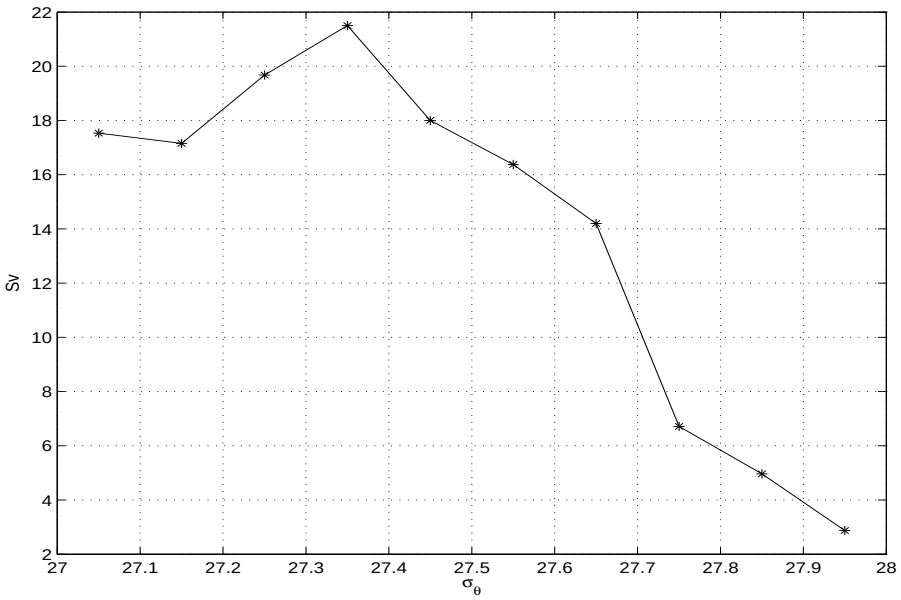

Figure 4.1: Annual mean transformation function $\overline{F(\sigma_\theta)}$ (Sv) integrated over the study domain. The computation follows Speer and Tziperman (1992). It spans the density range $27.05\sigma_\theta$-$27.95\sigma_\theta$ with a density bin width of $\Delta\sigma_\theta = 0.1\ kg/m^3$.

$27.35\sigma_\theta$ to $27.95\sigma_\theta$. As discussed in section 4.5, this requires obduction from underlying denser waters into the $27.1\sigma_\theta$, $27.2\sigma_\theta$, and $27.3\sigma_\theta$ density classes. At higher surface density, the negative slope, usually interpreted as "subduction", is likely associated with loss through entrainment by deep overflows of the Irminger Sea and the Iceland Basin, rather than by upper ocean subduction of the sort found in the subtropics.

The transformation rates are consistent with previous studies. Qiu and Huang (1995), using Levitus climatology, observed a similar obduction peak for subtropical densities. In addition, similar trends for the basin integral of the annual mean transformation function were obtained by Speer and Tziperman (1992) using the Isemer and Hasse (1987) dataset. However, since their data set did not extend to the Nordic Seas, they did not estimate annual mean transformation

for the densest water masses. Valdivieso Da Costa et al. (2005), using model data output and applying a kinematic approach, obtained a similar behavior of the basin integral of the annual mean transformation function.

4.4.2 Regional distribution of the transformation rates

To identify the origin of SPMWs characterized by particular potential densities the annual mean transformation function $\overline{F_{i,j}(\sigma_\theta)}$ is mapped on a regular $1°\times 1°$grid (Fig. 4.2). In order to track the flow involved in the transformation of a certain SPMW, we superimpose the streamlines of the surface flow computed from surface drifters from Brambilla and Talley (submitted). Each panel of Fig. 4.2 shows where the surface water of a certain density σ_θ, outcropping at the surface, changes its density toward higher or lower values driven by the air-sea heat flux. Positive (negative) values correspond to increasing (decreasing) of surface density, or in other words, to advection toward increasing (decreasing) density.

Each panel is dominated by positive (red) annual mean transformation values, suggesting that the subpolar gyre is characterized by a progressive densification of the surface layer that occurs proceeding northward through the gyre. Along the lightest isopycnals ($27.05\sigma_\theta$ - $27.35\sigma_\theta$), there are also a few locations with negative (blue) transformation rates. These are mostly located south of Cape Farvel (Greenland), on the Iceland-Faroe Ridge and at a few grid points in the Irminger Sea. Each negative value is due to the imbalance between

the local heating in spring-summer and the apparently weaker cooling that occurs in fall, which might suggest that these limited regions are characterized by a net positive buoyancy flux. However, the climatological buoyancy flux (Fig. 4.3) is negative everywhere in the domain. Thus, we attribute the small ($O(10^{-2})$ Sv) negative transformation values to uncertainties related to the computational procedure. Indeed, in addition to the winter outcrop, light densities ($27.05\sigma_\theta$ - $27.35\sigma_\theta$) outcrop also in summer at northern latitudes. At each grid location (i, j) the net transformation is the time integral of the negative density flux $f(x, y, t)$ (toward lighter density) in summer, and the positive density flux (toward greater density) in fall. However, since the ocean surface increases in density in fall more rapidly than in summer, the time discretization ($dt = 1.5$ $days$) causes an underestimate of the time integral for the fall period.

The location of largest diapycnal volume flux depends on the isopycnal, of course, and also follows the circulation tracked by the surface streamlines. The most intense transformations across the $27.05\sigma_\theta$, $27.15\sigma_\theta$, $27.25\sigma_\theta$, and $27.35\sigma_\theta$ isopycnals are located on the southern edge of the subpolar gyre and shift progressively northeastward in the Iceland Basin with increasing density (Figs. 4.2a, b, c, d). These regions are fed from the water coming from the eastward branch of the NAC, that subsequently splits into the northeastward branches through the Iceland Basin and Rockall Trough (Figs. 4.2a, b, c, d). The regions of most intense diapycnal volume flux across the $27.45\sigma_\theta$, $27.55\sigma_\theta$, $27.65\sigma_\theta$ isopycnals are located along the East Reykjanes Ridge Current, the Irminger Current and the East Greenland Current, and in the Nordic Seas along the Norwegian Current

(Figs. 4.2e, f, g).

Looking at each NAC branch, the region of intensified transformation proceeds downstream from lower to higher density. This is consistent with the progression of SPMW density along each current, as seen in Brambilla and Talley (submitted).

The Labrador Sea, Irminger Sea and Nordic Seas are characterized by intense diapycnal flux across the $27.65\sigma_\theta$ isopycnal (Fig. 4.2g), consistent with dense water formation (e.g. Pickart et al., 2003). This is further explored in section 4.5.

The regions of intense water mass transformation are associated with SPMW, identified by the minimum of potential vorticity along specific isopycnals ($27.3\sigma_\theta$, $27.4\sigma_\theta$, $27.5\sigma_\theta$). The regions of low potential vorticity identified as SPMW occupy only a limited portion of the intense transformation regions. Therefore, SPMWs participate in the shallow overturning circulation, but they might not entirely constitute it. Integrating the transformation rates across the $27.25\sigma_\theta$, $27.35\sigma_\theta$, $27.45\sigma_\theta$ isopycnals in the areas identified by the contours of low potential vorticity, we find a throughput of the $27.3\sigma_\theta$ and $27.4\sigma_\theta$ SPMW of $\sim$ 6 Sv compared with $\sim$ 19.5 Sv and 21.5 Sv overall for these densities (Fig. 4.1), while the throughput of $27.5\sigma_\theta$ SPMW is $\sim$ 8 Sv, compared with $\sim$ 18 Sv overall. This comparison clearly depends on the choice of low potential vorticity used to define the SPMW (Brambilla and Talley, submitted), but it does provide a useful approximation of the diapycnal transport for these specific SPMWs.

Figure 4.2: Regional distribution of the annual mean transformation function $\overline{F_{i,j}(\sigma_\theta)}$ (Sv). Values are plotted on a regular 1°× 1°grid. The black lines are the surface flow streamlines with a contour interval of 2cm from Brambilla and Talley (submitted). The computation extends over the entire study domain [10°N-75°N, 100°W - 20°W]. However just the portion of the domain with significant results is shown. Transformation across the isopycnals: a) 27.05σ_θ, b) 27.15σ_θ, c) 27.25σ_θ, d) 27.35σ_θ, e) 27.45σ_θ, f) 27.55σ_θ, g) 27.65σ_θ, h) 27.75σ_θ, i) 27.85σ_θ, and j) 27.95σ_θ.

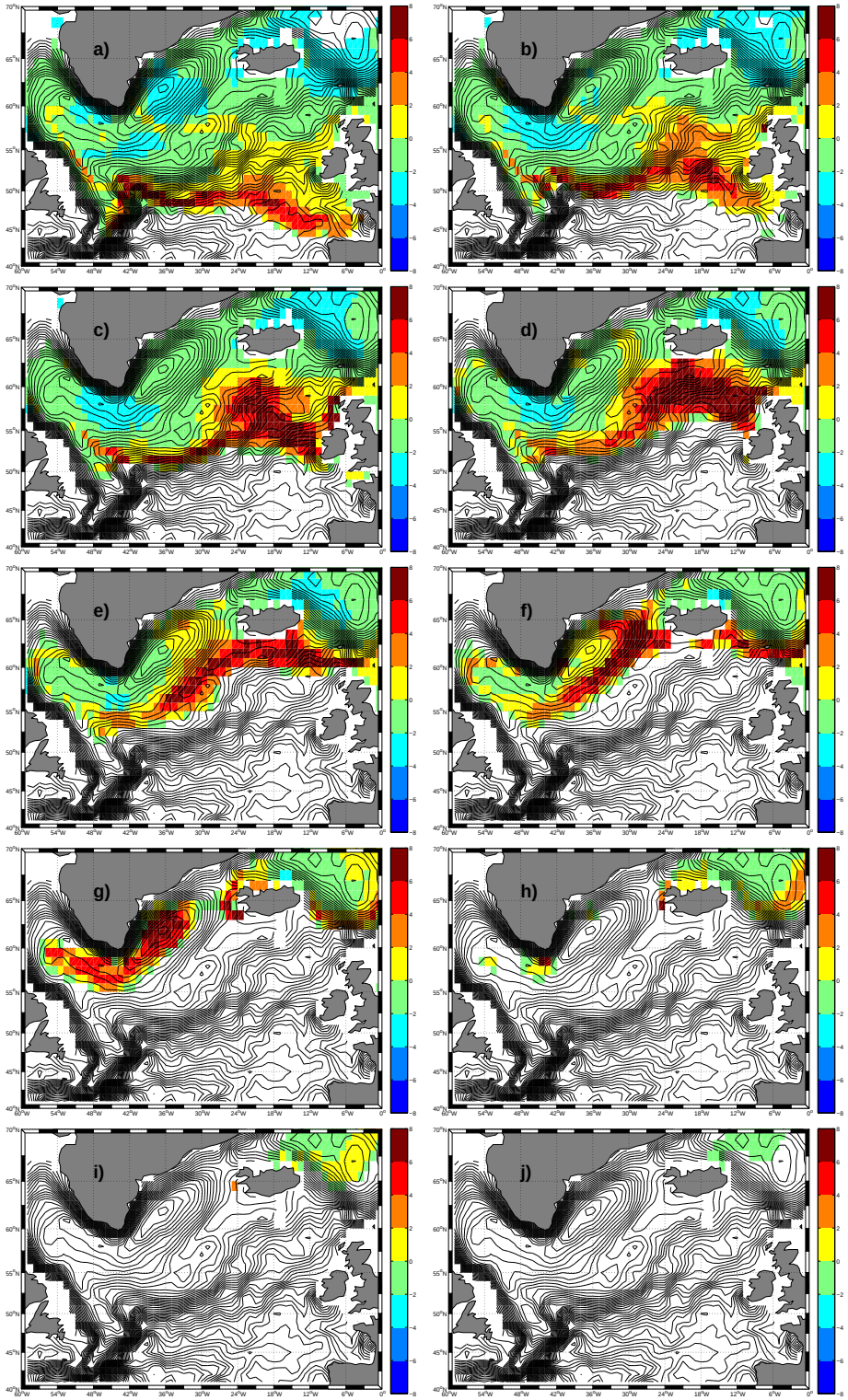
a)
b)
c)
d)
e)
f)
g)
h)
i)
j)

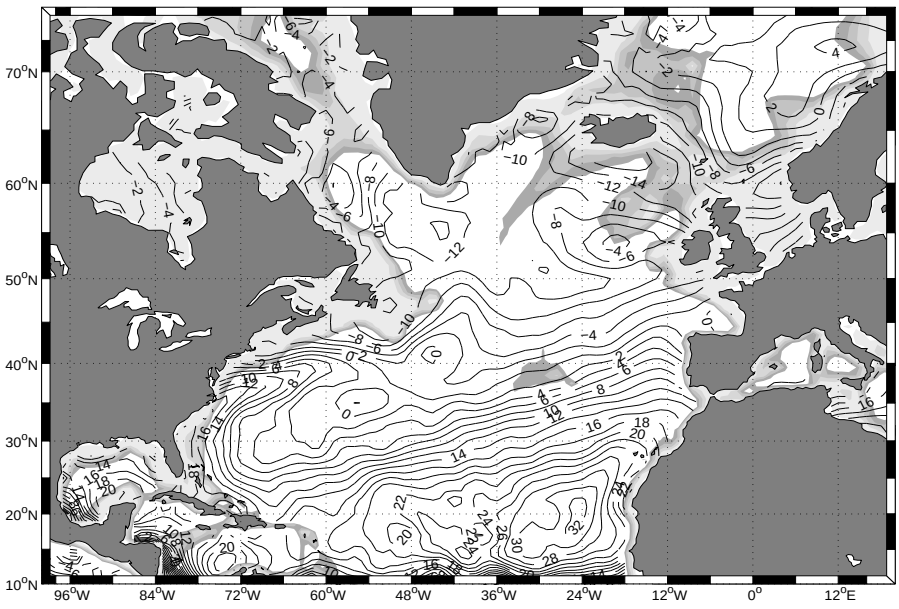

Figure 4.3: Annual mean buoyancy flux ($kgm^{-1}s^{-3}$) computed from the NOC air-sea fluxes (Grist and Josey, 2003)

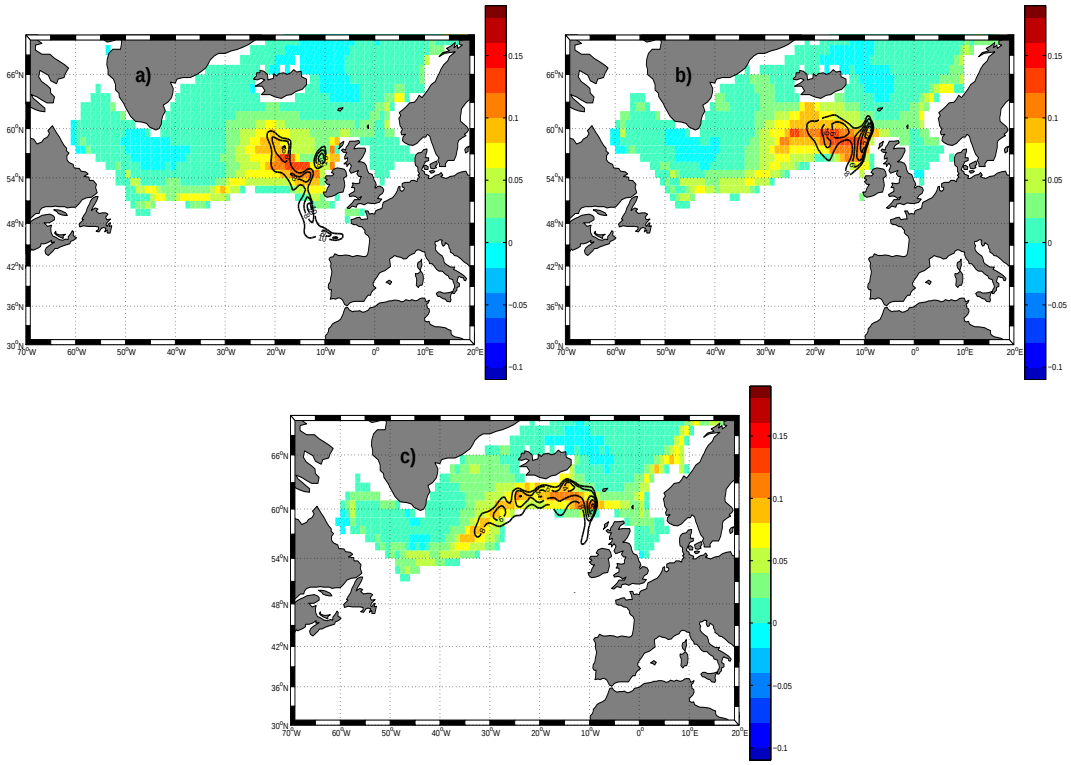

Figure 4.4: Regional distribution for the annual mean transformation function $\overline{F_{i,j}(\sigma_\theta)}$ (Sv) plotted on a regular 1°× 1°grid, as in Fig. 4.2. a) Transformation across the $27.25\sigma_\theta$ isopycnal. The black contours represent the minimum of potential vorticity computed on the $27.3\sigma_\theta$ isopycnal. The PV varies from 0 to $10\times10^{-13}cm^{-1}s^{-1}$. Contour interval is $2\times10^{-13}cm^{-1}s^{-1}$. b) Transformation across the $27.35\sigma_\theta$ isopycnal. The black contours represent the minimum of potential vorticity computed on the $27.4\sigma_\theta$ isopycnal. The PV varies from 0 to $8\times10^{-13}cm^{-1}s^{-1}$. Contour interval is $2\times10^{-13}cm^{-1}s^{-1}$. c) Transformation across the $27.45\sigma_\theta$ isopycnal. The black contours represent the minimum of potential vorticity computed on the $27.5\sigma_\theta$ isopycnal. The PV varies from 0 to $8\times10^{-13}cm^{-1}s^{-1}$. Contour interval is $2\times10^{-13}cm^{-1}s^{-1}$.

4.4.3 Temporal variability

The regional distribution of the transformation function (Fig. 4.4) showed the spatial correspondence between transformation and the location of SPMW of the same densities. Here, we investigate the temporal variability of the transformation function, using the basin integrated transformation function computed at each time step (Fig. 4.5). The temporal variability of transformation has been also shown in previous studies (e.g. Speer and Tziperman, 1992; Valdivieso Da Costa et al., 2005). However given the different data and the focus on specific isopycnals in our study, we considered this brief analysis useful to complete the discussion of SPMW transformation.

In Fig. 4.5, the sum of the time series of the estimated transformation rates corresponds to the annual transformation shown in Fig. 4.1. Positive transformations (toward higher density) occur in winter and fall when heat is lost from the ocean to the atmosphere; negative transformations (toward lighter densities) occur in late spring and summer, when heat is gained by the ocean.

The transformation that occurs during the cold months is associated with deep mixed layers and hence SPMW. In late fall, the mixed layer starts deepening and summer stratification tends to disappear. The isopycnal layer that outcrops at the surface is affected by the heat lost from the ocean to the atmosphere and is eventually transformed to another surface water mass of higher density. The new surface water mass is characterized by nearly uniform properties and corresponds to new SPMW. Thus, winter transformation dominates the diapycnal flux that

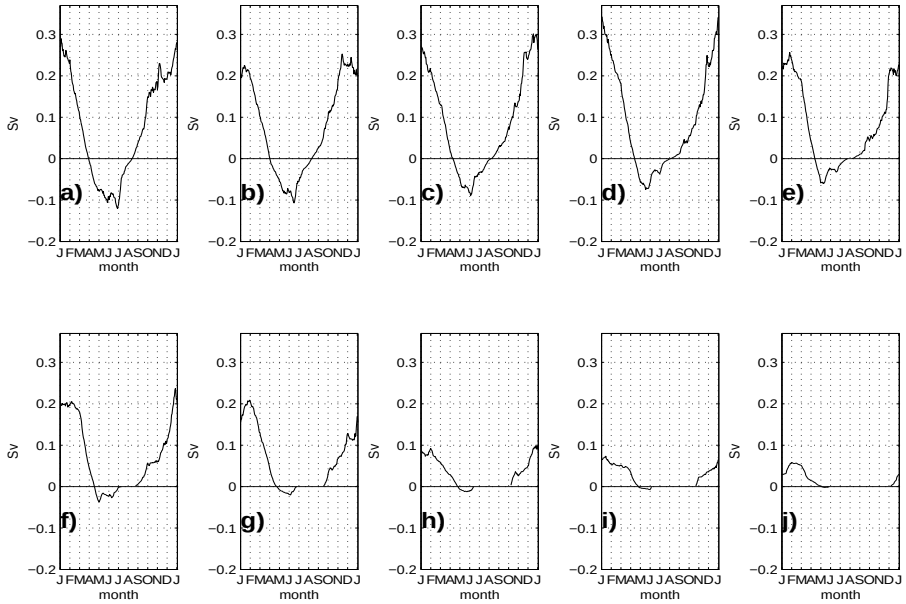

Figure 4.5: Time series of the transformation function (Sv), integrated over the study domain computed for each time $dt = 1.5days$. a) $27.05\sigma_\theta$, b) $27.15\sigma_\theta$, c) $27.25\sigma_\theta$, d) $27.35\sigma_\theta$, e) $27.45\sigma_\theta$, f) $27.55\sigma_\theta$, g) $27.65\sigma_\theta$, h) $27.75\sigma_\theta$, i) $27.85\sigma_\theta$, j) $27.95\sigma_\theta$.

creates SPMWs, as suggested by McCartney and Talley (1982).

The negative monthly values of water mass transformation (from dense to light densities) are due to the summer warming and restratification. Lighter densities ($27.05\sigma_\theta$ to $27.45\sigma_\theta$) are present at the surface in summer at more northern latitudes ($\sim 60°$N) than the winter outcrop; the denser isopycnals ($\sigma_\theta > 27.45$) outcrop just in winter in our study domain. For this reason, the negative values of the transformation rates water mass are larger at lighter densities (Fig. 4.5a, b, c, d, e) and smaller for higher density classes (Fig. 4.5f, g, h, i, j).

4.5 SPMW formation/obduction

The basin-integrated annual mean water mass transformation (Fig. 4.1) is the rate at which surface water masses change density due to air-sea fluxes. If the rates were constant for all the density classes considered, we could conclude that the densest SPMW originates, through transformation, from the lightest SPMW along an ideal pipeline completely isolated from the ocean interior. However, the transformation rate is not constant. This requires convergence or divergence, leading to formation and obduction of surface water masses that thus can affect the transport of SPMW.

We first estimate the volume of SPMW of each density class that is annually formed or obducted, by taking the derivative of the basin integral of the annual mean transformation function. Secondly, we qualitatively map formation/obduction in the $27.3\sigma_\theta$, $27.4\sigma_\theta$, $27.5\sigma_\theta$ isopycnal layers using the method described in section 4.3.2. By superimposing the absolute streamfunction of the corresponding isopycnal flow (from Brambilla and Talley (submitted)) on the formation map, it is possible to identify the paths followed by formed/obducted surface water.

4.5.1 Annual mean formation/obduction rates

The derivative of the basin-integrated annual mean transformation rates (Fig. 4.6) provides a rough approximation of the annual net production or

obduction of SPMWs (Speer and Tziperman, 1992; Nurser et al., 1999; Valdivieso Da Costa et al., 2005). Annual net obduction occurs at light densities, $\sim$ -2.5 Sv at 27.2σ_θ and $\sim$ -2 Sv at 27.3σ_θ, suggesting obduction into the mixed layer.

On the other hand, annual net water mass formation occurs at densities greater than 27.35σ_θ, suggesting that water mass transfers from the mixed layer to the ocean interior. The formation values for the 27.4σ_θ, 27.5σ_θ, 27.6σ_θ SPMWs are likely associated with entrainment of warm water into the deep overflows in both the Irminger Sea and the Iceland Basin. This interpretation is driven by the conclusion of the accompanying paper (Brambilla and Talley, submitted) that SPMW does not subduct in the eastern subpolar gyre.

In addition, in situ observations of the entrainment flux in the eastern subpolar gyre and the formation rates roughly agree. South of Iceland, Steele et al. (1962) measured deep southwestward transport of the order of 5 Sv choosing a level of no motion based on the T-S values. They pointed out that just 1.4 to 2 Sv of these 5 Sv was actual Nordic Seas overflow water, while the rest was due to entrainment of Atlantic water. Another estimate of the overflow and entrainment flux in the same region was obtained by Saunders (1996), who, using mooring measurements lasting one year, estimated that the transport south of Iceland, at $\sigma_\theta \geq 27.8$, has a mean value of 3.2 Sv with a standard deviation of 1.4 Sv. Of this, $\sim$ 1.5 Sv are Norwegian Sea water. Thus, the $\sim$ 3.5 Sv formation of the water mass at 27.4σ_θ that we compute is comparable with the upper limit of the observed entrainment rate. Analogously, in the Irminger Sea, Dickson and Brown (1994) estimated that the $\sim$ 3 Sv of Denmark Overflow Water (DOW) transport increases

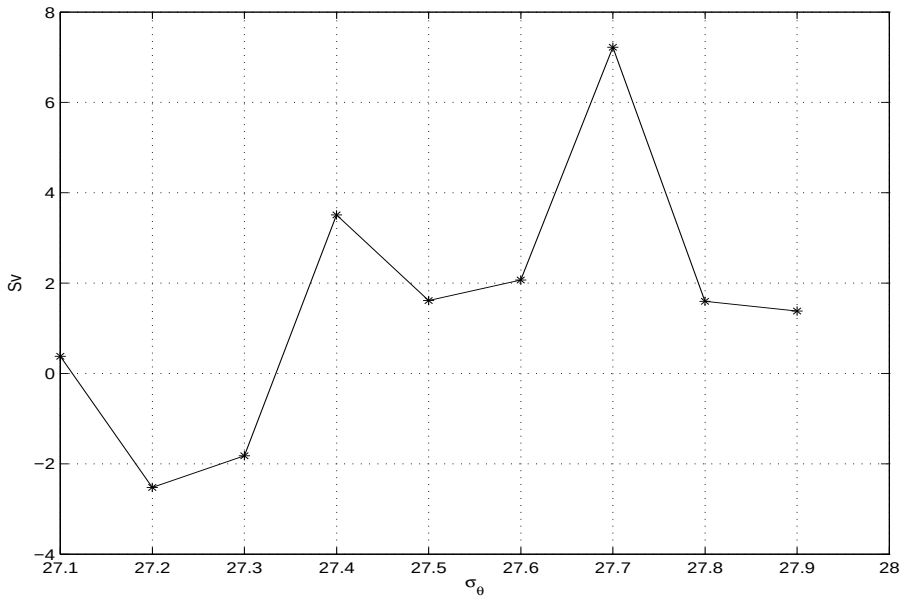

Figure 4.6: Annual mean formation function $\overline{M(\sigma_\theta)}$ (Sv) integrated over the study domain. The computation follows Speer and Tziperman (1992).

up to $\sim 5\ Sv$ in the first 160 km due to warm entrainment. Our formation rates on the order of 2 Sv for the $27.5\sigma_\theta$ and the $27.6\sigma_\theta$ SPMWs are comparable.

The larger formation rate obtained for the $27.7\sigma_\theta$ SPMW is also entrained in the dense flow that then participates in the formation of the Labrador Sea Water (LSW). The formation area of the $27.7\sigma_\theta$ SPMW in the Irminger Sea (Fig. 4.2g) is in agreement with the recent results from Pickart et al. (2003).

4.5.2 Regional distribution of the formation/obduction estimates

As explained in section 4.3.2, associating the annual formation rates integrated over the entire study domain with the corresponding outcropping areas,

we have been able to roughly represent the main regions and the spatially-averaged magnitude of the formation/obduction values on various isopycnal layers (as described in section 4.3.2). However, it should be noted that since the method is based on atmospheric data and not on direct observation of the vertical flux across the permanent pycnocline, the formation/obduction distribution maps shown here refer to processes that take place in the upper mixed layer. Therefore these maps do not identify the areas where the water is actually subducted/obducted across the permanent pycnocline. Advection within the mixed layer causes displacement between the formation regions in the mixed layer and subduction regions through the permanent pycnocline.

The isopycnal layer centered around $27.3\sigma_\theta$ (Fig. 4.7a) is characterized by relatively strong divergence in the center of the subpolar gyre, following the northeastward flow of the NAC current. This suggests that water from the ocean interior upwells into the mixed layer to replenish the loss of $27.3\sigma_\theta$ water mass. Hence, the $27.3\sigma_\theta$ water that is eventually transformed into the $27.4\sigma_\theta$ SPMW is not just part of the mixed layer but is diluted with water from the interior. Most of the divergence occurs along the main NAC and along the southern side of the Rockall Trough and Iceland Basin branches of the NAC.

The formation/obduction maps along the $27.4\sigma_\theta$ and $27.5\sigma_\theta$ isopycnal layers (Figs. 4.7b,c) differ significantly from the $27.3\sigma_\theta$ isopycnal. Both the $27.4\sigma_\theta$ and $27.5\sigma_\theta$ isopycnals are dominated by formation. The formation values on the $27.4\sigma_\theta$ isopycnal are larger than on the $27.5\sigma_\theta$ isopycnal.

Because of the limitation of these maps which cannot capture advection,

the formation areas of the $27.4\sigma_\theta$ and $27.5\sigma_\theta$ SPMW most likely do not coincide with the locations of subduction through the pycnocline. Nevertheless, the absolute streamfunctions on the $27.4\sigma_\theta$ and $27.5\sigma_\theta$ isopycnals clearly illustrate the path followed by the newly formed water masses (Figs. 4.7b,c). The $27.4\sigma_\theta$ SPMW follows both the northeastward Iceland Basin branch of the NAC and the southwestward East Reykjanes Ridge Current. The $27.5\sigma_\theta$ SPMW seems to follow the northeastward Iceland Basin branch of the NAC, the East Reykjanes Ridge Current and the Irminger Current.

Thus, we have observed that along the advection paths of each SPMW considered, not all the water transformed into a certain SPMW is subsequently transformed into a further denser one, and not all the water transformed into a denser SPMW is coming from the predecessor SPMW.

The maps shown in Fig. 4.7 cannot be directly compared with the subduction/obduction estimates computed directly at the base of the winter mixed layer by Marshall et al. (1993) and Qiu and Huang (1995). Here, in fact, we are computing the average formation/obduction in isopycnal layers represented by their winter outcrop regions. On the other hand, the sum of the formation/obduction estimates for all the outcropping isopycnal layers considered, at each grid point, might be interpreted as the subduction/obduction that occurs at the subpolar gyre surface, hence, it can be compared with Marshall et al. (1993) and Qiu and Huang (1995).

Fig. 4.8 shows the result of our exercise. The region south of $\sim 55°$N is characterized by divergence, consistent with the obduction shown by Marshall et al.

and Qiu and Huang. On the other hand, different from the mentioned results, north of $\sim 55°$N the subpolar gyre is characterized by formation. This result apparently contrasts with the expected upwelling due to the positive wind-stress curl in the subpolar North Atlantic. To the north the wind stress curl is positive and to the south it is negative, resulting in Ekman pumping and suction, respectively, which should drive obduction and subduction in these regions. However, as mentioned in section 4.5.1, formation/obduction resulting from the convergence/divergence of transformation has been associated with mass loss by entrainment, and not with classical subduction.

The major obduction region on this map is closely associated with the zero wind-stress curl. The least dense subpolar surface water is in the wind-driven obduction region and far enough from the northern sill that its mass balance is mainly affected by the wind. In contrast, the higher density surface water farther north, which is subject to wind driven obduction, actually loses mass, likely trough entrainment.

The surface density contours in March are also superimposed on Fig. 4.8. The $27.35\sigma_\theta$ isopycnal coincides with the boundary between the formation and obduction regions by definition because of the way that the maps were constructed from the basin-integrated transformations of Fig. 4.1.

Figure 4.7: Annual mean formation/obduction rates (m/year) $\overline{S_{i,j}}$ plotted on a 1°× 1°regular grid. Positive values (red) correspond to annual mean formation, negative values (blue) correspond to annual mean obduction. The formation/obduction regions do not necessarily coincide with where the subduction/obduction through the permanent pycnocline takes place because of advection within the mixed layer. a)$\overline{S_{i,j}(27.3\sigma_\theta)}$ and the streamfunction on the $27.3\sigma_\theta$ isopycnal. b)$\overline{S_{i,j}(27.4\sigma_\theta)}$ and the streamfunction on the $27.4\sigma_\theta$ isopycnal. c)$\overline{S_{i,j}(27.5\sigma_\theta)}$ and the streamfunction on the $27.5\sigma_\theta$ isopycnal. Streamfunctions are based on a surface drifter velocity reference and geostrophic shear from climatological hydrographic data (from Brambilla and Talley (submitted)).

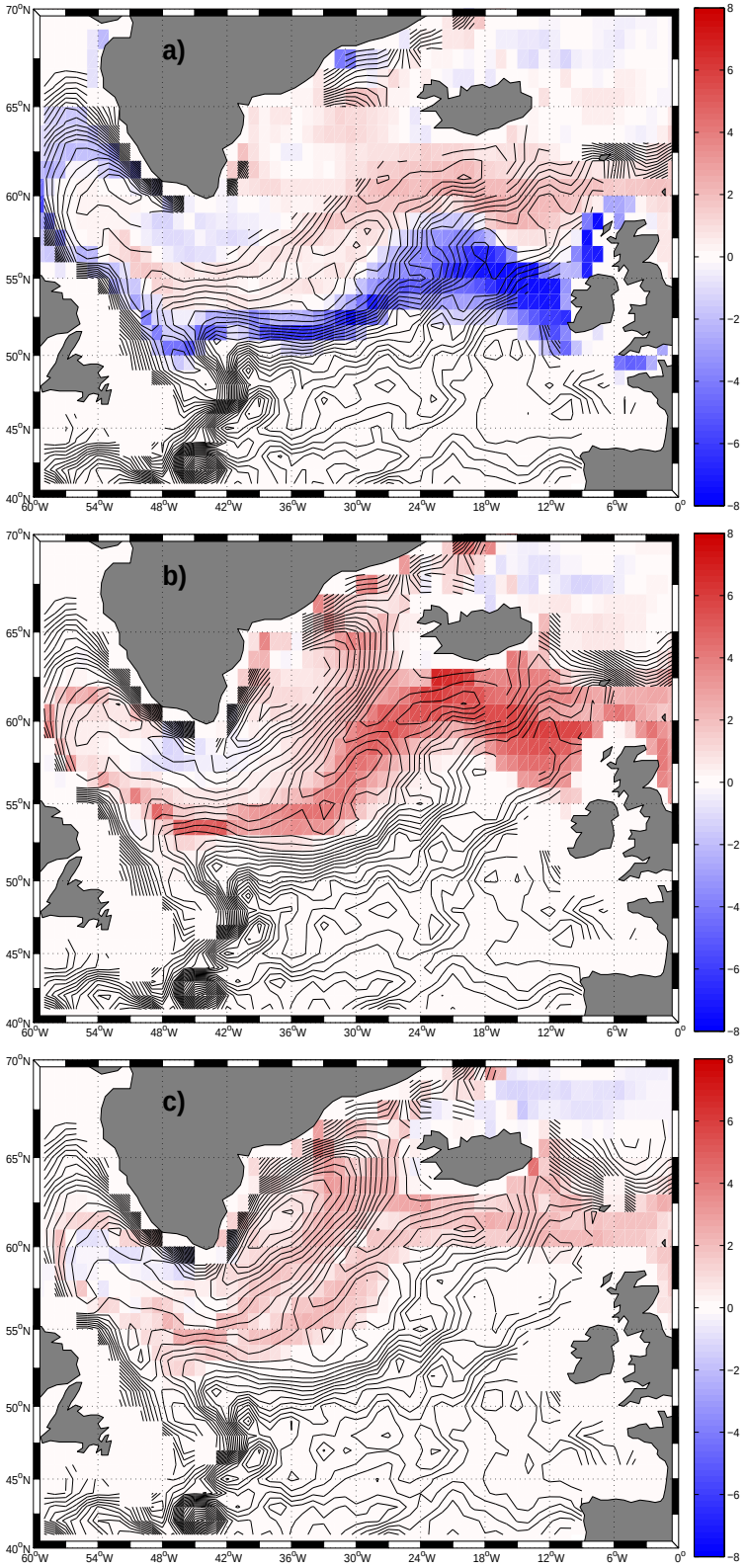
a)
b)
c)
70°N
65°N
60°N
55°N
50°N
45°N
40°N
60°W
54°W
48°W
42°W
36°W
30°W
24°W
18°W
12°W
6°W
0°
8
6
4
2
0
−2
−4
−6
−8

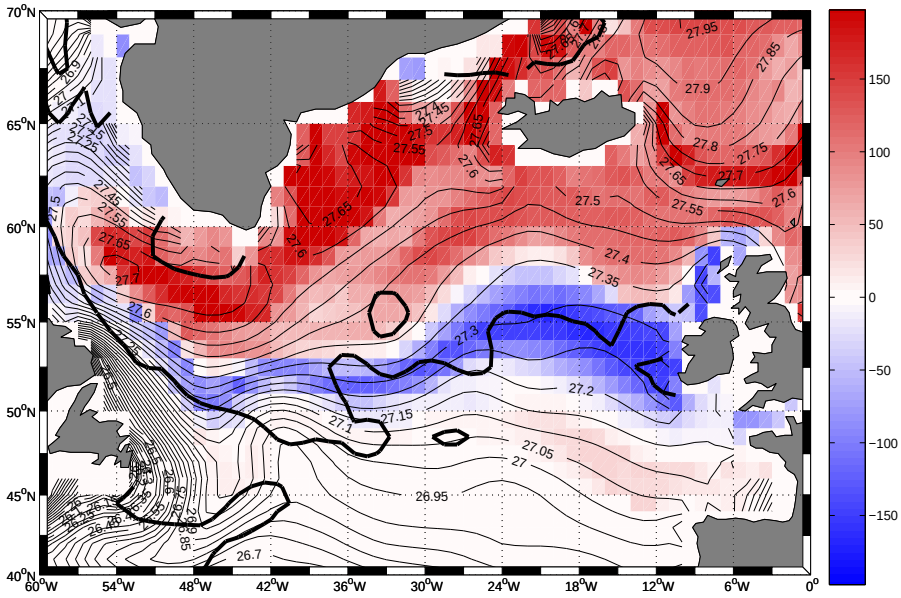

Figure 4.8: Annual mean formation/obduction rates (m/year) for densities $27.05\sigma_\theta$ - $27.95\sigma_\theta$ plotted on a 1°× 1°regular grid. Positive values correspond to annual mean formation, negative values correspond to annual mean obduction. Black thick contour is the zero wind stress curl from the NOC climatology. North of the thick black contour, the wind stress curl is positive; south of it, it is negative. Thin contours are the surface density from WOA01 climatology for March, Contour interval is $0.05kg/m^3$. No formation/obduction values are calculated for densities lighter than $27.05\sigma_\theta$ or greater than $27.95\sigma_\theta$.

4.6 Geostrophic transport

We showed in section 4.4 that the diapycnal volume flux driven by air-sea interaction causes the transformation of SPMW density. However the diapycnal volume flux might not be the only source of SPMW. Hence, we need to estimate the isopycnal flux contribution to SPMW. This consists of subsurface water on a given SPMW isopycnal that enters the SPMW region from the south and then joins the layer of newly formed SPMW that results from diapycnal transformation of less dense SPMW.

To estimate the isopycnal flux, we compute the baroclinic component of the geostrophic transport across the A24 WOCE hydrographic section from 1997 that crosses the eastern North Atlantic subpolar gyre from Greenland to Scotland, concentrating on the SPMW layer (Fig. 4.9a). The geostrophic transport is computed as a function of the potential density. The water column is divided in 29 layers between $27.25\sigma_\theta$ and $27.975\sigma_\theta$. Each layer has a constant density width of $0.025kg/m^3$. To these we add the upper layer between the ocean surface and the $27.25\sigma_\theta$ isopycnal. We have not carried out a full analysis of reference velocities for the geostrophic flow. We find that by examining results from a range of choices of a level of no motion, we obtain enough information to constrain our estimate of isopycnal transport.

Geostrophic transport with a level of no motion at 800m is shown for illustration in Fig. 4.9b. This choice allows a correct resolution of the dense water transport, which is southward and roughly balances the northward flow. (The total

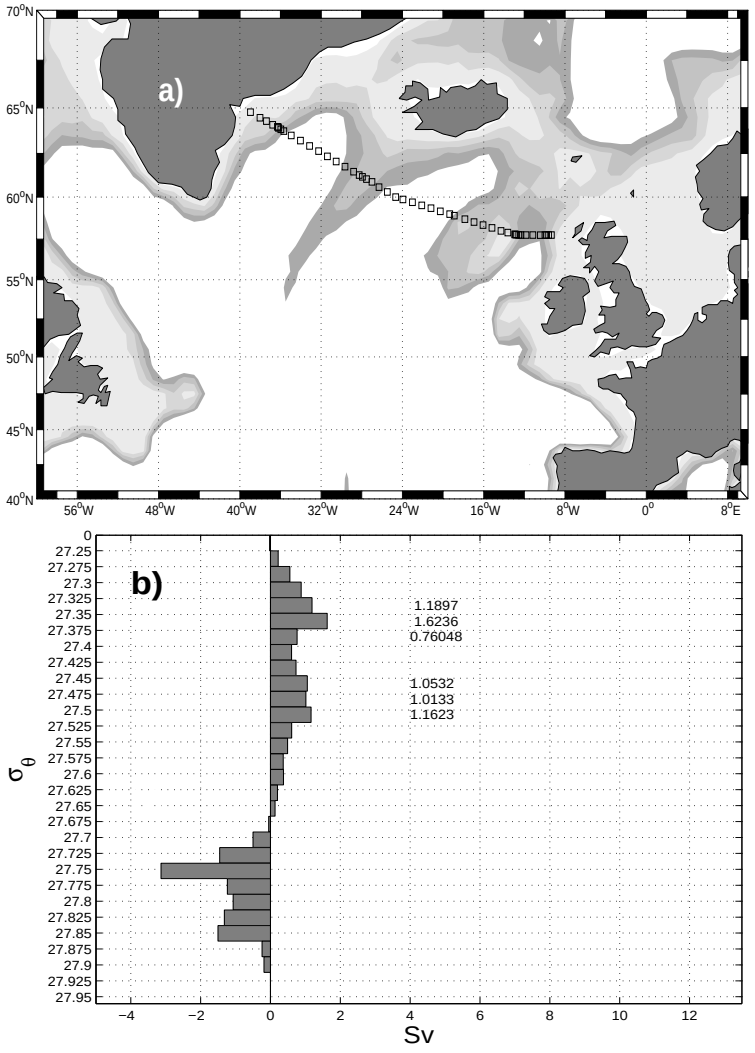

Figure 4.9: Geostrophic transport (Sv) measured across the A24 WOCE section. a) Location of the transect. Bathymetry is shaded. Darkest contour is 2000m, lightest contour is 10m. Contour interval is 500m. b) Geostrophic transport with level of no motion at 800m.

transport across the section with this choice is ∼1 Sv.) The real flow across this section likely has significant barotropic structure coupled with bottom-intensified, southward overflow. Despite the unrealistic level of no motion, this calculation is useful to describe the features of the shallow flow, characterized by two peaks of northward transport centered around $27.35\sigma_\theta$ and $27.475\sigma_\theta$. A different choice of level of no motion, although affecting the structure of the dense flow ($\sigma_\theta > 27.675$) and the net transport, does not cause any significant change in this shallow structure.

The transport associated with each of these peaks varies from a minimum on the order of 3 Sv, obtained with a level of no motion at 800m, to a maximum on the order of 8 Sv, obtained with a level of no motion at the bottom (not shown). These values represent 10%-40% of the basin-integrated diapycnal flux, thus suggesting that the diapycnal flux dominates SPMW transformation, and that the isopycnal flux is less than half of the diapycnal component.

4.7 Summary and conclusions

SPMWs are the thick surface water masses of the subpolar North Atlantic. Thus they constitute the surface layer affected by air-sea interaction. Therefore, we have considered it useful to study the transformation of SPMW in terms of the surface water mass transformation as described by Walin (1982) and Speer and Tziperman (1992). Different from the many previous studies of North Atlantic water mass transformation (Tziperman, 1986; Garrett et al., 1995; Garrett and Tandon, 1997; Nurser et al., 1999; Marsh, 2000; Speer and Tziperman, 1992; Speer et al., 1995; Speer, 1997; Marshall et al., 1999; Gulev et al., 2003; Valdivieso Da Costa et al., 2005), we presented the regional distribution of the annual mean transformation function on isopycnals, to localize the regions where SPMWs of various densities are transformed.

The estimates of the basin-integrated annual mean transformation, in agreement with previous studies and the transport of the upper limb of the meridional overturning circulation (McCartney and Talley, 1984; Krauss, 1986; Speer and Tziperman, 1992; Schmitz and McCartney, 1993; Schmitz, 1995; Ganachaud, 2003; Talley, 2003), varies from 21.5 Sv at 27.35σ_θ to 3 Sv at 27.95σ_θ. The average is 14$\pm$6.5 Sv. The regional distribution of the annual mean transformation function shows a very good correspondence between the intense transformation regions across the 27.25σ_θ, 27.35σ_θ, and 27.45σ_θ and the locations of the 27.3σ_θ, 27.4σ_θ, and 27.5σ_θ SPMWs, identified as low potential vorticity. However, we also observed that SPMWs are not as extended as the transformation

regions. It has been estimated that just ~ 6 Sv are associated with the the $27.3\sigma_\theta$ and $27.4\sigma_\theta$ SPMW, instead of the ~ 19.5 and 21.5 Sv estimated across the $27.25\sigma_\theta$ and the $27.35\sigma_\theta$ isopycnals. Analogously, the throughput of the $27.5\sigma_\theta$ SPMW is on the order 8 Sv, while the diapycnal flux across the $27.45\sigma_\theta$ isopycnals is ~ 18 Sv. Thus, we confirm the hypothesis of SPMWs as the link from the warm and salty water coming from the subtropical gyre to the dense water formed in the Labrador Sea and the Nordic Seas (e.g. McCartney and Talley, 1982; McCartney and Talley, 1984; Schmitz and McCartney, 1993; McCartney and Mauritzen, 2001), but they might not constitute the entire transport.

In addition, the analysis of the time series of the basin integrated transformation rates shows that the period from late fall through winter is characterized by the maximum transformation values. Therefore, we conclude that most of the diapycnal flux that creates the SPMWs occurs in winter, as already suggested by McCartney and Talley (1982).

The smooth density progression of the surface water masses transformed by air-sea flux confirms that a certain SPMW characterized by a specific density can be generally interpreted as the source and the predecessor of denser and lighter SPMW, in agreement with McCartney and Talley (1982). However, important constraints should be added to this statement, as follows.

1) The source/product chain for SPMW transformation is associated the current branch along which the SPMW is present (Brambilla and Talley, submitted). Transformation of the $27.2\sigma_\theta$ SPMW up to the $27.5\sigma_\theta$ SPMW, measured as the diapycnal flux across the 27.15-$27.45\sigma_\theta$ isopycnals, occurs along both the Rockall

Trough and the Iceland Basin branches of the NAC. The transformation from the $27.5\sigma_\theta$ SPMW up to the $27.7\sigma_\theta$ SPMW occurs along the East Reykjanes Ridge Current, the Irminger Current, and the East and West Greenland Currents.

2) The transport of a given SPMW along the corresponding isopycnal is characterized by subduction and obduction events along its path. Thus, in the overestimating possibility in which SPMW are defined as the entire outcropping region for a given density class, it is not correct to imagine the transformation of SPMW along an ideal pipeline along which the entire SPMW of a certain density becomes the SPMW with higher density value, contrary to McCartney and Talley's (1982) hypothesis. We have shown that the $27.3\sigma_\theta$ SPMW includes water upwelled from the interior to the surface layer. The $27.4\sigma_\theta$ and $27.5\sigma_\theta$ SPMW are instead characterized by downwelling into the ocean interior, occurring along both the northeastward flow from the Iceland Basin and Rockall Trough to the Iceland-Faroe Ridge, and along the East Reykjanes Ridge Current. In light of the results described in the companion paper (Brambilla and Talley submitted), where SPMW is observed within the mixed layer and not subducted into the interior, and the agreement with the North Atlantic entrainment rates reported in previous studies (e.g. Steele et al., 1962; Dickson and Brown, 1994; Saunders, 1996), the SPMW formation has been interpreted as water mass loss by entrainment into the deep overflows of the Irminger Sea and the Iceland Basin.

3) Finally, although the diapycnal volume flux is a dominant source of SPMWs, the contribution of isopycnal flux cannot be neglected. We infer, from estimating the geostrophic transport across the A24 WOCE section in the eastern North Atlantic

subpolar gyre, that the isopycnal contribution to the SPMW throughput might be 10% - 40% of the diapycnal flux.

References

Brambilla, E., and Talley, L. D., 2007: Subpolar Mode Water in the northeastern Atlantic. Part I: properties and circulation. Submitted.

Conkright, M. E., Antonov, J. I., Baranova, O., Boyer, T. P., Garcia, H. E., Gelfeld, R., Johnson, D., Locarnini, R. A., Murphy, P. P., O'Brien, T. D., Smolyar, I., and Stephens, C., 2002: World ocean database 2001, volume 1: Introduction. U.S. Gov. Printing Office, Wash., D.C. 167 pp.

Dickson, R. R., and Brown, J., 1994: The production of North Atlantic Deep Water: sources, rates, and pathways. *J. Geophys. Res.*, **99**, 12319–12341.

Ganachaud, A., 2003: Large-scale mass transports, water mass formation, and diffusivities estimated from World Ocean Circulation Experiment (WOCE) hydrographic data. *J. Geophys. Res.*, **108**(C7), 3213. doi: 10.1029/2002JC001565.

Garrett, C., Speer, K., and Tragou, E., 1995: The relationship between water mass formation and surface buoyancy flux, with application to Phillips' Red Sea model. *J. Phys. Oceanogr.*, **25**, 1696–1705.

Garrett, C., and Tandon, A., 1997: The effects on water mass formation of surface mixed layer time-dependence and entrainment fluxes. *Deep-Sea Res. I*, **44**, 1991–2006.

Grist, J. P., and Josey, S. A., 2003: Inverse analysis adjustment of the SOC air-sea flux climatology using ocean heat transport constraints. *J. Clim,*, **16**, 3274–3295.

Gulev, S., Barnier, B., Knochel, H., Molines, J. M., and Cottet, M., 2003: Water mass transformation in the North Atlantic and its impact on the meridional circulation: insights from ocean model forced by NCEP-NCAR reanalysis surface fluxes. *J. Clim,*, **16**, 3085–3110.

Hanawa, K., and Talley, L. D., 2001: Mode Waters. In *Ocean Circulation and Climate - Observing and Modelling the Global Ocean*, editors J. C. G. Siedler, and J. Gould, 372–386. Academic Press edition.

Isemer, H.-J., and Hasse, L., 1987: The Bunker Climate Atlas of the North Atlantic Ocean. Vol2: Air-Sea interaction. *Springer-Verlag*, 218pp.

Krauss, W., 1986: The North Atlantic Current. *J. Geophys. Res.*, **91**, 5061–5074.

Lumpkin, R., and Speer, K., 2003: Large-scale vertical and horizontal circulation in the North Atlantic Ocean. *J. Phys. Oceanogr.*, **33**, 1902–1920.

Marsh, R., 2000: Recent variability of the North Atlantic thermohaline circulation inferred from surface heat and freshwater fluxes. *J. Clim,*, **13**, 3239–3260.

Marshall, J., Jamous, D., and Nilsson, J., 1999: Reconciling thermodynamic and dynamic methods of computation of water-mass transformation rates. *Deep-Sea Res. I*, **46**, 545–572.

Marshall, J. C., Nurser, A. J. G., and Williams, R. G., 1993: Inferring the subduction rate and period over the North Atlantic. *J. Phys. Oceanogr.*, **23**, 1315–1329.

Masuzawa, J., 1969: Subtropical mode water. *Deep-Sea Res.*, **16**, 463–471.

McCartney, M. S., and Mauritzen, C., 2001: On the origin of the warm inflow to the Nordic Seas. *Prog. Oceanogr.*, **51**, 125–214.

McCartney, M. S., and Talley, L. D., 1982: The Subpolar Mode Water of the North Atlantic. *J. Phys. Oceanogr.*, **12**, 1169–1188.

McCartney, M. S., and Talley, L. D., 1984: Warm-to-cold water conversion in the northern North Atlantic. *J. Phys. Oceanogr.*, **14**, 922–935.

Nurser, A. J. G., Marsh, R., and Williams, R., 1999: Diagnosing water mass formation from air-sea fluxes and surface mixing. *J. Phys. Oceanogr.*, **29**, 1468–1487.

Perez-Brunius, P., Rossby, T., and Watts, D. R., 2004: Transformation of the warm waters of the North Atlantic from a geostrophic streamfunction perspective. *J. Phys. Oceanogr.*, **34**, 2238–2256.

Pickart, R., Straneo, F., and Moore, G. W. K., 2003: Is Labrador Sea Water formed in the Irminger Sea? *Deep-Sea Res. I*, **50**, 23–52.

Qiu, B., and Huang, R. X., 1995: Ventilation of the North Atlantic and North Pacific: Subduction versus obduction. *J. Phys. Oceanogr.*, **8**, 2374–2390.

Read, J. F., 2001: CONVEX-91: Water masses and circulation of the Northeast Atlantic subpolar gyre. *Prog. Oceanogr.*, **48**, 461–510.

Saunders, P. M., 1996: The flux of dense cold overflow water southeast of Iceland. *J. Phys. Oceanogr.*, **26**, 85–95.

Schmitz, W. J., 1995: On the interbasin-scale thermohaline circulation. *Rev. Geophys.*, **33**(2), 151–174.

Schmitz, W. J., and McCartney, M. S., 1993: On the North Atlantic circulation. *Rev. Geophys.*, **31**, 29–49.

Speer, K., 1997: A note on average cross-isopycnal mixing in the North Atlanticocean. *Deep-Sea Res. I*, **44**, 1981–1990.

Speer, K., and Tziperman, E., 1992: Rates of water mass formation in the North Atlantic ocean. *J. Phys. Oceanogr.*, **22**, 93–104.

Speer, K. G., Isemer, H. J., and Biastoch, A., 1995: Water mass formation from revised [COADS] data. *J. Phys. Oceanogr.*, **25**, 2444–2457.

Steele, J. H., Barrett, J. R., and Worthington, L. V., 1962: Deep currents south of Iceland. *Deep-Sea Res.*, **9**, 465–474.

Talley, L. D., 1999: Mode waters in the subpolar North Atlantic in historical data and during the WOCE period. *WOCE Newsletter*, **37**, 3–6.

Talley, L. D., 2003: Shallow, intermediate, and deep overturning components of the global heat budget. *J. Phys. Oceanogr.*, **33**, 530–559.

Tandon, A., and Zhao, L., 2004: Mixed layer transformation for the North Atlantic for 1990-2000. *J. Geophys. Res.*, **109**, C05018. doi:10.1029/2003JC002059.

Tziperman, E., 1986: On the role of interior mixing and air-sea fluxes in determining the stratification and circulation of the oceans. *J. Phys. Oceanogr.*, **16**, 680–693.

Valdivieso Da Costa, M., Mercier, H., and Treguier, A. M., 2005: Effects of the mixed layer time variability on kinematic subduction rate diagnostics. *J. Phys. Oceanogr.*, **35**, 427–443.

Walin, G., 1982: On the relation between sea-surface heat flow and thermal circulation in the ocean. *Tellus*, **34**, 187–195.